DISS. ETH NO. 24980

Towards Two-Dimensional Polymers at the Air/Water Interface: Synthesis, Characterization, and Application

A thesis submitted to attain the degree of

DOCTOR OF SCIENCES of ETH ZURICH

(Dr. sc. ETH Zurich)

presented by
Vivian Clarissa Müller
MSc ETH Interdisciplinary Sciences

born on 09.06.1989
citizen of Germany

accepted on the recommendation of

Prof. A. D. Schlüter, examiner
Prof. N. D. Spencer, co-examiner
Prof. R. Zenobi, co-examiner
Prof. R. Spolenak, chair

2018

Für meine Familie

ETH
Eidgenössische Technische Hochschule Zürich
Swiss Federal Institute of Technology Zurich

Towards Two-Dimensional Polymers at the Air/Water Interface: Synthesis, Characterization, and Application

Doctoral Thesis

Vivian Clarissa Müller
MSc ETH Zurich

February 26th, 2018

Accepted on the recommendation of: Prof. A. D. Schlüter, examiner
Prof. R. Zenobi, co-examiner
Prof. N. D. Spencer, co-examiner
Prof. R. Spolenak, co-examiner
Department of Materials, ETH Zürich

Abstract

Two-dimensional materials, such as molybdenum disulfide and graphene, have attracted much attention in the past decade. Two-dimensional polymers, as a subclass of two-dimensional materials, are defined as free-standing films composed of single layers of monomers that are covalently connected to give tesselated, ordered structures.

The study of two-dimensional polymers synthesized at the air/water interface represents a major analytical challenge, particularly in terms of structure elucidation. In this thesis, two amphiphilic monomers that differ in terms of flexibility and complexity were studied with regard to their behavior at the interface, their polymerization, and the structure of the obtained polymerized films.

To this end, various analytical techniques were employed, both at the air/water interface and after transfer of the film onto solid substrates, in order to prove the chemical connectivity between monomer units, estimate the conversion of the polymerization, study the packing of the monomers and to show that all criteria defining a two-dimensional polymer were fulfilled. These techniques included Brewster angle microscopy (BAM), scanning electron microscopy (SEM), atomic force microscopy (AFM), fluorescence microscopy, scanning tunneling microscopy (STM), tip-enhanced Raman spectroscopy (TERS), X-ray photoelectron spectroscopy (XPS), UV-vis spectroscopy, selected area electron diffraction (SAED) and variable angle spectroscopic ellipsometry (VASE).

The chemical connectivity was successfully proven in the case of one monomer using TERS, backed up by DFT calculations and confocal Raman spectra of synthesized reference compounds. A value for the conversion was estimated based on the TERS results and was further corroborated by XPS and a UV-vis study. It was also shown that all five definition criteria for a two-dimensional polymer were fulfilled. In the second case, not all aspects of structure elucidation could be resolved in a satisfactory way. This was mainly attributed to the differences in flexibility and complexity between the monomers. Nevertheless, indirect spectroscopic evidence could be furnished and this monomer proved particularly suited for a preliminary study exploring the option of performing polymerizations post-transfer on solid substrates. Furthermore, this study showed the possibility of using the fluorescent monomer films for optical recording or optical data storage.

In this thesis, the introduction will give a short overview of the techniques used to synthesize two-dimensional polymers along with their advantages and drawbacks. The challenges of structure elucidation will be considered together with the methods that are suited for this endeavour and that were used within the scope of this work. The photochemical and photophysical properties of anthracenes will be discussed in detail, as they often function as reactive units of monomers for two-dimensional polymerizations. Likewise, the spectroscopic signature of anthracene derivatives in various spectroscopies will be reviewed as it is of relevance for the structure elucidation of two-dimensional polymers. The main part is divided in three chapters: in chapter 3, the structure elucidation of monomer **1** is presented. Following that is chapter 4 about the structure elucidation of monomer **2** alongside with a comparison of the structure and properties of the two monomers. Finally, in chapter 5, the suitability of monomer **2** and monomer **3** films as an optical recording device will be assessed.

Zusammenfassung

Zweidimensionale Materialien wie Molybdändisulfid und Graphen haben in der letzten Dekade für viel Aufmerksamkeit gesorgt. Zweidimensionale Polymere, eine Unterkategorie der zweidimensionalen Materialien, sind als freistehende Filme definiert, welche aus einer einzelnen Schicht Monomere bestehen, die kovalent miteinander verknüpft sind und somit in einer geordneten, getäfelten Struktur resultieren. Die strukturell-chemische Untersuchung von zweidimensionalen Polymeren, die an der Wasser-Luft-Grenzfläche erzeugt wurden, stellt eine große Herausforderung dar, auf Grund der geringen Probungsmengen und ihrer Porösität. Die Untersuchung von zwei amphiphilen Monomeren, die unterschiedliche Flexibilität und Komplexität aufweisen, auf ihr Verhalten an der Wasser-Luft-Grenzfläche, ihre Polymerisierung und die Struktur der erhaltenen polymerisierten Filme hin ist Gegenstand dieser Arbeit.

Zur Durchführung der Charakterisierung wurden diverse analytische Methoden angewendet, welche eine Untersuchung der Filme sowohl an der Wasser-Luft-Grenzfläche als auch nach Übertragung auf feste Substrate ermöglichten. Um die chemische Verknüpfung zwischen Monomeren, den Umsatz der Polymerisierung, die Packung der Monomere und die Erfüllung aller Kriterien, welche die Definition der zweidimensionalen Polymere umfasst, zu untersuchen, wurde auf Methoden wie Brewster Winkelmikroskopie, Rasterelektronenmikroskopie, Rasterkraftmikroskopie, Fluoreszenzmikroskopie, Rastertunnelmikroskopie, spitzenverstärkte Ramanspektroskopie, Röntgenphotoelektronenspektroskopie, Elektronenabsorptionsspektroskopie und SAED zurück gegriffen.

Die chemische Verknüpfung und der Umsatz ließen sich in einem Fall erfolgreich durch spitzenverstärkte Ramanspektroskopie nachweisen, deren Ergebnisse wiederum durch Dichtefunktionaltheorieberechnungen sowie die Aufnahme konfokaler Ramanspektren synthetisierter Vergleichsverbindungen gestützt wurden. Des Weiteren konnten die Ergebnisse mittels Röntgenphotoelektronenspektroskopie und Elektronenabsorptionsspektroskopie abgesichert werden.

Im zweiten Fall gelang die chemisch-strukturelle Untersuchung des Films nicht vollumfänglich, was auf Unterschiede in der Monomerflexibilität und -komplexität zurückgeführt wurde. Nichtsdestotrotz fanden sich Anhaltspunkte für die chemische Verknüpfung und Struktur. Gerade dieses Monomer stellte sich als besonders geeignet heraus für

einen Exkurs in die Thematik der Polymerisierung auf festen Substraten und in die Einsatzmöglichkeiten fluoreszenter Monomerfilme als optische Datenspeicherungselemente.

Die Einleitung dieser Arbeit gibt zunächst einen kurzen Überblick über die Synthesemethoden zweidimensionaler Polymere und deren Vor- und Nachteile. Die Herausforderung der Strukturaufklärung, sowie die Methoden, welche potentiell dafür geeignet sind und im Rahmen der Arbeit dann auch verwendet wurden, werden genauer diskutiert. Ferner wird die Kategorie der Anthracene, die häufig als reaktive Einheit für Monomere zweidimensionaler Polymere verwendet werden, detailliert beschrieben und ihre charakteristische Photodimerisierungsreaktion vorgestellt. Ihre spektroskopische Signatur ist für die chemische Strukturaufklärung von zweidimensionalen Polymeren von Bedeutung, deshalb wird sie in diversen Spektroskopien analysiert. Der Hauptteil dieser Arbeit gliedert sich in drei Teile: Der erst Teil (Kapitel 3) präsentiert die chemisch-strukturelle Untersuchung von Monomer **1** und dessen Polymerisierungsprodukt. Kapitel 4 legt dasselbe für Monomer **2** sowie dessen Polymerisierungsprodukt dar und vergleicht im Anschluss die beiden Monomere. Sodann wird wird die Eignung der Filme von Monomer **2** und Monomer **3** im Bereich der optischen Datenspeicherung untersucht (Kapitel 5).

Parts of the thesis have been taken from the following publications:

V. Müller, F. Shao, M. Baljozovic, M. Moradi, Y. Zhang, T. Jung, W. B. Thompson, B. King, R. Zenobi, A. D. Schlüter *Angew. Chem. Int. Ed.* **2017**, *56*, 15262-15266.
Contribution of authors: *V. Müller*: preparation of Langmuir films, UV-vis spectroscopy, fluorescence, AFM, SEM, BAM, synthesis of reference compounds; *F. Shao*: confocal and tip-enhanced Raman spectra, simulation of Raman spectra; *M. Baljozovic*: X-ray photoelectron spectroscopy; *M. Moradi*: AFM scratching; *Y. Zhang*: simulation of Raman spectra; *T. Jung*: supervisor of M. Moradi and M. Baljozovic; *W. B. Thompson*: synthesis of monomer; *B. King*: supervisor of W. B. Thompson; *R. Zenobi*: supervisor of F. Shao; *A. D. Schlüter*: supervisor of V. Müller.

F. Shao, V. Müller, Y. Zhang, A. D. Schlüter, R. Zenobi, *Angew. Chem. Int. Ed.* **2017**, *56*, 9361–9363.
Contribution of authors: *F. Shao*: confocal and tip-enhanced Raman spectra, simulation of Raman spectra; *V. Müller*: preparation of Lang-

muir films, AFM; *Y. Zhang*: simulation of Raman spectra; *A. D. Schlüter*: supervisor of V. Müller; *R. Zenobi*: supervisor of F. Shao.

V. Müller, T. Hungerland, M. Baljozovic, T. Jung, N. D. Spencer, H. Eghlidi, P. Payamyar, A. D. Schlüter *Adv. Mater.* **2017**, *29*, 1701220.
contribution of authors: *V. Müller*: preparation of Langmuir films, imaging/bleaching with CLSM, fluorescence recovery by heating, excitation spectroscopy, UV-vis spectroscopy; *T. Hungerland*: synthesis of monomer, SEM, BAM, AFM; *M. Baljozovic*: X-ray photoelectron spectroscopy; *T. Jung*: supervisor of M. Baljozovic; *N. D. Spencer*: scientific discussion; *H. Eghlidi*: scientific discussion; *P. Payamyar*: redaction of manuscript; *A. D. Schlüter*: supervisor of V. Müller, P. Payamyar.

Acknowledgements

First and foremost I would like to thank Prof. A. Dieter Schlüter for giving me the opportunity to work on this interesting and versatile project. It was through his excellently taught classes that I first turned my attention towards polymer chemistry. Throughout my PhD, I have highly appreciated his encouragement to pursue the topics that fascinate me the most. His continuous support throughout my studies is highly appreciated.

Coming from a synthetic chemistry background, I had to learn about a plethora of microscopic and spectroscopic techniques used for studying two-dimensional polymers. I would like to thank the ”Langmuir guys” for sharing their knowledge about Langmuir films, surface science spectroscopies and microscopies, namely, Wenyang Dai, Dr. Payam Payamyar, and Dr. Tim Hungerland for introducing me to the experiments conducted at the Langmuir trough, cleaning procedures for various substrates, and giving me introductions to the various microscopes. Wenyang, I was particularly impressed with your extensive knowledge of the literature on two-dimensional materials and I think you do not know how much I appreciated the personalized tweezers that you provided me with. Payam, I enjoyed our numerous scientific discussions in the Langmuir room and group kitchen, as well as the interest you showed in general in my research. Special thanks also for granting me insight into the fascinating culture of Iran. I am particularly indebted to Dr. Tim Hungerland for giving me an introduction to the fluorescence microscope and for letting me continue and finish up research on molecular paper.

On the same note, I enjoyed numerous collaborations during my PhD. My collaborators not only gave me an insight into new techniques, but also into different mindsets. I am greatly indebted to Dr. Wei-Chih Liao, Dr. Feng Shao, Mina Moradi, Olha Popova, Dr. Milos Baljozovic, and Dr. Haoyuan Qi for their enthusiastic work. Wei-Chih, thank you for measuring the DNP-NMR spectra of my films. Feng, thank you for the commitment to our project, measuring the TER spectra and carrying out the DFT calculations. I greatly enjoyed working with you! Mina, Olha, and Milos, thank you for introducing me to XPS and STM, all our interesting discussions, and making the PSI lab my second 'work home'.

I would like to thank Prof. Dr. Thomas Jung, supervisor of Mina, Olha, and Milos, for supporting our collaboration, granting access to his UFO-like equipment room and showing interest in the topic of two-dimensional polymers. I would also like to thank Prof. Dr. Renato Zenobi, supervisor of Feng, for his support during our collaboration and his interest in this field.

I would like to thank Dr. Thomas Schweizer for providing me with numerous home-made devices, like my quartz cell for photo-reactions and an extended irradiation set-up for the trough. Thank you furthermore for repairing many group instruments that are of vital importance to the whole of the group.

I would like to thank Daniela Zehnder for all administrative support.

I would like to thank Dr. Martin Kröger for the image processing scripts that he wrote in order to interpret images of stretched two-dimensional polymers. Similarly, Gregor Hofer's contribution in this regard is greatly appreciated.

Many thanks go to my two very motivated students, Lukas Rochlitz and Moritz Hansen. They did great synthetic work in the lab and I wish them all the best for their scientific future.

I would like to thank Prof. Dr. Benjamin T. King for providing me with the monomer that I did a big part of my work on.

For access to the scanning electron microscope, I would like to thank Prof. Dr. Andre Studart. For access to optical microscopes, I would like to thank Prof. Dr. Paul Smith and Prof. Dr. Jan Vermant. For access to atomic force microscopes, I would like to thank Prof. Dr. Nicholas D. Spencer. For access to and maintenance of their confocal laser scanning microscopes, I would like to thank ScopeM, in particular Dr. Tobias Schwarz. For access to the fluorimeter, I would like to thank Prof. Dr. Pablo Rivera Fuentes. For access to the photoreactor, I would like to thank Prof. Dr. François Diederich. For access to their recycling GPC and an introduction to it, I would like to thank Prof. Dr. Helma Wennemers and Nellie Ochs, respectively.

The atmosphere in a PhD group greatly influences the PhD experience. I was very lucky to do my PhD in a group where members supported each other and where scientific problems were avidly discussed during coffee breaks (not so much at lunch when everyone was starving), which led to much fruitful output. In this regard many thanks go to the Polymer Chemistry group, in particular to Dr. Bernd Deffner, Dr. Chiara Gstrein, Dr. Payam Payamyar, Dr. Tim Hungerland, Ralph Lange, Daniel Messmer, Gregor Hofer, Philipp Tanner, and Dr. Sandra Serrano-Luginbühl. I would like to particularly thank Daniel Messmer for correcting my thesis.

On a similar note, I would like to thank Sophie Haberland, Dr. Sandra Serrano-Luginbühl, Jasmine Egli, and Dr. Martina Minges, my friends from my undergrad studies for sharing this experience with me. All doing a PhD at the same time meant that usually at least one of us had had a frustrating day in the lab when we met and I'm glad that we were able to put these things aside to enjoy ourselves after a hard day of work.

Coffee group 1: Dr. Anatol Schwab, Sophie Haberland, Dr. Elisabeth Schäfer and Dr. Jovana Milic – thank you for all the funny discussions! But also for supporting me scientifically by formulating the week's goal anew every Monday and by debating scientific questions. Jovana, I greatly admire your work ethic and determination, as well as your dedication to the topic of

women in science. Sophie, thank you for providing me insight into how to set up DFT calculations. Lisa, your cleverness in scientific and interpersonal matters always impressed me very much and I will try to channel your spirit in these affairs. Also, you are definitely my favorite aperol spritz drinking in the sun companion! Anatol, you were like a personal encyclopedia for chemistry and always had good input whenever I was stuck with something, in particular when it came to tricky work-ups.

Coffee group 2 or the Roche alumni: Alina Tirla, Nicole Hauser and Maryline Dong, thank you for distracting me from work and for all the fun things that we did together, as well as providing me insight into the instrument repertoire available at LOC and the Altmann group.

Great thanks to Daniel Messmer, Gregor Hofer, Richard Bernitzky, Moh Divandari, Stan van de Poll, and Jay Colman for distracting me from work every second Tuesday evening. I very much enjoyed our DnD sessions!

I would also like to thank the other members of the SAM board for enthusiastically working alongside me to organize all kinds of events at the D-MATL: thank you Christian Mathis, Max Kory, Florian Thöle, Martina Cihova, Ella Dehghani, Moh Divandari, Murielle Schreck, Stefano Danzi, Kilian Dietrich, Volker Schnabel, Paolo Testa, and Yvonne Gombert!

So many thanks go to Jay Colman, true hero of my PhD, who never once complained if I got home late, tired, in an ugly mood or all three of those. Your love, constant support and amazingly excellent culinary skills kept me going even when the going got tough. Furthermore, I truly appreciated the adventurous weekend activities and holiday trips you planned for us. I look forward to tackling the rest of our lives together.

I am deeply grateful to my parents, Prof. Dr. Hans-Peter Müller and Renate Borrmann, for their constant support at all times. From an early age on you taught me the value of education and even though I landed in the dull, dry natural sciences, your interest in what I was doing never wavered. Mom, you're the best! Thank you for proof-reading my theses, dealing with all

the administrative issues arising when living abroad and for never losing patience with me when I vanished from the face of the Earth during tough PhD times. Dad, thank you in particular for critical input on my theses, sending me interesting texts from social sciences to proof-read and for financing life in expensive Switzerland. Many thanks also go to my sister, Laura, truly the best sibling of the world. Thanks to Isolde Borrmann, my aunt, who never showed any interest in my PhD but a lot of interest in my life in general.

Many thanks go to Harriet von Oelhafen, my godmother, who proudly followed my achievements during life and supported me in my choices. Your video training and your lessons on communication skills are extremely valuable, way beyond my academic career. Just as many thanks go to my other godmother, Gerburg Reis, who hosted me whenever I needed a home in Bavaria away from home in Berlin.

Abbreviations

1D	One-dimensional
2D	Two-dimensional
3D	Three-dimensional
AFM	Atomic Force Microscopy
aq.	aqueous
BAM	Brewster Angle Microscopy
CC	Column Chromatography
CLSM	Confocal Laser Scanning Microscope
COF	Covalent Organic Framework
comb.	combined
DAA	Diazaanthracene
DFT	Density Functional Theory
FRAP	Fluorescence Recovery After Photobleaching
Ftf	Face-to-Face

FWHM	Full Width at Half Mean
GI-SAXS	Grazing Incidence Small Angle X-ray Spectroscopy
GI-XRD	Grazing Incidence X-ray Diffraction
h_{AFM}	Height Value Measured by Atomic Force Microscopy
h_{calc}	Height Value Based on Calculations
HMBC	Heteronuclear Multiple Bond Correlation Experiment
HOESY	2D Heteronuclear Nuclear Overhauser Effect Spectroscopy
HOPG	Highly-Oriented Pyrolitic Graphene
HSQC	Heteronuclear Single Quantum Coherence Experiment
HR	High Resolution
IR	Infrared
J	Spin-Spin Coupling Constant (Hz)
LB	Langmuir-Blodgett
LED	Light-emitting Diode
LEED	Low Energy Electron Diffraction

MALDI	Matrix-assisted Laser Desorption/Ionization
MMA	Mean Molecular Area
MS	Mass Spectrometry
NMR	Nuclear Magnetic Resonance
org.	organic
PMT	Photomultiplier Tube
ppm	Parts Per Million
rGPC	Recycling Gel Permeation Chromatography
rt	Room Temperature
SAED	Selected Area Electron Diffraction
SAM	Self-Assembled Monolayer
SCF	Self-Consistent Field
SEM	Scanning Electron Microscopy
SP	Surface Pressure
SPM	Scanning Probe Microscopy
STM	Scanning Tunneling Microscopy
TEM	Transmission Electron Microscopy
TERS	Tip-enhanced Raman Spectroscopy
TLC	Thin Layer Chromatography

TOF	Time-of-flight
UV	Ultraviolet
vis	Visible
XPS	X-ray Photoelectron Spectroscopy
XRD	X-ray Diffraction

Contents

Acknowledgements **vii**

Abbreviations **xiii**

Contents **xvii**

I Introduction **1**

1 Background **3**
- 1.1 Definition of Two-Dimensional Polymer 3
- 1.2 Synthetic Approaches 5
  - 1.2.1 Top-Down Approaches 6
  - 1.2.2 Bottom-Up Approaches 8
- 1.3 Structure Elucidation of Two-Dimensional Polymers 11
  - 1.3.1 Challenges of Structure Elucidation 11
  - 1.3.2 Suitable Analytical Techniques 13
  - 1.3.3 The Class of Anthracenes 16

2 Aims and Motivation **23**

II Results and Discussion **27**

3 Structure Elucidation of Films Based on Tetrafluoroanthracene-Based Monomer 1 **29**
- 3.1 Monomer Features 29
- 3.2 Film Formation and Behavior at the Air/Water Interface . . . 31

3.2.1 Evidence of π-π Stacking 32
3.3 Film Thickness 36
3.3.1 Thickness Determination by AFM 36
3.4 Mechanical Coherence of the Irradiated Film 40
3.5 Proof for [4+4]-Cycloaddition 42
3.5.1 X-ray Photoelectron Spectroscopy 42
3.5.2 Synthesis of Reference Compounds 46
3.5.3 UV-Vis Spectroscopy 48
3.5.4 Confocal and Tip-Enhanced Raman Spectroscopy . . . 51
3.6 Evidence for Structure 56
3.6.1 Brewster Angle Microscopy 56
3.6.2 Estimation of the Conversion 59
3.6.3 Determining Defects 62
3.6.4 Imaging techniques 64

4 Structure Elucidation of Diazaanthracene-Based Monomer 2 73
4.1 Characteristics of Monomer **2** 74
4.2 Evidence for π-π stacking 76
4.3 Absorption and Excitation Spectroscopy 77
4.4 Mechanical Coherence of the Irradiated Film and its Origin . 79
4.5 Film Thickness Determination by AFM 82
4.6 Comparison of Monomers **1** and **2** 83

5 Towards Applications: Molecular Paper 87
5.1 Choice of Monomer 89
5.2 Molecular Paper 89
5.2.1 Monomer **2** 89
5.2.2 Monomer **3** 94
5.3 Origin of Writing 100

III Conclusion and Outlook 107

6 Conclusion 109

7 Outlook 115

IV Experimental **119**

8 Sample preparation **121**
8.1 Langmuir trough 121
8.2 Preparation of Substrates 122
8.3 Polymerization and Film Transfer 123

9 Analytical techniques **125**
9.1 Brewster Angle Microscope (BAM) 125
9.2 Scanning Electron Microscopy (SEM) 125
9.3 Atomic Force Microscopy (AFM) 125
9.4 Scanning Tunneling Microscopy 126
9.5 Confocal and Tip-enhanced Raman Spectroscopy 127
9.6 DFT calculations 128
9.7 UV-Vis spectroscopy 129
9.8 Fluorescence and excitation spectroscopy 129
9.9 X-Ray Photoelectron Spectroscopy (XPS) 129
9.10 Confocal Laser Scanning Microscope (CLSM) 130
9.11 Photoreaction 130

10 Synthetic Procedures **133**
10.1 1,2,3,4-Tetrafluoroanthracene **4** 134
10.2 Tetrafluoroanthracene Dimer **5** 135
10.3 Dianthracene **7** 136

11 NMR Spectra **137**

Bibliography **151**

Curriculum Vitae **163**

Part I

Introduction

Chapter 1

Background

Following their discovery by Herrmann Staudinger at the beginning of the 20th century, polymers became important in various areas affecting our everyday life. The need for ever improving, new polymeric materials directed the attention of researchers towards finding synthetic methods to obtain control over not only the molecular weight of the polymers,[1–4] but also over their topology. From brush-like structures found in dendronized polymers,[5] to star polymers,[6] ladder polymer,[7] and dendrimers,[8] all kinds of architectures have been investigated.[9]

Exploring two-dimensional topologies of polymers leads to yet a further class of polymers: two-dimensional polymers. Although studies towards these materials began in the first half of the 20^{th} century with the work of Gee,[10,11] the isolation of graphene, a single-layer of annulated benzene rings, in 2004[12] brought about a flurry of research in the domain of single-atomic layer materials in the following decades.[13–15] Novoselov and Geim themselves were awarded the Nobel prize for their discovery in 2010. Graphene can be considered as a prototype of a two-dimensional polymer.

1.1 Definition of Two-Dimensional Polymer

What is a two-dimensional polymer? A two-dimensional polymer is an "atomically thin, laterally 'infinite', structurally precisely defined, covalently bonded sheet".[16] This definition encompasses several characteristics: The monomers possess at least three binding sites, so that they can create a two-dimensional tessellated structure upon polymerization. This tesselated structure exhibits a high internal order and its height corresponds to that of one layer of monomer. Furthermore, the monomer units are covalently bonded and the resulting polymer films are sufficiently strong to be free-standing. A graphic representation of this definition is shown in fig. 1.1.

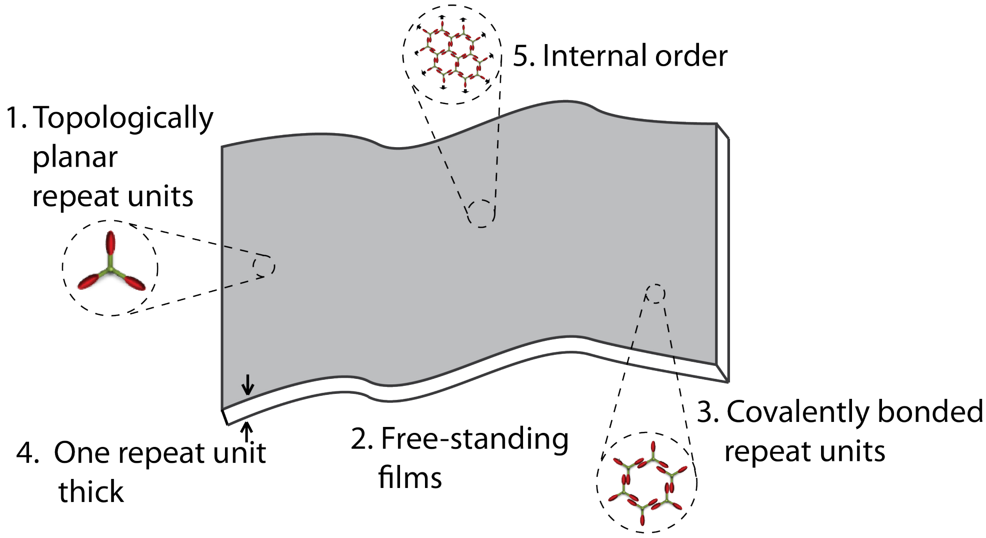
5. Internal order
1. Topologically planar repeat units
4. One repeat unit thick
2. Free-standing films
3. Covalently bonded repeat units

Figure 1.1: Schematic representation of a two-dimensional polymer.

While the definition of a two-dimensional polymer is restricted to monolayers of *covalently connected*, periodic repeat units, the more general term of two-dimensional material will be applied to all other two-dimensional materials where the criteria of covalent bonds and periodicity are not met.

Before going into a detailed analysis of the synthetic approaches to two-dimensional polymers, potential applications of two-dimensional polymers should be mentioned.

As a rather young class of material the full potential of two-dimensional polymers has not been thoroughly investigated. Possible future applications of two-dimensional polymers could be found in diverse fields, for example as new dielectrics, in gas separation, in miniaturized optical devices, in non-linear optical devices, and in catalysis. Some of these applications immediately result from the characteristic structure of two-dimensional polymers, for example, gas flow dynamics change when going from a bulk material to ultra-thin membranes, where they approach ultimate permeation.[17] Similarly, having a large surface-to-volume ratio is highly beneficial for catalysis.

In two-dimensional polymers this ratio is essentially at its maximum. The high order and extreme thinness of the films could aid in the miniaturization of optical devices. While these applications have not been explored so far, first steps have been taken to investigate some of them.[18]

1.2 Synthetic Approaches

Monomers that have at least three reactive sites are required for the synthesis of two-dimensional polymers. These sites can then react with their neighbors to give a regularly tesselated sheet. One can distinguish between reactions under kinetic control and thermodynamic control.[19] In the former, the monomers are assembled and preorganized before bond formation, then reactions that are generally irreversible are carried out. Under thermodynamic control, dynamic bonds are formed which allow for error correction as they are reversible. While kinetic bond formation usually leads to more stable bonds, the advantage of thermodynamic bond formation lies in its capability of correcting defects that have formed during polymerization.

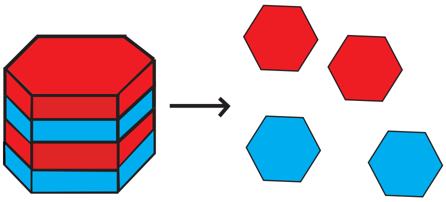

Figure 1.2: Top-down approach.

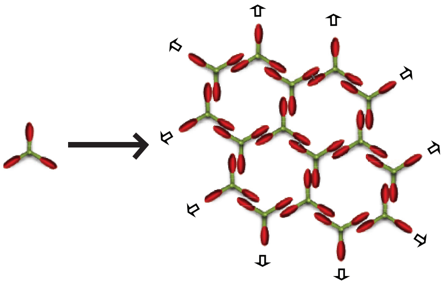

Figure 1.3: Bottom-up approach.

The various synthetic approaches to two-dimensional polymers can be divided into two main categories: the top-down approach (fig. 1.2), which comprises synthesis from layered structures, and the bottom-up approach (fig. 1.3), which includes synthesis at an interface and on-surface synthesis.

In the following, a brief overview will be given of the top-down approaches and the bottom-up approaches, along with their advantages and drawbacks. The types of chemistry used in these approaches will be discussed in their corresponding sections. The air/water interface or Langmuir approach will be discussed in more detail, before evaluating the analytical methods used to elucidate the structure of two-dimensional polymers. In the context of the evaluation of analytical methods, the compound class of anthracenes, one of the reactive units often used in monomers for two-dimensional polymerization in both top-down and bottom-up approaches, will be discussed.

1.2.1 Top-Down Approaches

In the top-down approach, a layered material is synthesized in bulk and then exfoliated down to the single sheet. Covalent organic frameworks (COFs) and the single-crystal approach fall into this category.

Covalent Organic Frameworks

Covalent organic frameworks (COFs) are synthesized in bulk as covalently bonded networks with a high porosity.[19] They have potential applications in catalysis,[20–22] optoelectronics,[23–26] and gas capture and storage.[27–29] The shape-persistent monomers are reacted under dynamic covalent bond forming conditions. This means that in order to correct defects in their structure arising during synthesis, their chemistry relies on reversible reactions, allowing the annealing of structural defects (thermodynamic bond formation control).

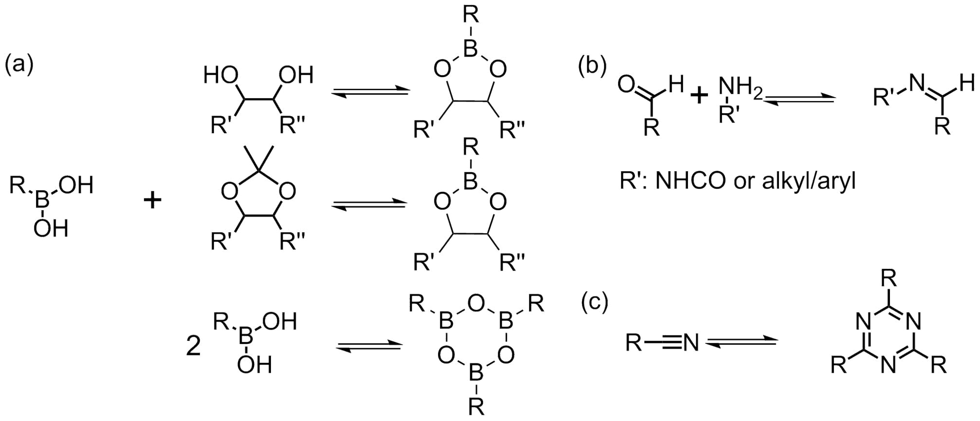

Figure 1.4: (a) Boron ester or boronic acid-based chemistry used in the synthesis of COFs. (b) Condensation chemistry of carbonyl groups with amines or hydrazines used in the synthesis of COFs. (c) Condensation chemistry of nitriles used in the synthesis of COFs.

Typical chemistries used in this approach are boron condensation (to give the boronic ester-linked COF),[30–33] carbonyl condensation (with amines or hydrazines to give the imine- or hydrazone-linked COF, respectively)[34–38] or trimerization of nitriles (giving triazine-based COFs),[39–41] see fig. 1.4.

While the dynamic covalent bond formation chemistry enhances the structural perfection, it has the drawback of creating weak bonds susceptible to hydrolysis that cannot withstand exfoliation conditions which are necessary to obtain single-sheets. Therefore, attempts to isolate single sheets by this approach have so far failed.

Single Crystal Approach

A further top-down approach is the single crystal approach where a trifunctional monomer is crystallized in a way that results in a suitable packing for polymerization. In such a packing, all reactive sites are close enough to each other to react and the resulting sheets are stacked in a layered assembly, such that they can be separated from one another. Typically, photochemical reactions are used, most notably anthracene [4+4]-cycloadditions or [2+2]-cycloadditions of olefins. Irradiation of the crystal results in photoreaction of the reactive moieties, leading to an internally structured polymer crystal. This crystal is then exfoliated in order to obtain monolayer sheets. Because pre-organization is achieved before the reaction, no error correction is required and chemistries can be used that result in stable, covalent bonds (kinetic bond formation control). This in turn enables exfoliation down to the single-layer.

The advantage of this method lies in the facilitated characterization of the crystal (by crystallographic methods) and in the low concentration of defects.

A main drawback is the limitation in lateral sheet size of the two-dimensional polymers. The lateral sheet size is not only limited by the size of the crystal, but also by domain formation within the crystal. These limitations lead to a reduction of the lateral sheet sizes obtained. Additionally, harsh exfoliation conditions can lead to a further reduction in sheet size. The exfoliation can be considered an additional disadvantage since it results in sheets varying in both lateral sheet size and thickness. The isolation and characterization of the ensuing sheets represents a further challenge, comparable to the characterization of two-dimensional polymers obtained at the air/water interface.

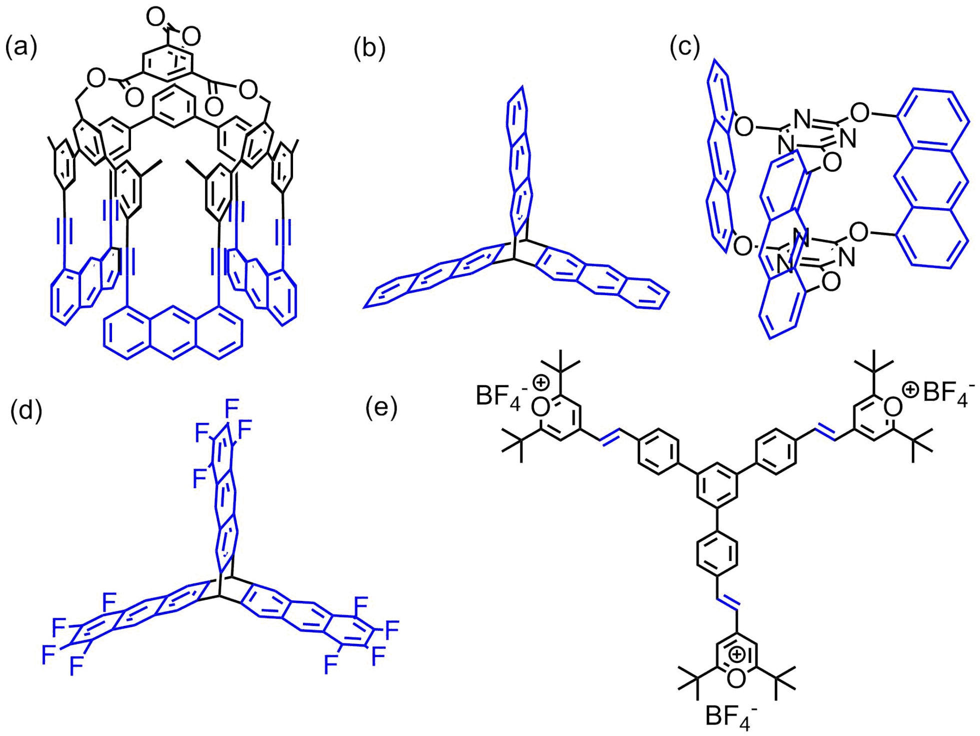

Figure 1.5: Monomers used in the single-crystal approach. Their reactive units are highlighted in blue. Structures (a), (b), (c), (d), and (e) can be found in [42], [43], [44], [45], and [46], respectively.

Despite these drawbacks, the single-crystal approach has so far brought forth the highest number of systems that can confidently be classified as two-dimensional polymers, see fig. 1.5.[42–46]

1.2.2 Bottom-Up Approaches

In the bottom-up approaches, the monomers are organized in a way that directly yields single monolayers upon polymerization. While this circumvents the exfoliation step, the characterization of the ensuing sheets is inherently difficult. In the following, different bottom-up approaches are presented, before going into detail about the characterization required for these single sheets.

On-Surface Synthesis

In this approach, shape-persistent monomers are sublimed onto a crystalline metal surface and heated up to induce molecular diffusion and to activate covalent bond-forming reactions. The chemistry involved can be the same as the one used for COFs described in the top-down approach,[47–49] but often aryl-aryl couplings, such as Ullmann coupling, are used.[50–52] Further reported syntheses involve halogenated porphyrins[53] and phtalocyanines.[54] In the latter cases, the metal surface induces homolytic cleavage of the halogens to generate radical species which can then recombine and thus start lateral growth.

The advantage of this approach is that the ensuing polymer can be directly characterized by scanning tunneling microscopy (STM) or high-resolution atomic force microscopy (HR-AFM) to determine its structure, domain sizes and defects. Unfortunately, the lateral size of the two-dimensional polymers obtained in this way is limited to ca. 100 nanometers, as during monolayer growth on the metallic surface the monomers often start building a second layer on top of the first.[50] The approach is further restricted by the choice of monomers which have to be sublimable to be suitable for this technique.

Interfacial Approach

In this rather new approach, reactions between monomers are confined to the liquid/liquid interface. This can be achieved in a system where monomers reside in the organic phase (solvent) and the catalyst necessary for the reaction between monomers resides in the aqueous phase. Thus reaction between monomers only occur at the interface between these two media. As the liquid/liquid interface is less sharply defined than the air/water interface[55] and as there is usually some residual solubility of the aqueous phase in the organic phase and vice-versa, the approach lacks control of the interfacial synthesis which results in multilayer synthesis instead of single-layer synthesis.[56–58]

Air/Water Interface or Langmuir Approach

In principle, the air/water interface approach could be included in the section about interfacial approach. However, compared to liquid-liquid interfaces, the air/water interface is a sharp interface.[59] This has the advantage that the molecules clearly orientate themselves at this interface (provided that they are amphiphilic) which cannot be said for the aforementioned liquid-liquid interface approach.

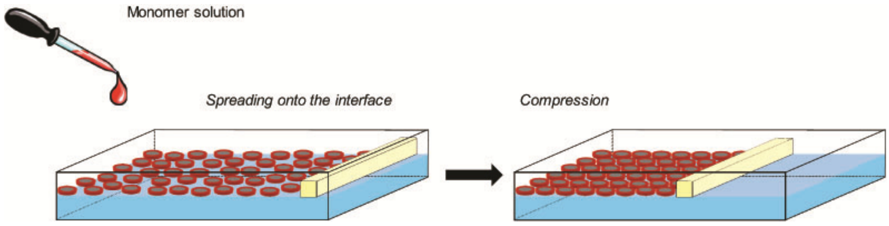

Figure 1.6: Langmuir approach

Thus, the Langmuir approach to two-dimensional polymers consists of first synthesizing a trifunctional, amphiphilic monomer. A solution of this monomer is then deposited on the water surface of a Langmuir trough, where the amphiphilic nature of the monomer helps orientate it such that its hydrophilic part will be immersed in the water, while its hydrophobic part is exposed to the air. Compression of the monomers leads to formation of a monomer monolayer (see fig. 1.6). This layer is then brought to polymerize, the reactions taking place between reactive units of neighboring monomer units. Molecular organic frameworks consist of monomers connected by metal ions which are injected into the subphase of the Langmuir trough after the deposition of the monomers at the air/water interface. While molecular organic frameworks are also synthesized at the air/water interface, they fall into the category of two-dimensional materials and therefore will not be considered further. This restricts polymerization chemistries used at the air/water interface to photoreactions such as the [4+4]-cycloaddition that also figure prominently in the single crystal approach and imine chemistry which has been discussed in the section about COFs. Polymerization leads to a highly structured network due to the preorganization of the reactive units. This is a further example of a kinetic bond formation approach, as the mobility on water in principle allows for error correction. Transfer of the formed film onto a suitable substrate and characterization via various techniques is necessary in order to elucidate the connectivity and the structural perfection of the formed sheets.

The advantage of this method is that only small amounts of material (a few hundred μg) are required to carry out a multitude of experiments. Furthermore, large lateral sheet sizes can be obtained. However, structure elucidation of the film is challenging, since many analytical methods lack the required sensitivity for the quantities probed in the ultrathin sheets which are on the order of ng–μg, depending on the size of the probed area. Indeed,

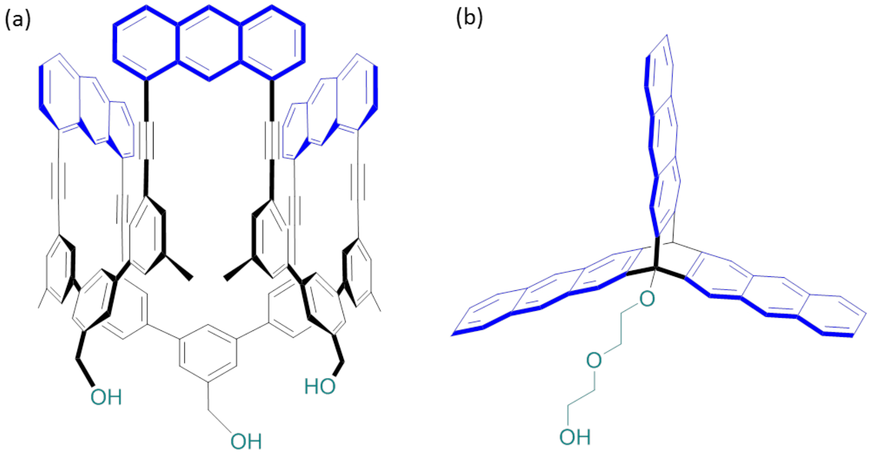

Figure 1.7: Monomers used for the synthesis at the air/water interface or Langmuir approach. Their reactive units are highlighted in blue, the hydrophilic part is highlighted in cyan. Structures (a) and (b) can be found in references [60–62] and [63], respectively.

there are very few publications where the structure of the films synthesized at the air/water interface has been shown by STM or HR-AFM;[63] a study evidencing both the chemical connectivity and the structure of the polymer has yet to be published. Microscopic techniques are mainly used to assess the quality and homogeneity, as well as the height of the film. Structure elucidation of the sheets has proven particularly challenging and so far, has not been achieved in our group.

1.3 Structure Elucidation of Two-Dimensional Polymers

1.3.1 Challenges of Structure Elucidation

In going from one dimension to two dimensions, the analytical techniques used for characterization of polymers change from techniques commonly used for the characterization of organic molecules to techniques used for surface characterization. Nuclear magnetic resonance (NMR) spectroscopy, mass spectrometry (MS), and gel-permeation chromatography (GPC) which are often used to determine the dispersity and the molecular weight of one-dimensional polymers are either not sensitive enough or simply unsuitable for two-dimensional polymers as they would require dissolving or destroying the sheets. New characterization methods have to be identified that are suitable for the characterization of two-dimensional polymers.

For a full characterization of a two-dimensional polymer

1. its thickness,
2. its capability to be free-standing,
3. its crystallinity,
4. the size of its domains,
5. and the nature of its covalent connectivity

have to be assessed.

These assessment criteria do not only have to be explored for a material to be called a two-dimensional polymer but also correspond to the typical parameters that are determined for one-dimensional polymers, in particular criteria 3–5.

Regardless of whether a top-down or bottom-up approach is used to synthesize a two-dimensional polymer, characterization at the single-layer sheet level is necessary and poses considerable analytical challenges. There are several reasons for this. First of all, the quantities of material present in a monomolecular layer are too small to be characterized by most analytical techniques, particularly in regard to (5), the nature of covalent connectivity. Secondly, the structural complexity of most two-dimensional polymers, especially when compared for example to graphene, impedes structure elucidation as the newly formed bonds whose existence has to be shown are obscured by a complicated matrix of chemically similar atoms and bonds. Thirdly, the porosity and thus high flexibility of a single-layer sheet allows the formed network to deform in such a way that the crystalline order is no longer apparent when the geometric order is lost. This phenomenon is illustrated in fig. 1.8. The problem is further exacerbated by the conformational changes the sheet might experience upon transfer from the air/water interface to solid substrates or upon exfoliation from the single-crystal. It can lead to a distortion of the film such that imaging techniques can no longer resolve the structure unless they achieve atomic resolution. Finally, the occurence of domains within the sheet obstructs all investigations that rely on long-range crystallinity (TEM, LEED). They can be formed due to grain boundaries between domains of differing crystallinity or of the same crystallinity but offset by a few degrees with respect to one another.

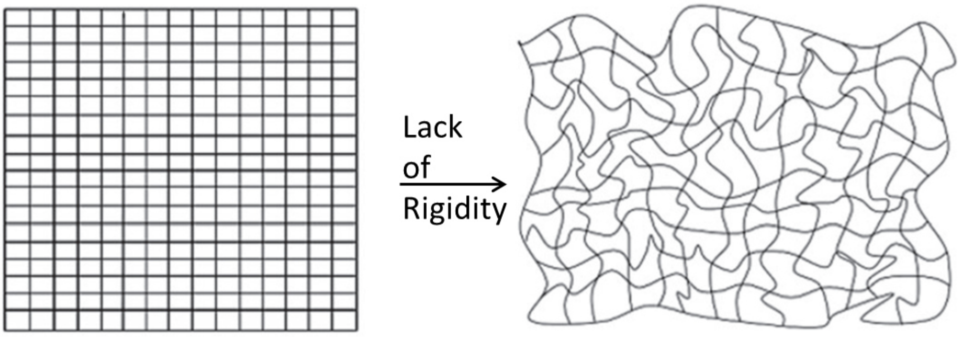

Figure 1.8: Loss of crystallinity as a result of flexibility. Figure adapted from reference [64].

Despite these difficulties, several analytical techniques commonly used for surface characterization were identified as suitable in this challenge. Note that the techniques presented here are not an exhaustive compendium of all analytical techniques that would allow studying the obtained films, but that the focus is rather on the techniques that were actually used within this thesis.

1.3.2 Suitable Analytical Techniques

In this section, analytical techniques suitable for assessing criteria 1–4 will be discussed in this order, while a separate subchapter is dedicated to the elucidation of the chemical connectivity (5).

In order to determine the thickness (1), atomic force microscopy (AFM) could be applicable.

Atomic Force Microscopy In atomic force microscopy, a sharp tip mounted on a cantilever is brought into close contact with a surface and the force between tip and surface is measured. A change of the force is registered by a laser beam trained on the cantilever and reflected onto the detector, such that small changes in the position of the cantilever are accompanied by the reflected light reaching the detector at a different position. This allows correcting the position of the cantilever, thus creating a feedback loop. Keeping either the force or the distance to the sample constant, the topography of the surface can be imaged by raster scanning the surface. Molecular resolution can be achieved.[65] Depending on which force is monitored, different properties of the surface can be probed with a high resolution.[66–68] In the context of this work, imaging the films created at the air/water interface allows determining the topography of the film, as well as the height of the film when the topography is determined at a film fold, edge or crack.

The free-standingness of the film (2) is an important criterion that the films have to fulfill in order to meet the definition of a two-dimensional polymer and it also allows drawing conclusions about the percolation within the sheet. In order to exhibit mechanical coherence, a certain amount of bonds have to be formed between neighboring monomers. The exact percentage depends on the packing of the monomers and is predicted by percolation theory.[69,70] The percentage is termed bond percolation threshold.[71] Thus, the capability of spanning a grid gives a lower threshold for the conversion reached in a two-dimensional polymerization. To determine whether a film is capable of being free-standing (2), transfer onto a holey substrate could be conducted and the capability to span the substrate investigated by scanning electron microscopy (SEM).

Scanning Electron Microscopy With a scanning electron microscope, the sample is imaged by raster-scanning the sample with an electron beam.[72] The electrons of the beam interact with atoms in the sample, producing secondary electrons, backscattered electrons, X-rays and other signals, thus giving information about the topography and composition of the sample.[73] For surface sensitive analysis, low-energy secondary electrons are collected to produce high-resolution images of the sample. These electrons originate from the first few nanometers of the sample. A three dimensional image is obtained since the number of secondary electrons emitted depend on the angle of the primary beam and the sample, with a perpendicular arrangement leading to less secondary electrons than lower angles. The resolution of the SEM depends on the spot size of the electron beam and SEM does not allow imaging of individual atoms like transmission electron microscopy, but recently sub-nanometer resolutions have been reported.[74]

Transmission electron microscopy (TEM) or selected area electron diffraction

(SAED), high-resolution atomic force microscopy (HR-AFM), and scanning tunneling microscopy (STM) are commonly used for surface characterization and could be used to assess the homogeneity, cristallinity (3) and domain sizes of a two-dimensional polymer (4). As atomic force microscopy was already discussed in the section about thickness determination, it will not be discussed here.

TEM or SAED The transmission electron microscope was developed in the 1930s by Ruska and Knoll.[75,76] It images thin specimens or a specimen that is suspended on a grid by probing it with an electron beam that passes the specimen and is then detected, creating an image that is determined by the interaction of the electron beam with the sample. Due to the small de Broglie wavelength of electrons, atomic resolution can be achieved. Selected area electron diffraction allows measuring the diffraction pattern in chosen areas of thin films and is therefore suitable for species where domain formation is expected, such as two-dimensional polymers. Thus, different crystalline domains of the film can be investigated by this technique.[77]

Scanning Tunneling Microscopy Scanning tunneling microscopy (STM) is based on similar principles as AFM with the difference that surfaces are imaged by monitoring the tunneling current between the probing tip and the conducting surface. Monitoring the tunneling current enables probing the molecular orbitals of the species on a conducting substrate. The STM achieves atomic resolution and is therefore suitable for investigating the structure and crystallinity of the two-dimensional polymer.[78]

Thus, there are several microscopic techniques available that allow investigating the crystallinity, provided the transfer of the films from the air/water interface does not obscure it too much.

Finally, the nature of the polymer's connectivity (5) is best assessed by choosing methods tailored to the specific, reactive units of the monomers. By choosing sensitive techniques where both monomer and polymer should give characteristic, distinct signals the probability to determine the chemical connectivity between the monomer units is maximized. In order to choose the appropriate methods for this endeavor, the properties of anthracenes, the reactive subunit that comprises the monomers studied in this thesis, are presented in the following section along with cues how these characteristics can be used in terms of analytical techniques.

1.3.3 The Class of Anthracenes

As in the case of one-dimensional polymers, the polymerization chemistry used for two-dimensional polymerization has to be high-yielding in order to obtain high conversion in the two-dimensional polymer. It is for this reason that high-yielding photoreactions are preferred. Anthracenes are often used in the design of monomers as their photoreaction has been shown to be quantitative in the single crystal.[79] For this reason, the chemistry of anthracenes will be discussed, along with characteristic spectroscopic properties of both anthracenes and their dimers.

Photoreaction of Anthracenes

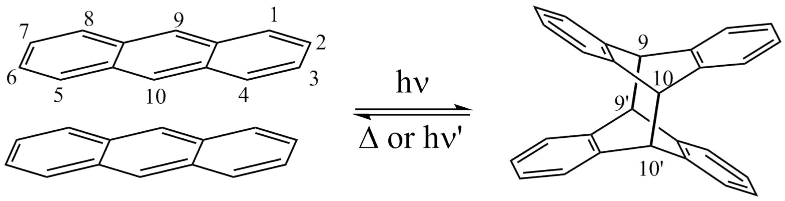

Figure 1.9: [4+4]-cycloaddition of anthracenes to give the anthracene dimer.

The anthracene dimerization and its reversibility was first observed in 1867 by Fritzsche.[80,81] The photoreaction, shown in fig. 1.9, and its scope in terms of substrates has been studied extensively over the years.[82] These studies showed that the photoreaction readily gives the 9,9′,10,10′-dimer in most solvents.[83] The reaction proceeds rapidly, with rates of k_{dim} on the order of 0.5–2.3 x $10^9 M^{-1} s^{-1}$, unless bulky substituents are present on the the 9- and/or 10-position of the anthracenes, which slow down the dimerization reaction to the point where it does not proceed at all due to steric hindrance (e.g. 9,10-diethylanthracene).[84]

The product of the photoreaction of anthracenes is also concentration-dependent: While oxidation to endoperoxides cannot compete with photodimerizations at substrate concentrations of 10^{-3} M or higher, it can be observed at concentrations lower than 10^{-3} M. Ruling out the occurence of oxidation as a side reaction during polymerization is of great importance for monomer systems based on anthracenes.

Packing Motifs of Anthracenes

The potential packing motifs of anthracenes are shown in fig. 1.10. In arenes, the edge-to-face and end-to-face interactions are more commonly observed than the face-to-face π-π interactions.[85]

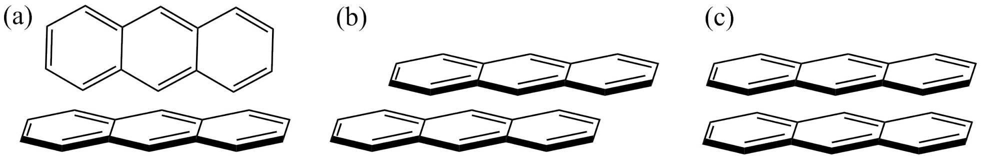

Figure 1.10: Packing motifs of anthracenes: edge-to-face (a), slipped parallel (b), and face-to-face (or parallel) stacking (c).

The preferred packing can be tuned by substitution of the anthracenes. Any substitution that leads to a polarization of the anthracene, for example substitution with halogens, can influence the packing motif. To illustrate this on the example of smaller arenes, a computational study of the packing of benzene-fluorobenzene dimers found that the face-to-face and parallel-displaced packing is strongly favored compared to edge-to-face packings, by as much as 4.5 kcal/mol.[86] This tendency was also observed experimentally.[87–91] The influence of substitution was also studied on a broader range of arenes, including anthracenes.[92–94]

A further way to influence the packing is by preventing certain types of packing through the introduction of bulky substituents or by incorporating the anthracenes within a molecule such that certain types of packings can no longer be achieved.

These results showed that the preference for edge-to-face stacking in arenes can be overcome by careful design considerations. These considerations were implemented into the design of monomer candidates for two-dimensional polymerizations.

Fluorescence and Absorption Spectroscopy of Anthracenes

The [4+4]-cycloaddition of anthracenes in the solid state proceeds via excimer formation. An excimer is defined as "a dimer which is associated in an excited electronic state and dissociated in its ground electronic state".[95,96] While it is unclear whether excimer fluorescence and photodimerization are competing processes in solution or whether the excimer formation is a required intermediate during the photoreaction,[97] it is evident that excimer formation can only occur when an anthracene pair exhibits a certain proximity.[98] Excimer formation in aromatic molecules can be observed by excimer emission in the fluorescence spectrum and is characterized by broad, unstructured fluorescence between 400–600 nm. In solution, the formation of excimers is concentration-dependent. This is because occurence of excimer fluorescence can be correlated with proximity of the aromatic units[96] and an at least partial overlap of the π-π planes.[99–102] Kato *et al.* have brought forth the theory that the extent of π-π overlap in the planes of aromatic molecules influences the emission maximum and FWHM of the excimer fluorescence, see fig. 1.11.[103–106] As this theory was developed considering phases of liquid crystals, the observation should be considered as a relative and not an absolute estimate for anthracene overlap, its validity only applicable within one particular anthracene system. It nevertheless gives a first indicator of how fluorescence could aid in determining the orientation of anthracene-bearing monomers at the air/water interface. Recent work has further investigated the correlation between anthracene packing and exhibited fluorescence.[94,107]

While fluorescence spectroscopy conducted with a fluorimeter is a bulk technique, confocal laser scanning microscopy allows imaging samples with a so-called lambda scan, recording the fluorescence spectrum in each pixel of the image and therefore allowing for a laterally resolved fluorescence image.[108,109] Recent advances in fluorescence microscopy could in principle permit recording the fluorescence on the nanometer scale.[110] Studying the fluorescence in different parts of a monomer film obtained from the air/water interface could allow drawing conclusions on the orientation of the molecules within the film and on the domain size, if the domains differ in their packing. This only holds true if the monomer film is not disrupted during transfer from the air/water interface.

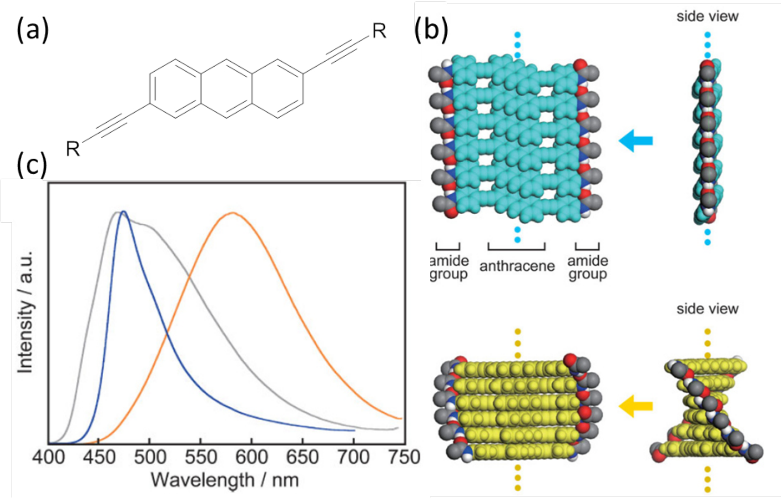

Figure 1.11: When the anthracene-based compound shown in (a) adopts different packings (b), their fluorescence spectra are affected accordingly (c). The broadest emission (orange spectrum) is observed for the cubic phase, which corresponds to the lower packing in (b) where the anthracenes are parallel. For the columnar packing shown above, where the anthracenes are slipped parallel, a narrower, blue-shifted emission is observed (blue spectrum). In the former case, the π-π overlap is maximized. The grey spectrum shows the emission from the isotropic phase. Taken from [106].

Anthracenes are fluorescent, while their photoproducts (dimers or endoperoxides) are not. The disappearance of fluorescence can be used to monitor the consumption of anthracene-bearing monomers, although as noted before, it does not give an indication of the product formed. Furthermore, measuring the excimer fluorescence of a two-dimensional polymer film can indicate a proximity of reactive units, while monitoring its intensity depending on wavelength (an excitation spectrum) gives a measure for the purity of the film. Fluorescence spectroscopy is a highly sensitive technique and is therefore suitable for studying two-dimensional polymers.

UV-vis absorption spectroscopy, while ca. 1000 times less sensitive than fluorescence spectroscopy, can still be sensitive enough to detect the absorption of a monolayer, particularly in the case of anthracene-based monomers. Anthracenes not only absorb strongly, but exhibit a characteristic signature in the absorption spectrum, consisting of a strong absorption band at 250 nm, corresponding to the $^1A_{1g} \rightarrow {}^1B_{3u}$ transition (to the long axis of the molecule), and an absorption corresponding to the $^1A_{1g} \rightarrow {}^1B_{2u}$ (short axis

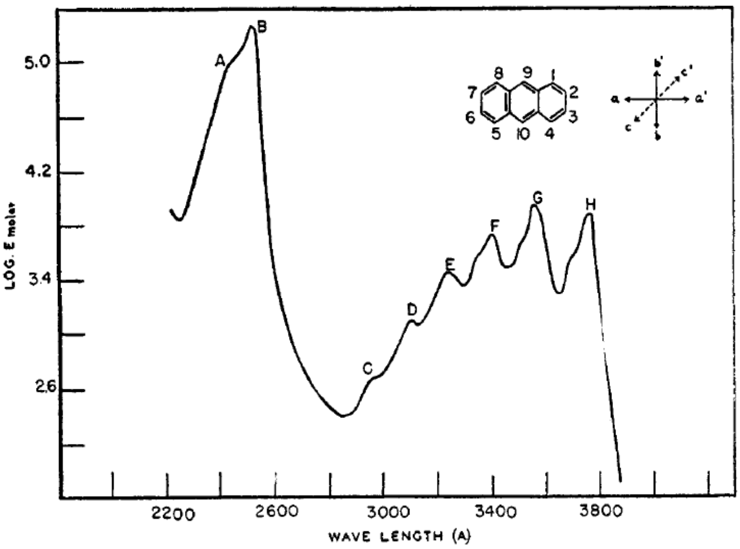

Figure 1.12: UV-vis absorption spectrum of anthracene in ethanol, taken from ref. [111]

of the molecule) which is split up into several smaller, equally spaced bands between 300–400 nm, the vibrational fine structure of the aromatic system, see fig. 1.12.[112–115] Substitution on the anthracenes alters the spectrum. Enlarging the π system leads to a bathochromic shift of the spectrum. A substitution that breaks the symmetry of the system leads to a gradual loss of the fine structure bands, thus making them less discernible.[111,116] They do not disappear but rather begin merging up to the point where the fine structure resembles more of a broad, unstructured peak. It is noteworthy that the shift on the main peak and the shift on the hyperfine structure does not necessarily occur to the same extent.[111] Interestingly, slight shifts of the vibrational fine structure have been correlated with changes in the relative orientation of anthracene pairs along the long and short axis[117,118] and even been used to calculate the orientation between anthracene pairs.[119] While in principle one can deduce from this something about the relative orientation of anthracene neighbors in a monomer film, a study of how exactly the absorption spectrum is influenced by the orientation of the anthracenes would be necessary before drawing any conclusions. Anthracene itself has been investigated in this regard[119] but since substitution of the anthracene also influences the appearance of the spectrum, a thorough crystallization and spectroscopic study of the monomer system would become necessary, something that is not feasible within the scope of this thesis. The method should nevertheless be mentioned within this discussion of potentially useful methods for the characterization of two-dimensional polymers.

Anthracene dimers are no longer conjugated and thus their absorption spectrum is considerably blue-shifted. In addition, the vibrational fine structure observed in extended aromatic systems is lost. This pronounced difference in the spectra allows for a quick differentiation between anthracenes and reacted anthracenes. Contrary to fluorescence spectroscopy, one can observe not only the disappearance of the bands characteristic to anthracenes, but also the formation of a new band at shorter wavelengths.

Raman Spectroscopy of Anthracenes and TERS

Anthracene itself has 33 Raman-active vibrations.[120] Since substitution of anthracenes has a strong impact on the number and type of vibrations, they will not be discussed here, but rather the reader is referred to the discussion in the literature.[121,122] Contrary to infrared (IR) spectroscopy, Raman spectroscopy is not affected by the presence of water, as water is a weak Raman scatterer. This is of great importance in the case of Langmuir-Blodgett films which by their nature still have layers of water attached to them. Furthermore, in Raman microscopy higher lateral resolutions can be achieved than in IR microscopy, as shorter wavelengths are used for excitation.

While confocal Raman is not nearly sensitive enough to detect Raman signals of a monolayer, tip-enhanced Raman spectroscopy, which is 10^6–10^9 times more sensitive, could be suitable to detect the Raman spectrum of a monolayer.[123] TERS combines Raman spectroscopy with scanning probe microscopy (SPM), either in an AFM or STM. The SPM enables obtaining a lateral resolution well below the diffraction limit, as the resolution will depend on the sharpness of the tip and not on the wavelength of the exciting laser. For TERS, the tip of the microscope is brought into close contact with the metallic surface and illuminated with a focused laser, thereby creating surface plasmons between the tip and the surface. As a result, an enhanced electromagnetic field is created between tip and surface that intensifies Raman scattering in the vicinity of the tip, thereby enhancing the collected Raman signal that is characteristic of the probed compounds.

X-ray Photoelectron Spectroscopy

X-ray photoelectron spectroscopy (XPS) relies on the photoelectric effect.[124] When a photon impinges on a surface, it can cause an electron bound to an atom or ion to be ejected from it. The kinetic energy of this electron will correspond to the initial energy of the photon minus the binding energy that needs to be overcome in order to eject the electron. While both initial energy and measured kinetic energy can be determined, one can calculate the binding energy of the electron. This binding energy is characteristic of the element and of the chemical environment that is was released from. The selectivity for thin layers is accomplished due to the fact that liberated electrons have a limited free path length, thus if they are excited within the bulk they are lost to detection. This restricts characterization to the topmost layers (up to 10 nm) of the material. XPS therefore reveals information on both the speciation and elements of thin films.[125] In the case of anthracenes and their photodimers, there is only a slight increase of sp^3-hybridized carbon compared to sp^2-hybridized carbon which will make it challenging to differentiate the two cases.

Thus, most techniques suitable for the structure elucidation and characterization of two-dimensional polymers are most often also used to characterize thin films. The list of techniques presented here is by no means exhaustive but serves as an introduction to the plethora of analytical techniques used within this work.

Chapter 2

Aims and Motivation

The air/water interface approach used for synthesizing two-dimensional polymers holds great promise because it provides access to macroscopic monolayer sheets and obviates the need for exfoliation; however, to this day, there is hardly any system that can confidently be termed as a two-dimensional polymer that was synthesized at the air/water interface. This can mainly be attributed to the challenging nature of the structure elucidation at the single-layer level, particularly to the small analytical quantities studied. These problems are also of relevance in the top-down approaches. In order to make the claim of having synthesized a two-dimensional polymer, the single-layer sheets obtained after exfoliation from the bulk have to be thoroughly characterized. In both cases, the same analytical techniques are of interest.

The presented thesis focuses on the study of single-layer films obtained from trifunctional, amphiphilic, anthracene-bearing monomers assembled and irradiated at the air/water interface and then transferred onto solid substrates.

The main goals of this thesis are to study monomers at the air/water interface that may react to give two-dimensional polymers and to characterize their films in terms of thickness, structure and chemical connectivity. This is done in order to determine whether they can indeed be classified as two-dimensional polymers and to identify which analytical techniques are of use for the future characterization of new monomer candidates.

Two monomers **1** and **2** will be investigated in this regard and their behaviors at the air/water interface compared.

Furthermore, the possibility of performing the polymerization post-transfer will be explored with monomer **2** and a third monomer, monomer **3**. This is of particular interest in order to achieve large-area two-dimensional polymers.

The structures of the three fluorescent monomers are shown in fig. 2.1. Polymerizing directly on the solid substrate opens up the world of writing onto fluorescent monolayers of the monomers by a quenching of the fluorescence; the films of monomers **2** and **3** will be investigated in this regard, in an effort to explore a first potential application of these materials and to determine the mechanism behind the writing.

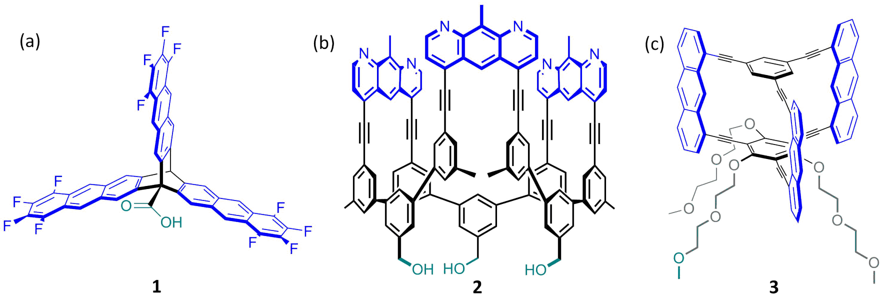

1 2 3

Figure 2.1: Monomers studied within this thesis. Their reactive units are marked in blue, their amphiphilic part in cyan. Monomer **1** (a) will be discussed in chapter **3**, monomer **2** (b) in chapter **4** and **5** and monomer **3** (c) in chapter **5**.

In the following, a brief outline of the thesis is presented. In the first part of this thesis, monomer and polymer films obtained from monomer **1** will be studied by various techniques, aiming at assessing the monomer's behaviour at the air/water interface, film homogeneity, thickness, mechanical coherence, and at elucidating the bond formed between repeat units, as well as its structure. For this purpose, various analytical techniques for the study of these extremely thin films mentioned beforehand are used.

In the second part of this thesis, monomer **2** is studied in a similar fashion, though in less detail. Due to their differences in complexity and rigidity, monomers **1** and **2** exhibit distinct behaviors at the air/water interface which will be discussed.

A potential application as molecular paper will be explored thereafter for the monomer films of monomers **2** and **3**. First steps are undertaken to use the films in an application: the monomer films' suitability for optical applications in miniaturized devices is investigated.

Part II

Results and Discussion

Chapter 3

Structure Elucidation of Films Based on Tetrafluoroanthracene-Based Monomer 1

3.1 Monomer Features

As was discussed in detail in the introduction, structure elucidation of monolayer sheets remains extremely challenging due to the small sample size of the sheets (ng-μg, depending on sampled area), their structural complexity and their large mesh size. The large mesh size results in flexibility of the sheets which can obscure crystalline ordering and facilitate lateral contraction of the sheet.

Several of these considerations influenced the design of monomer **1**. It was closely related to a monomer that reacted to give a two-dimensional polymer sheet whose structure had been successfully characterized by STM.[63] Monomer **1**, is a rigid, amphiphilic, propeller-shaped molecule (see fig. 3.1a). Its rigidity could be beneficial to avoid issues arising from an increased flexibility of the polymer films. The polar carboxylic acid orientates the molecule at the air/water interface such that it is immersed in water, while the rest of the molecule remains in the air. Its three reactive units consist of 1,2,3,4-tetrafluoroanthracenes. These tetrafluoroanthracenes enhance the propensity of the molecules to undergo *face-to-face* stacking due to favorable dipole-dipole interactions and a favorable molecular electronic quadrupole moment between the fluorinated (electron-rich) and non-fluorinated (electron-poor) part of the anthracene (head-to-tail packing).[126–128] This design was chosen in order to favor the desired packing of the monomers at the air/water interface.

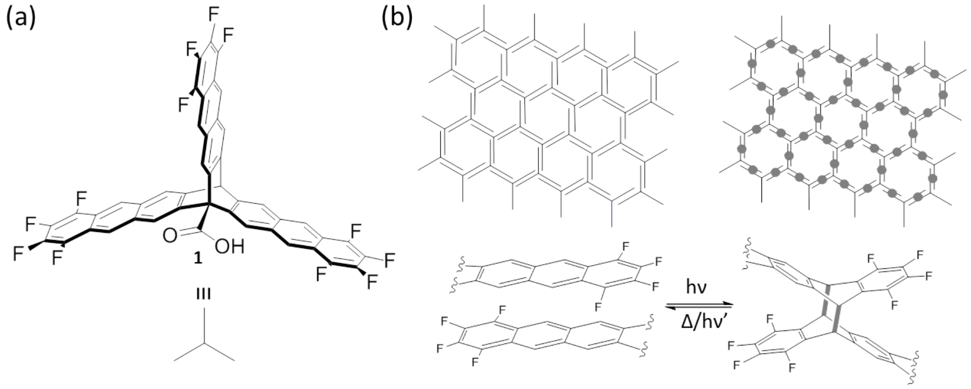

Figure 3.1: (a) Structure of monomer **1**. (b) A top view of a potential packing the monomers could adapt at the air/water interface which would result in the tetrafluoroanthracenes being paired. Via a [4+4]-cycloaddition, neighboring tetrafluoroanthracene units of monomers undergo dimerizations to give the polymer. The [4+4]-cycloaddition reaction can be reversed by heating or irradiation at a shorter wavelength.

The monomer was thus reduced to its most fundamental components: the three reactive units and a polar group that made it amphiphilic and helped orientate it at the air/water interface. This basic design was chosen in order to reduce the structural complexity as much as possible, in view of a characterization of chemical bonds which would profit from such simplicity.

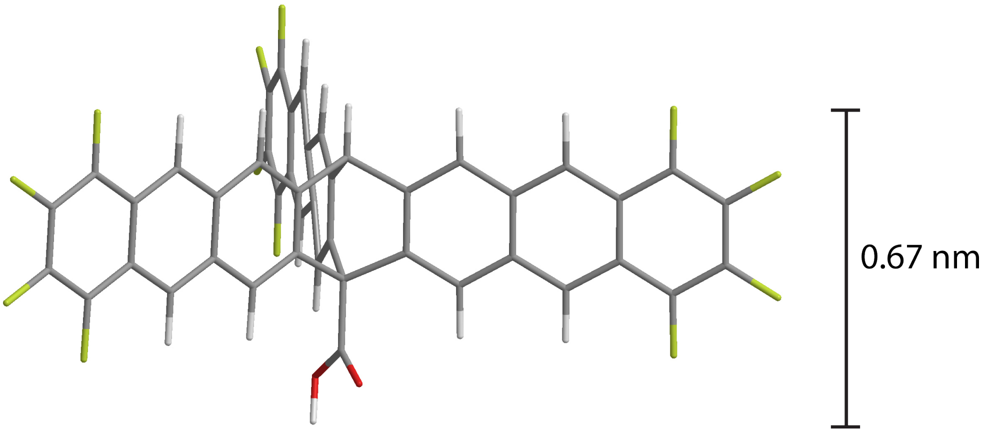

Figure 3.2: MM2 geometry optimized molecular model of monomer **1**.

The monomer has a height of 0.67 nm as determined by a MM2 geometry optimization and the tetrafluoroanthracene has a length of 8 Å.

The packing it may adopt at the air/water interface is shown in fig. 3.1b. Under irradiation, the tetrafluoroanthracenes can undergo [4+4]-cycloaddition to form the corresponding tetrafluoroanthracene-dimers. This reaction can be reversed by irradiation at a shorter wavelength or by heating. Further alternative packings are discussed in the next section (see fig. 3.3), as is the behavior of the monomer at the air/water interface.

3.2 Film Formation and Behavior at the Air/Water Interface

After spreading a solution of the monomer at the air/water interface of a Langmuir trough, the film formation during compression of the LB trough barriers was monitored by Brewster angle microscopy. The images revealed that from the moment of monomer deposition, laterally extended domains were present (see fig. 3.4a). During compression, these islands exhibited a very rigid behaviour. Pushing the domains against each other often resulted in tearing rather than coalescence of the domains. Therefore, the exact manner of deposition strongly influenced the quality of the monomer film. For this reason, a dilute solution of 0.2 mg/mL was used for the experiments.

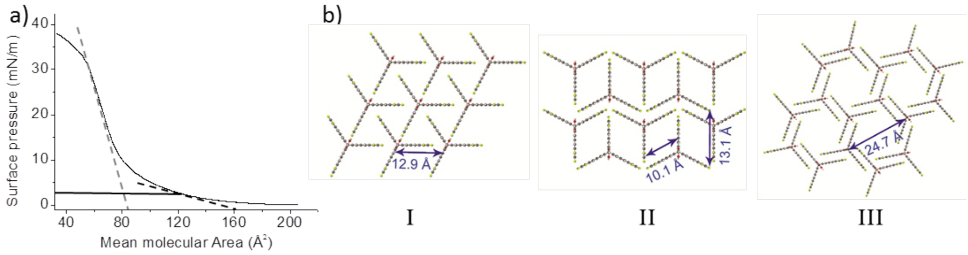

Figure 3.3: (a) Isotherm measured upon compression of monomers. (b) Three packings the monomers may assume at the air/water interface.

The target surface pressure for transfer experiments was determined by consulting the isotherm measurements and BAM images. At a surface pressure of 2 mN/m, a laterally extended film was observed (see fig. 3.4b). The mean molecular area (MMA) at this pressure was determined to be 160 Å (see fig. 3.3a), which corresponds to the value calculated for the proposed packing III, shown in fig. 3.3b. Packing I and II would result in mean molecular areas of 144 and 112 Å, respectively. Compressing to higher surface pressures led to a reduction of the MMA to 85 Å which is too low for either of the alternative packings I and II. This phenomenon has been observed previously for a structurally related monomer.[63] In theory, a mean molecular area of 85 Å could correspond to double layer formation. Indication for this was found with AFM scratching experiments and XPS measurements. As packing III was the only one amenable to two-dimensional polymer formation, a surface pressure of 2 mN/m was used for all experiments henceforth. After compression to this surface pressure, the monomer film did not change appearance over time, but remained stationary, an observation that is in line with the rigidity observed beforehand with the Brewster angle microscope (see fig. 3.4). On the contrary, the surface pressure dropped sharply upon start of irradiation and then gradually recovered. This is in line with the fact that in the postulated packing, the area per monomer unit in the polymer was smaller than it was in the monomer packing. The film therefore contracted upon irradiation which led to a drop in surface pressure. With a rigid monomer that has a high propensity to adopt a certain favored packing, a fast polymerization would occur if the tetrafluoroanthracenes of the monomers were closely packed. As mentioned above, tetrafluoroanthracenes have a high propensity to stack *face-to-face*, the fluorinated ring of one anthracene interacting strongly with the non-fluorinated ring of another. This would result in a close packing of tetrafluoroanthracenes and, by extension, a fast polymerization, and would account for the rapid drop in surface pressure observed. In line with this hypothesis is the observation that using an irradiation source of lower intensity leads to a less drastic decrease of the surface pressure at the start of irradiation. Using the weakest irradiation source did not lead to decrease in the surface pressure at all which may indicate that the reaction rate of the polymerization and the speed of the barrier compression are similar enough to compensate the contraction of the film.

3.2.1 Evidence of π-π Stacking

Such a *face-to-face* stacking should result in the formation of excimers in the fluorescence spectrum of the film. To assess the fluorescence, the monomer film was transferred onto quartz and the fluorescence spectrum of the film

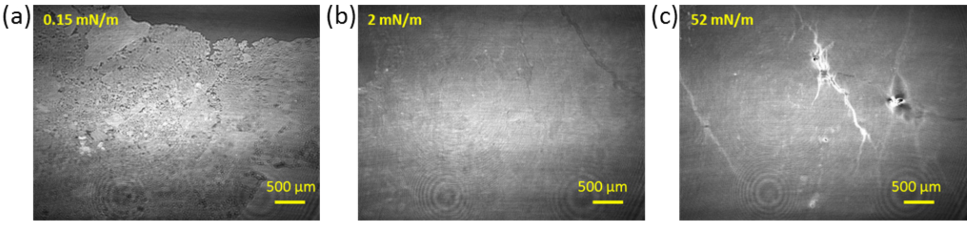

Figure 3.4: BAM images of the film after deposition of the monomer solution (a), compression to the target surface pressure (b) and at very high surface pressure (c).

was measured. The spectrum was then compared to the fluorescence spectrum of the monomer in acetonitrile. In case of the film, one could observe a broad, unstructured fluorescence which is characteristic of excimers. Meanwhile, the monomeric fluorescence that the monomer showed in solution was not observed, see fig. 3.5a.

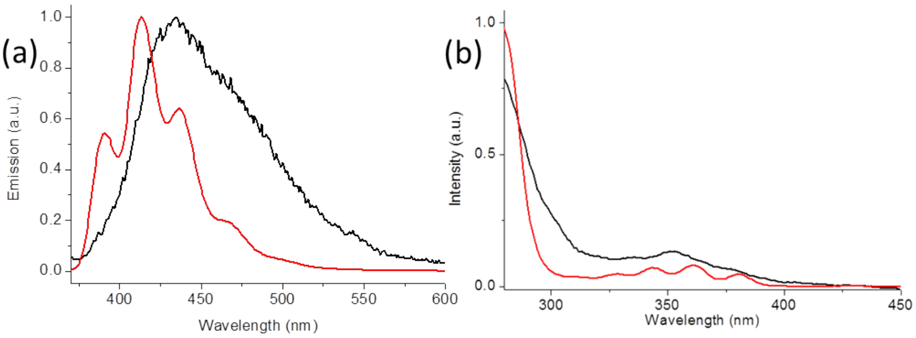

Figure 3.5: (a) Fluorescence of the monomer in acetonitrile (2 μM, red) and of the monomer film on quartz (black). The film reveals no monomeric emission. (b) Comparison of the excitation spectrum of the monomer film on quartz recorded between 270–480 nm with a detection wavelength of 500 nm (black) and absorption spectrum of the monomer in solution (red).

To confirm that the observed fluorescence stemmed exclusively from the monomer, the excitation spectrum of the monomer film on quartz was measured. For this, the emission intensity at λ = 500 nm was monitored while sweeping the excitation range between 270–480 nm. If the fluorescence at that wavelength was solely due to emission from the monomer, the excitation spectrum should exhibit the same characteristics as the absorption spectrum of the monomer. If, however, some fluorescent impurity was responsible for the emission, the excitation spectrum should differ and also show peaks of the impurity.[129] The excitation spectrum of the monomer film on quartz indeed matched the absorption spectrum of the monomer measured in solution, as the main peak and the characteristic vibrational fine structure of anthracenes in the range of 300–380 nm were conserved (see fig. 3.5b). Slight blue shifts of ca. 10 nm were observed between the monomer absorption spectrum in solution and the excitation spectrum of the monomer film on quartz. These shifts could be due to the change of environment from solution to solid state as this influences the vibrational freedom of the molecules.[111] Furthermore, the spectra differ in terms of increased scattering in the case of the absorption spectrum which further decreases the signal-to-noise ratio. Overall, the two spectra do resemble one another and no new distinct peak could be observed. This finding confirmed that only the monomer was responsible for the excimer fluorescence.

Additionally, a TERS study provided some indirect evidence for π-π stacking in the case of the LB monomer film. The molecular orientation of the monomers within an LB film was investigated and compared to the orientation of the monomers within a spin-coated sub-monolayer. In order to study the molecular orientation, TERS mapping was carried out on the film on Au(111) on an area of 100 x 100 nm^2 with a resolution of 5 nm/pixel. In the case of the densely packed LB film of packing III (see fig. 3.3b), this resolution would correspond to approximately 10 monomers per pixel. Within this map, the peak ratio of the bands at 1604 and 1445 cm^{-1} was plotted. Both bands are orientation-dependent and thus their ratio may provide insight on the orientation of the molecules within the pixel. A comparison of the peak ratio map of the monomer LB film to the spin-coated sub-monolayer, which can be seen in fig. 3.6, showed that the orientation within the LB film was much more homogeneous than in the case of the spin-coated layer.

These findings indicated that the synthesis at the air/water interface led to an orientation of the molecules prior to the transfer onto solid substrate. Furthermore, during TERS acquisition, the orientation of the molecules was less influenced by the imaging conditions, which can be ascribed to the π-π stacking that locks the orientation of the molecules. In the case of the spin-coated sub-monolayer, on the other hand, the orientation of the molecules was random, as the deposited molecules had no incentive to orientate themselves in a particular manner on the Au(111) crystal (fig. 3.6b and fig. 3.6d).

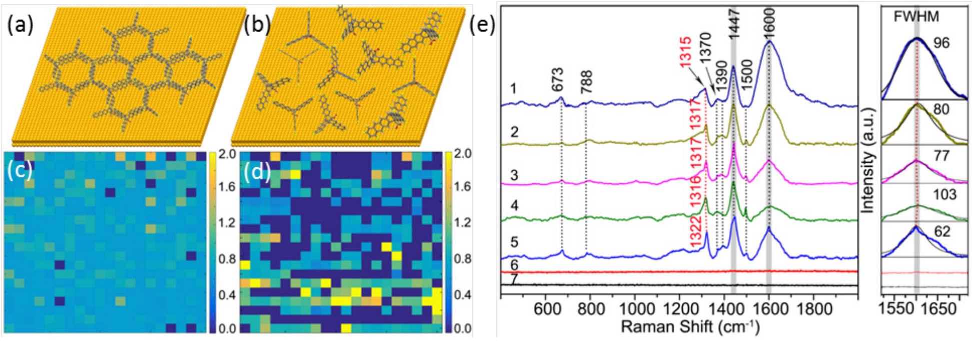

Figure 3.6: Schematic representation of LB monomer film (a) and spin-coated sub-monolayer (b). TERS mapping of the 1600/1445 cm^{-1} peak ratio of LB monomer film (c) and spin-coated submonolayer (d). (e) Left: spectra of different regions in the spin-coated sub-monolayer (1–4) compared to a spectrum of the monomer LB film (5). The spectrum of bare Au(111) is shown in (6) while the spectrum collected with a retracted tip is shown in (7). Right: Lorentzian line fitting of the peak at 1600 cm^{-1} which reveals narrower FWHM for the LB film.

The fluctuation of the molecular orientation could also be a result of thermal diffusion, molecular restructuring on the surface, different adsorption geometries, and molecular restructuring on the surface, which play a role in ambient TERS,[130–132] but which would be experienced in both LB and spin-coated film and can therefore be ruled out as a cause for the fluctuation of the molecular orientation. The homogeneous orientation within the LB film seems to be a consequence of, and thus indirect evidence for, π-π stacking between tetrafluoroanthracenes of neighboring monomers.

The fact that the molecules in the LB film are more strongly locked in position due to intermolecular interactions and are less prone to fluctuation was furthermore reflected in the linewidths of the peaks in the spectra. The linewidth (FWHM) of the peak at 1600 cm^{-1} in the spectrum of the monomer LB film was significantly smaller than the linewidths of the same peak encountered in the spectra of the random sub-monolayer spectrum. In the case of the spin-coated submonolayer the linewidths varied from 77–103 cm^{-1} while it was only 62 cm^{-1} in the case of the LB monomer film. The larger linewidth in the sub-monolayer was attributed to enhanced mobility of the monomers. A similar effect has been observed in the literature when comparing TER spectra collected at room temperature to TER spectra recorded at low temperatures.[130]

The narrower linewidths of the peaks in the TER spectra of the monomer LB film and mapping of the peak intensity ratio showed that the monomer LB film exhibits a much more homogeneous orientation than that of the spin-coated sub-monolayer, which can be attributed to intermolecular π-π stacking. These findings corroborate that *face-to-face* stacking between tetrafluoroanthracene moieties takes place, which had already been indicated by the presence of excimer fluorescence in the fluorescence spectrum of the monomer LB film.

Coming back to the different packings presented in fig. 3.3b, both packing II (MMA: 112 Å) and III (MMA: 160 Å) would account for the presence of excimer fluorescence and the evidence of π-π stacking in the Raman spectra. Although neither could be excluded on the basis of these two findings, the mean molecular area of 160 Å at a surface pressure of 2 mN/m was more in line with packing III. While packing II could also enable monomers to react to form linear polymers, the film would contain residual unreacted anthracenes. In the following sections, whenever experimental evidence emerges that would allow excluding one of the two packings on the basis of the presence or absence of unreacted tetrafluoroanthracenes, it will be pointed out and discussed.

3.3 Film Thickness

Brewster Angle Microscopy (see fig. 3.19) showed that the film has uniform thickness at the air/water interface. To determine the thickness, the films were characterized by AFM.

3.3.1 Thickness Determination by AFM

To determine the film height and thereby whether the films form a monolayer at the air/water interface, several experiments were carried out. The question of whether or not the film is a monolayer was crucial. For one, it is one of the five conditions that have to be fulfilled for the polymer to qualify as two-dimensional polymer. For another, the presence of excimer emission in the case of the monomer film and the conclusions drawn with regard to the packing relied on the monomers being confined to two dimensions. Finally, a TERS study of the polymer gave an estimation of conversion (see section 3.6.2) which can be correlated to the structure *via* percolation theory, based on the assumption that the monomer units reside in just one layer. The film height was therefore assessed by two methods, namely AFM height analysis at edges and folds of the film, and AFM scratching experiments in the film.

a)

0.793
0.83
0.955
0.745
0.782
0.805
0.895
1.106
0.964
0.692
0.762
0.777
0.815
0.868
1.006
1.066
1.066
0.892
0.937
0.872
0.875
0.945
0.944
0.961
1.053
1.059
0.837
0.989
0.91
Ø 0.903
± 0.109

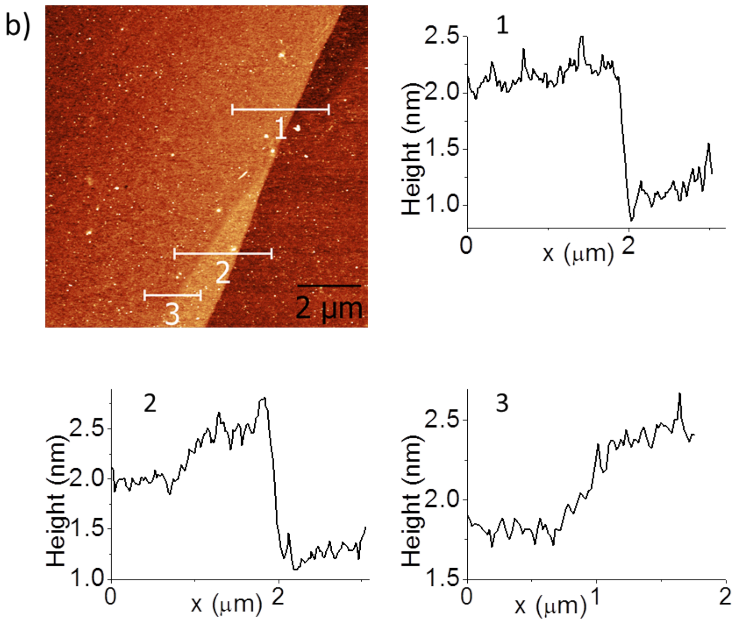

Figure 3.7: (a) Film heights recorded at edges of irradiated film on SiO_2/Si wafers. The values were collected on several samples and edges. (b) Example of an image of an irradiated LB film edge and fold on SiO_2/Si, with the height curves recorded at different locations of the edge.

AFM height analysis was carried out after transferring both the monomer film and the irradiated film onto SiO_2/Si wafers that were partially covered with a strip of mica during transfer. Removal of the mica strip after transfer of the LB film created a film edge where the film height could be measured. While the mica created a clear edge where the film height could be determined, it also left some residual mica specks on the wafer (bright spots in the image of fig. 3.7b) and in some cases removal of the mica resulted in the film being dragged across the SiO_2/Si wafer. For these reasons, film heights were also measured at cracks and holes of the film that occured occasionally (see fig. 3.8b). In the case of the monomer LB film, the film height was

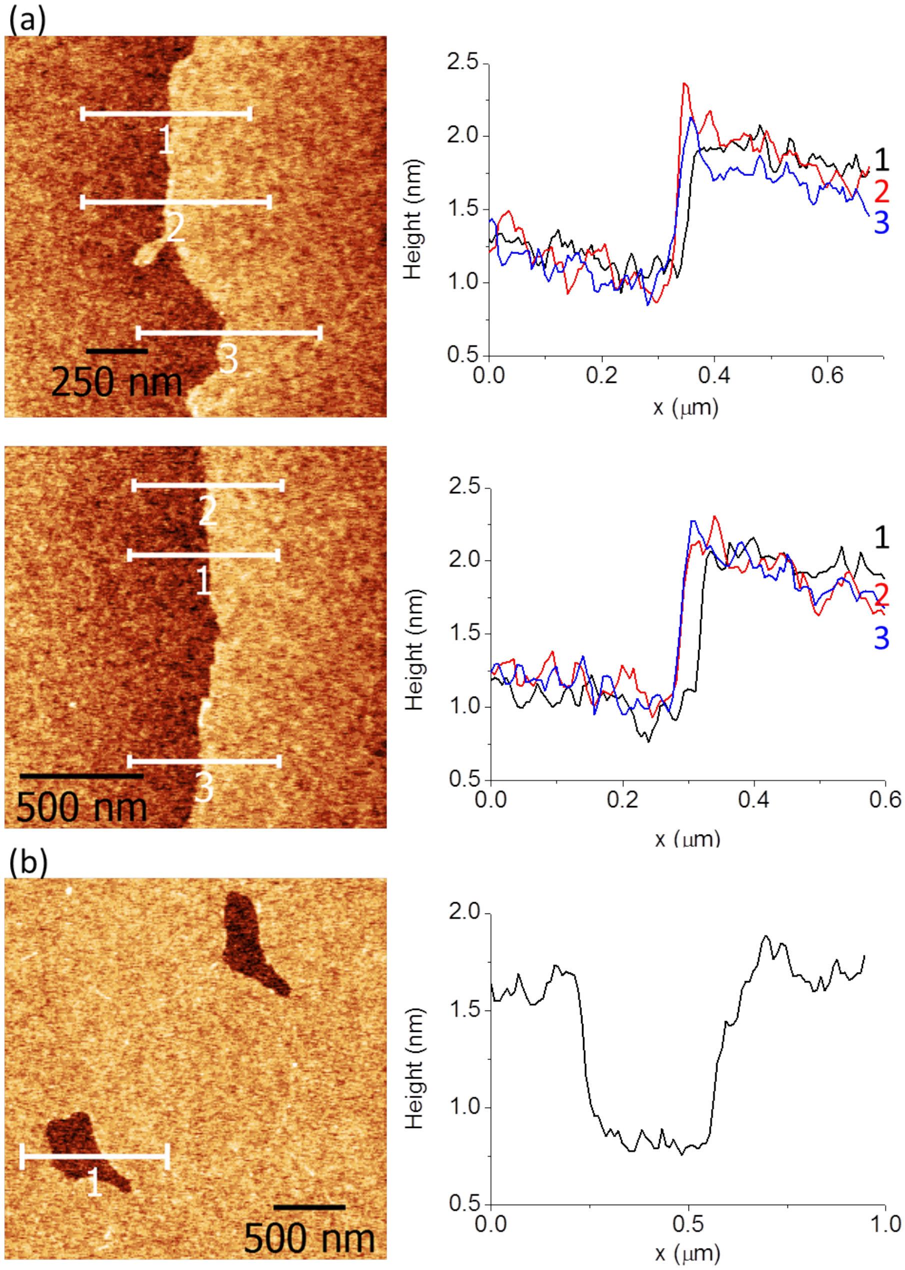

Figure 3.8: (a) Images of monomer LB film edges on SiO_2/Si and the corresponding height measurement curves. (b) Film heights were also measured in cracks of the monomer LB film.

determined to be h_{AFM} = 0.9 nm (± 0.1 nm). The monomer film exhibited more holes and cracks than the irradiated film, which may be due to the lack of covalent bonds that weakens the coherence of the film during transfer. For the irradiated film, the same height was obtained (see fig. 3.7a). These values were slightly larger than what would be expected for the films (h_{AFM} = 0.9 nm compared to h_{calc} = 0.7 nm). However, the values that were measured at a fold of the irradiated film were lower than at an edge. At the fold, shown in fig. 3.7b, a thickness of h_{AFM} = 0.7 nm was measured, which is closer to what the molecular model predicted (see fig. 3.2). Slightly higher values have been obtained before for LB films measured with the AFM at film edges.[18,62] One reason could be the presence of residual water trapped underneath the film. This scenario is realistic, considering the carboxylic acid moieties of the monomers most likely form a hydrogen bonding network when immersed in water at the air/water interface. Regardless of whether water layers were the reason behind the additional 0.2 nm thickness recorded at film edges, all recorded values were in agreement with the thickness of a monolayer and well below the value that a double layer would result in.

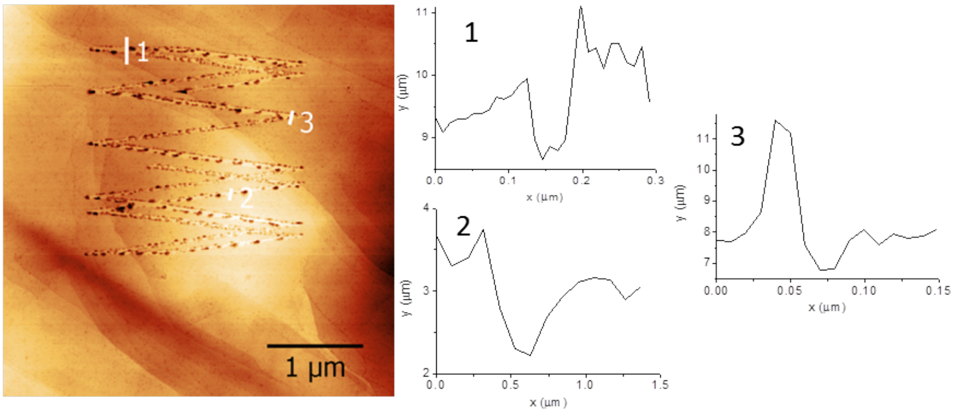

	curve 1			curve 2			curve 3			ø	±
height (nm)	0.6	0.5	1.2	1.0	0.7	1.0	0.9	1.0	0.9	0.9	0.2

Figure 3.9: (a) AFM image of an irradiated LB film on HOPG scratched with an AFM tip, the height curves at different places of the scratching and the values extracted from these curves.

Similar thickness values were also obtained in film scratching experiments. For these experiments, AFM tips at a high setpoint voltage were driven across the film in order to scratch it. The voltage was high enough to break the film but did not leave any trace on HOPG, the underlying substrate, which was tested in a separate experiment on a bare HOPG substrate. It was therefore possible to assess the film's thickness. This method also indicated a thickness of 0.9 nm for the film, albeit with a slightly higher standard deviation of 0.2 nm. The higher standard deviation may be due to the fact that the scratching pushes aside the film, creating high piles on each side of the scratch (see fig. 3.9a). These additional residues obstruct a precise measurement of the film height which explains the higher standard deviation. Nevertheless, all values for the film heights obtained by AFM-based methods were in good agreement with one another and with the molecular model and showed that the synthesized LB films consist indeed of a monolayer.

3.4 Mechanical Coherence of the Irradiated Film

To assess the mechanical coherence of the monomer and polymerized films, they were transferred onto TEM grids of various mesh sizes. In fig. 3.10a, a grid of the smallest mesh size, 20 x 20 μm^2, is shown that the monomer film was transferred onto. Aside from some residual material in one corner of a hole, marked with a red circle, the grid was completely unspanned. In the case of the monomer film, the film was not capable of spanning any holes of the grid, regardless of the mesh size. The monomer film simply fell through the grid, leaving the grid uncovered.

In fig. 3.10b, two images of grids with varying mesh size are shown. Both grids were covered with irradiated film and showed spanning of the film over large areas. Contrary to the monomer film, the irradiated film showed significantly enhanced mechanical coherence, routinely spanning holes the size of 50 x 50 μm^2 and in some cases even holes up to the size of 155 x 155 μm^2. These findings showed that upon irradiation, a chemical transformation took place that considerably enhanced the mechanical coherence of the film. The chemical transformation brought about by irradiation of the monomers at the air/water interface must have produced covalent bonds to result in such a dramatic change in mechanical coherence. Mere intermolecular interactions such as π-π stacking are not sufficient to account for the film spanning, as evidenced by the lack of grid spanning in the case of the monomer film.

In fig. 3.10b, an SEM image shows that a hole of the size 155 x 155 μm^2 was spanned by the irradiated film which, assuming an MMA of 160 Å and

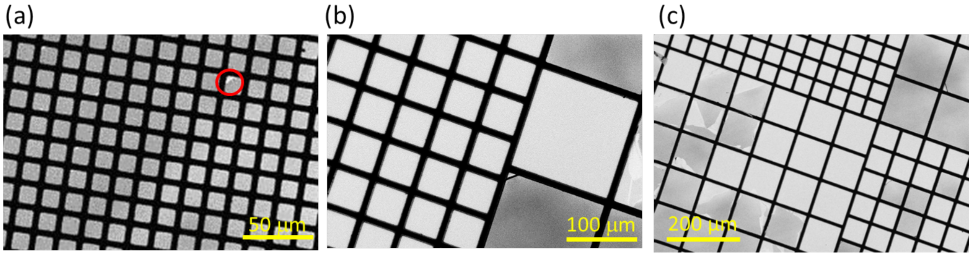

Figure 3.10: (a) 20 x 20 μm^2 holes of the grid are not spanned by the monomer film.(b) Left: the 50 x 50 μm^2 holes of the grid are completely spanned by the irradiated film and even a 155 x 155 μm^2 hole is completely spanned, reflecting considerable mechanical coherence of the film. Right: The 100 x 100 μm^2 holes are spanned over a large area.

a bond percolation threshold of 65%, corresponds to at least 10^{10} reactive units that must have reacted in order to exhibit the necessary mechanical coherence. In the image of fig. 3.10c, 9 squares, each the size of 100 x 100 μm^2 are spanned continuously, the film extending towards the holes of smaller mesh size as well. Even if one assumes cracks on the struts, the images show that larger areas of the grid can be spanned by the irradiated film.

Assuming that packing III of fig. 3.3b is the one adapted by the monomers at the air/water interface, the fact that spanning is observed means that at least 65% of all tetrafluoroanthracene moieties had to have reacted, according to percolation theory.[69,70] This value is a lower threshold for the conversion that must have taken place in order to reach this mechanical coherence. A more precise estimate is given in section 3.6.2.

The evidence for π-π stacking that was collected suggested that the mechanical coherence of the irradiated film may be due to covalent bonds formed between tetrafluoroanthracenes of neighboring monomers. To prove the occurence of the [4+4]-cycloaddition and the formation of C-C bridgehead bonds, the monomer film and the irradiated film were studied by different methods, including X-ray photoelectron spectroscopy (XPS), UV-vis spectroscopy and confocal and tip-enhanced Raman spectroscopy. The study of the type of covalent bond formed during irradiation and responsible for the enhanced mechanical coherence is the topic of the next section.

3.5 Proof for [4+4]-Cycloaddition

In order to identify the chemical bond formed during irradiation, spectroscopic methods that are sensitive enough to detect monolayers were used. These included UV-vis, TERS and XPS. In order to identify characteristic bands of the monomers and the dimers in Raman spectroscopy and UV-vis spectroscopy, reference compounds were synthesized. In this section, the XPS results will be discussed first. Then, the synthesis of reference compounds for UV-vis spectroscopy and TERS is presented, followed by the UV-vis spectroscopy and TER studies.

3.5.1 X-ray Photoelectron Spectroscopy

XPS spectra were collected of the monomer LB film and the irradiated LB film. For this, both were transferred onto Au/glass substrates in order to facilitate evaluation of the carbon peak. The Au $4f_{7/2}$ peak was set to a binding energy of 284 eV. It must be noted that all peaks, both in the fluorine and in the carbon spectra, are ca. 0.8 eV lower than they are expected. One possible explanation could be that the Au $4f_{7/2}$ peak itself is shifted, which has been observed before.[133] For the discussion, the peak binding energies that result from the Au $4f_{7/2}$ peak being at 284 eV are used.

The results of the measurement are shown in fig. 3.11. In order to deconvolute the peaks, literature of previously studied fluorinated aromatic systems was considered.[134–138] The study of this literature revealed that the C sp^2, C sp^3, C-F, and C_α-CF carbons are at distinct binding energies in fluorinated aromatic systems. This was also the case for the monomer and irradiated films: peaks at binding energies corresponding to C sp^2, C sp^3, C_α-C-F, C-F and COOH carbons could be identified and distinguished in both monomer and polymer film.

In the monomer film, at the same binding energy as the COOH peak, was a further feature that may arise from the interaction of the fluorinated carbons with the π electronic system of the neighboring tetrafluoroanthracene unit (see fig. 3.11a). This feature disappeared upon polymerization. Further changes in the aspect of the peaks were observed between monomer and irradiated film. In tables 3.1 and 3.2 the quantification tables for the deconvoluted C1s peaks can be found. In the irradiated film, the peak at 285.3 eV (peak C1s-2), which corresponds to the binding energy of C-C and C-O

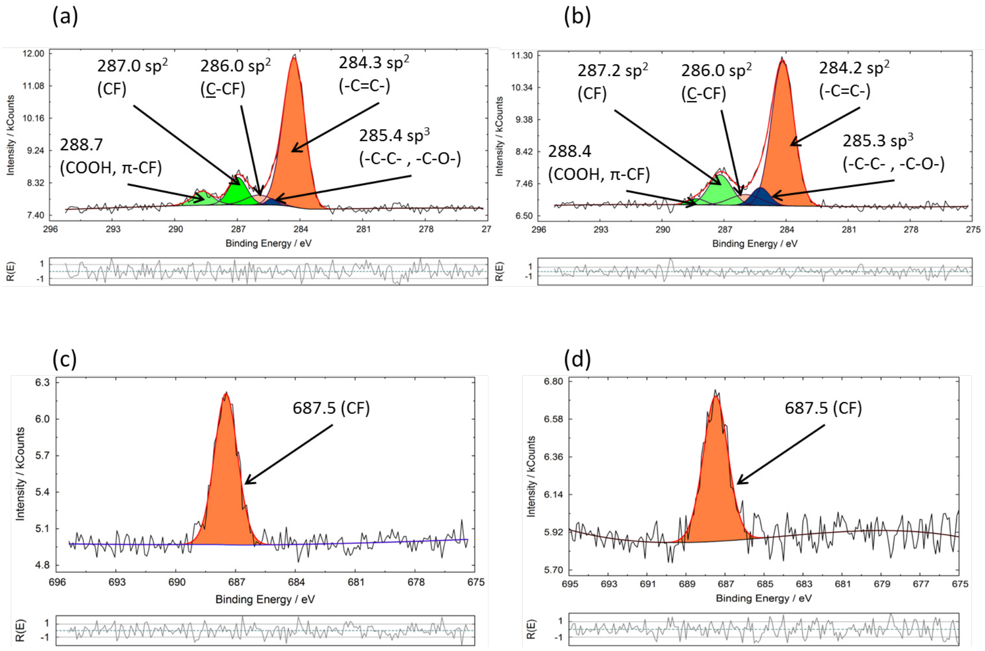

Figure 3.11: (a) C1s spectrum of the monomer film on Au/glass.(b) C1s spectrum of the irradiated film on Au/glass. F1s spectrum of the monomer (c) and polymerized film (d).

sp^3, increased roughly 4-fold in intensity compared to what was found in the case of the monomer film. This increase in sp^3 content is to be expected upon polymerization. Usually, a quantification of the peak at 285.3 eV would be difficult due to the fact that it is at the same binding energy as carbon-based impurities. However, in this particular case, it was possible due to the very similar F/C ratios on both monomer film and irradiated film sample, which indicate that the level of impurities was at the same level for both samples, see tab. 3.3. The ratio of 0.13 or 0.14 is lower than what would be expected (12 F / 45 C $\approx$ 0.26) which showed that some residual impurities contribute to the carbon peak. The F1s peak did not change in appearance between the two samples. Both the peak maximum and shape remained the same, see fig. 3.11c, d. This is consistent with what has been observed before in fluorinated aromatic systems, namely that the F1s peak is barely influenced by the chemical environment of the carbon that the fluorine is attached to.[136,137]

However, not all peak intensities changed in the expected way when comparing monomer and polymer film. While the peak reflecting the sp^3 content

Table 3.1: Quantification table for the C1s peak of the monomer film. The area gives the area of the deconvoluted peaks and the normalized area has been adjusted using the given sensitivity values. The quantity (Q) gives the relative amounts of carbon, while normalized Q gives it in relation to the total amount of carbon in order to compare it to the polymer film.

Peak name	Energy (eV)	Area/cps (eV)	Sensitivity factor	Norm. Area	Quantity (Q)	Norm. Q ($\div$ Σ)
C1s-1	284.3	1106.4262	19.387	57.07052	24.43	0.739
C1s-2	285.4	23.1683	19.367	1.19628	0.51	0.015
C1s-3	286	90.65018	19.367	4.68065	2	0.060
C1s-4	287	173.43725	19.348	8.96409	3.84	0.116
C1s-5	288.7	101.91398	19.349	5.26714	2.26	0.068
Σ					33.04	

Table 3.2: Quantification table for the C1s peak of the irradiated film. The area refers to the area of the deconvoluted peaks and the normalized area has been adjusted using the given sensitivity values. The quantity (Q) gives the relative amounts of carbon, while normalized Q gives it in relation to the total amount of carbon in order to compare it to the monomer film.

Peak name	Energy (eV)	Area/cps (eV)	Sensitivity factor	Norm. Area	Quantity (Q)	Norm. Q ($\div$ Σ)
C1s-1	284.2	1307.0456	19.366	67.49177	27.68	0.688
C1s-2	285.3	131.73791	19.377	6.79867	2.79	0.069
C1s-3	286	134.95794	19.367	6.96845	2.86	0.071
C1s-4	287.2	281.24742	19.348	14.53625	5.96	0.148
C1s-5	288.4	44.14571	19.359	2.28037	0.94	0.023
Σ					40.23	

increased fourfold, as would be expected upon polymerization, the peak at 284.3 eV (peak C1s-1) which corresponds to the sp^2 hybridized carbons only decreased by a tenth, instead of the expected third. The C1s-3 peak which corresponds to the carbons α to the fluorinated carbons should not change at all between monomer and polymer film, however, one can observe a slight increase. Similarly, the C1s-4 peak which corresponds to the fluorinated carbons should remain the same in the two systems, while the quantification table revealed a slight increase in the case of the irradiated film. The C1s-5 peak is particularly difficult to comment on as it not only corresponds to the C=O component but also has a feature that arises due to π-π interactions.

The reason for these deviations could be due to the fitting or due to the fact that the measurements were not recorded at a synchrotron facility and therefore lack the precision required for these small quantities. One can also not rule out the presence of residual unreacted monomers which would make interpretation of the peak quantities even more difficult. Whatever the reason, it was these discrepancies that prompted us to not exclusively rely on the XPS data for a quantification of the polymerization extent and to look for additional methods to prove the polymerization *via* [4+4]-cycloaddition.

Table 3.3: Quantification table for the F1s peak of polymer (P) and monomer (M) film. The total amount of carbon of monomer and polymer film from tab. 3.1 and 3.2 were used to compare the amount of fluorine found.

Peak name	Energy (eV)	Area/cps (eV)	Sensitivity factor	Norm. Area	Quantity (Q)	F/C ratio
F1s (P)	687.6	1061.9298	80.443	13.20102	5.41	0.13
F1s (M)	687.5	916.35021	80.443	11.3913	4.88	0.14

In summary, the XPS data showed that all features that are expected to be present, such as fluorinated carbons, carbons α to fluorinated carbons, carboxylic acid carbons and sp^2 and sp^3 carbons could be found and that they were at distinct binding energies. The increase of the sp^3 content in case of the irradiated film was consistent with the calculated change in the sp^3 ratio for the proposed [4+4]-cycloaddition between neighboring monomer units that may have brought about the enhanced mechanical coherence observed on holey grids. Finally, a feature is attributed to the interaction of the C-F carbons with the π system of a neighboring monomer disappeared upon irradiation which is consistent with the proposed reaction as it would lead to a break of the conjugation in the π system of the tetrafluoroanthracenes. However, the quantification of the other peaks deviated too much from the expected values to rely on this method for quantification. Therefore, while these results supported our hypothesis, it was necessary to conduct further experiments to corroborate the polymerization mechanism by independent methods and to estimate a value for the conversion taking place.

3.5.2 Synthesis of Reference Compounds

In order to identify characteristic bands of anthracenes, tetrafluoroanthracenes, and their respective dimers in UV-vis and Raman spectroscopy, reference compounds were synthesized.

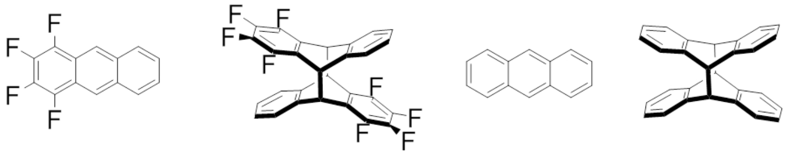

4 **5** **6** **7**

Figure 3.12: Reference compounds used in the UV-vis absorption and the confocal Raman studies. The synthesis of compounds **4**, **5**, and **7** is shown in fig. 3.13.

The reference compounds are shown in fig. 3.12. Their syntheses are depicted in fig. 3.13.

Reference compound **4** was obtained *via* a three-step synthesis, using a slightly modified literature procedure.[139,140] The synthesis started out by reduction of *N*-methylphthalimide to give isoindole **8**. The reaction time of the reduction had to be increased to 2.5 h as the reaction time stated in the literature (1 h) led to a mixture of the isoindole and the partially reduced phthalimide. Increasing the reaction time allowed to obtain **8** spectroscopically pure, as judged by ^{1}H NMR, and, since **8** is sensitive to light and oxygen, it was used directly in the next step without further purification.

Using *n*-butyllithium, tetrafluoroaryne was generated from pentafluorochlorobenzene. This species was reacted with the isoindole **8** to give the epiminoanthracene **9**. This step was particularly low-yielding, as the conversion only reached 50% and due to the fact that a large amount of side products were formed, as judged by TLC of the reaction mixture. Arynes are unstable and prone to react quickly, thereby forming a variety of sideproducts. Despite these side products, compound **9** was used directly in the next reaction without further purification due to its low stability. Subjecting **9** to Cope elimination led to the loss of the *N*-methyl group and re-aromatization to give reference compound **4**. Compound **4** was subjected to column chromatography and was obtained spectroscopically pure, as judged by ^{1}H NMR and ^{13}C NMR. The overall synthesis was low-yielding (5%), mainly due to

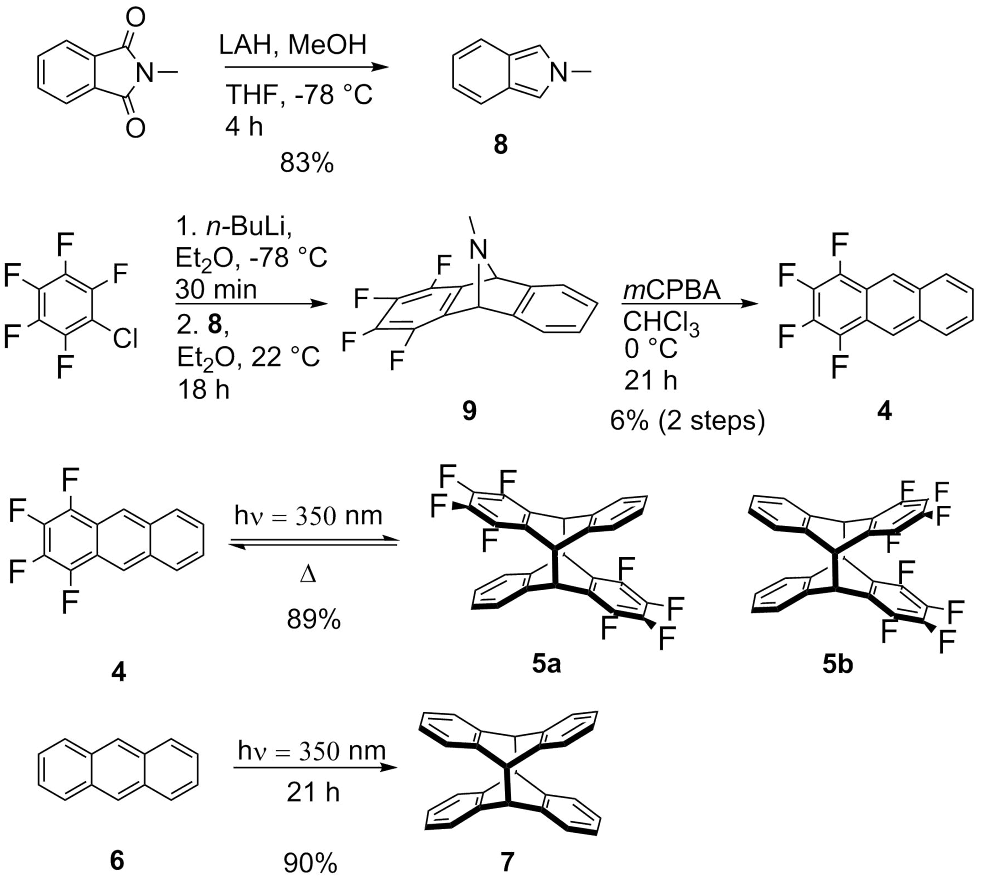
LAH, MeOH
THF, -78 °C
4 h
83%
8
1. n-BuLi,
Et2O, -78 °C
30 min
2. 8,
Et2O, 22 °C
18 h
9
mCPBA
CHCl3
0 °C
21 h
6% (2 steps)
4
hν = 350 nm
Δ
89%
4
5a
5b
hν = 350 nm
21 h
90%
6
7

Figure 3.13: Synthesis of reference compounds **4**, **5**, and **7** for UV-vis spectroscopy and Raman spectroscopy studies.

the second step which has a low conversion and was prone to side reactions.

In order to obtain the dimer **5**, **4** was subjected to a photoreaction at a wavelength of λ = 350 nm, which led to a single isomer. In order to obtain its crystal structure, dimer **5** was recrystallized from toluene at 60 °C, which led to reversion of the [4+4]-cycloaddition. Subjecting the dissolved crystals of **4** to a further photoreaction led to a 2:1 isomer mixture which corresponded to compounds **5a** and **5b**. Of these isomers, one was the head-to-tail dimer and the other was the head-to-head dimer. Despite extensive study by NMR experiments, including HSQC, HMBC, ^{19}F-^{13}C correlation spectra and HOESY, it was not possible to unambiguously assign the isomers. The in-depth discussion of the NMR spectra is presented in section 10.2.

Reference compound **7** was obtained from compound **6** by photoreaction at 350 nm in high yield. During the reaction, compound **7** precipitated due to decreased solubility, which minimized work-up to a mere washing procedure to remove unreacted **6**.

With these compounds at hand, the UV-vis and confocal Raman spectra of compounds **4**, **5**, **6**, **7**, and monomer **1** were recorded. In the next section, the results of the UV-vis study will be presented, followed by the results of the TERS study.

3.5.3 UV-Vis Spectroscopy

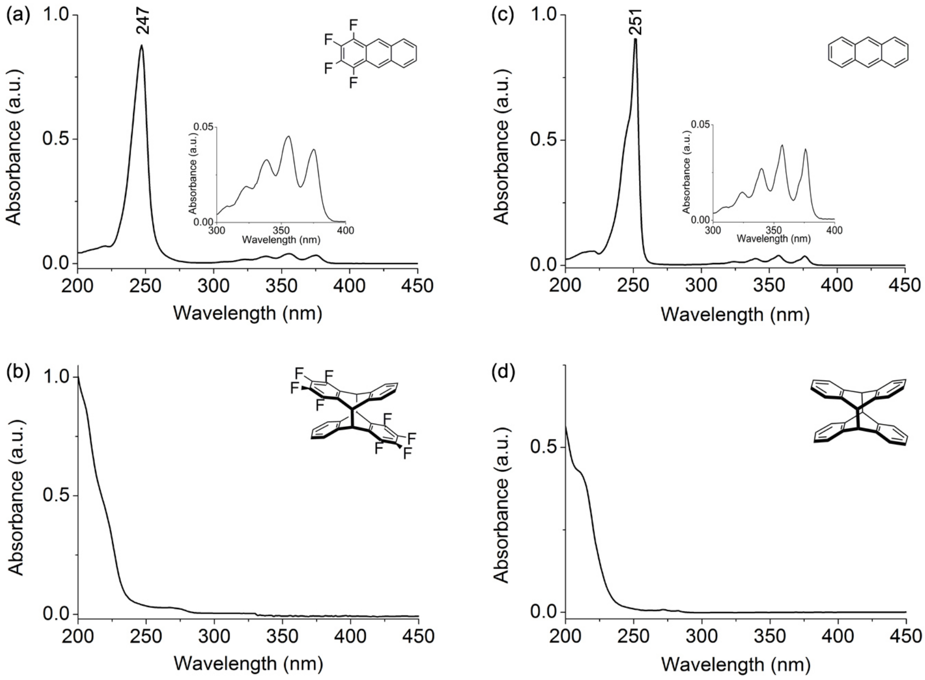

Figure 3.14: (a) Solution UV-vis spectrum of compound **4**. (b) Solution UV-vis spectrum of compound **5**, the dimer of **4**. (c) Solution UV-vis spectrum of **6**. (d) Solution UV-vis spectrum of compound **7**. **4** and **6** were recorded in acetonitrile, **5** and **7** in cyclopentane.

The UV-vis spectra of the reference compounds in solution are shown in fig. 3.14. In the case of compound **4** and **6**, the typical UV-vis signature of anthracenes could be observed: a strong signal at 250 nm and the typical vibrational fine structure between 300–400 nm. Both the main peak and the fine structure completely disappeared in the case of the corresponding dimers, **5** and **7**. Instead, an intense band at shorter wavelengths, namely 200–220 nm, appeared which is consistent with a reduction of the conjugation in the π system of the anthracenes.

These spectra were subsequently compared to the UV-vis spectra of the monomer LB film and the irradiated LB film. It was expected that the tetrafluoroanthracene moieties would be the main contributors to the UV-vis spectrum of the monomer. This expectation was confirmed by a comparison of the UV-vis spectrum of compound **4**, the UV-vis spectrum of the monomer **1** in solution and the UV-vis spectrum of the monomer LB film on quartz (see fig. 3.15a). A distinct bathochromic shift of the main peak of $\Delta\lambda$ = 28 nm was observed between the spectrum of **4** to the spectrum of the monomer **1** in solution, yet the overall appearance in terms of features of the spectrum remained unchanged. The exact cause for the bathochromic shift is not quite clear. Usually, a bathochromic shift can be observed upon an extension of the conjugation system. While there are three tetrafluoroanthracene moieties in the monomer, the system is not fully conjugated. One would therefore not necessarily expect a bathochromic shift. However, it is well known for aromatic compounds that substitution of the ring leads to a bathochromic displacement of the curve with little change in the overall shape of the absorption curve, with the exception of some loss in resolution of the vibrational fine structure.[111] This phenomenon would account for the observed changes between the spectrum of compound **4** in solution and the spectrum of the monomer **1** in solution. One other explanation could be homoconjugation between the tetrafluoroanthracenes.[141] The further slight bathochromic shift of $\Delta\lambda$ = 9 nm between the monomer in solution and the monomer LB film on quartz could be due to increased dipole-dipole and quadrupole interactions,[142,143] that arise due to π-π stacking but it could also be due to the change from solution to the solid environment.

As was the case for compounds **5** and **7**, the UV-vis spectrum of the irradiated LB film showed none of the features characteristic in the UV-vis spectra of anthracenes. The main peak at 250 nm had unequivocally disappeared, but the signal-to-noise ratio did not allow for a statement on the vibrational fine structure around 350 nm. A new distinct peak at 200–220 nm was observed instead, consistent with what was observed for the anthracene dimers (see fig. 3.15b). The increase in scattering observed in the irradiated LB film was consistent with an increase in grain size as one would expect upon polymerization and thereby contraction of the film.

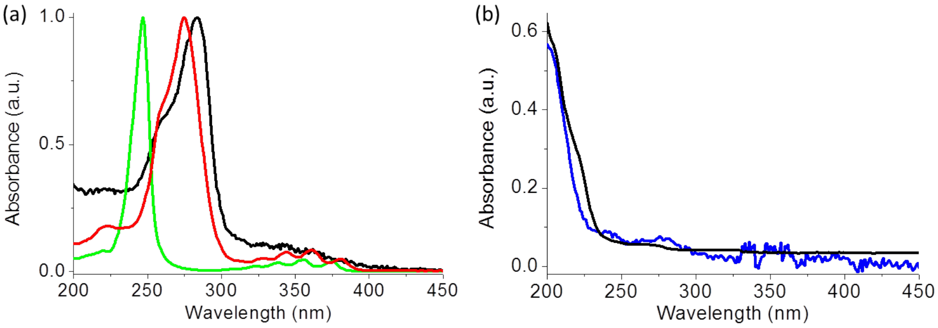

Figure 3.15: (a) Solution UV-vis spectrum of compound **4** (green) and monomer **1** (red). The UV-vis spectrum of the monomer LB film on quartz is shown in black. (b) UV-vis spectrum of the irradiated LB film on quartz (blue) compared to the solution UV-vis spectrum of dimer **5** (black).

Similar to the XPS results, the findings of the UV-vis study were consistent with the hypothesis that the proposed mechanism was at the basis of the enhanced mechanical coherence. The UV-vis spectra of **5** and the irradiated LB film were very similar. The UV-vis spectra of **4** and the monomer also show great similarity, confirming that the main contribution to the spectrum arises from the tetrafluoroanthracene moieties. The broadening and slight bathochromic shift observed in the spectrum of the monomer film relative to the spectrum of the monomer in solution could be due to π-π stacking, but could also arise due to the shift from solution to a solid environment. The disappearance of the main band at 250 nm indicates that all the tetrafluoroanthracene moieties were consumed during irradiation. Assuming that the disappearance of the tetrafluoroanthracene moieties means that they were transformed into their corresponding dimers, the conversion would be considerably higher than the minimum value of 65% given by percolation theory. Unfortunately, the wavelength range where the dimer and the irradiated LB film absorb is a region where a great number of small molecules absorb (i.e aromatic compounds, conjugated double bonds) and is by no means singularly characteristic for anthracene dimers. An estimate of the extent of polymerization is given in the section on conversion (see section 3.6.2) and is subject to some uncertainty due to the increased noise in the case of the irradiated LB film. In order to unambiguously identify the newly formed species, the system was analyzed by a further, orthogonal analytical method, namely confocal Raman and tip-enhanced Raman spectroscopy.

3.5.4 Confocal and Tip-Enhanced Raman Spectroscopy

Confocal Raman spectra of the reference compounds and monomer **1** were recorded. Furthermore, the spectra were simulated using DFT at the B3LYP/ 6-31G(d) level for the reference compounds and monomer **1** that had reacted with three tetrafluoroanthracenes. This was done in order to identify characteristic differences between unreacted anthracenes and their dimers. The simulated and measured spectra are shown in fig. 3.16. A comparison showed that the simulation and measured powder spectra agreed well.

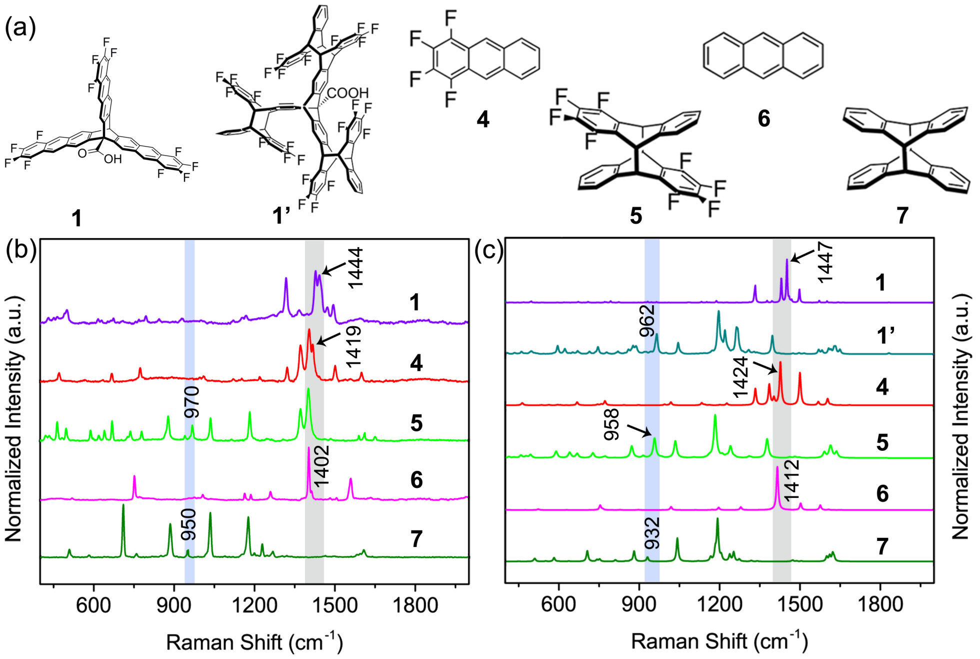

Figure 3.16: (a) Chemical structures of the reference compounds. (b) Confocal Raman spectra of monomer **1** and reference compounds **4**, **5**, **6**, and **7**. (c) The corresponding calculated spectra and an additional calculated spectrum for monomer **1** that has reacted with three tetrafluoroanthracene moieties. The boxes in light blue and grey show the characteristic regions.

For compound **4**, **6**, and monomer **1**, the bands at 1419, 1402, and 1444 cm^{-1} were identified as anthracene ring breathing mode vibrations. For monomer **1**, a further contribution to this band could be due to the bridge bicyclic core (triptycene). These bands were absent in the spectra of compounds **5**, **7**, and the simulated dimer **1′**. Instead, new bands at 950–970 cm^{-1} appeared that were absent in the case of unreacted anthracenes. These bands were identified as corresponding to the bridge head C-C stretching vibrations. Thus, both types of compounds exhibited distinct characteristic vibrations that allowed unambiguous identification of anthracene and its dimer species and thereby provided the opportunity to differentiate between monomer and polymer LB film.

Confocal Raman spectroscopy is not sensitive enough to record the spectrum of a monolayer. TERS, on the other hand, is 10^6–10^9 times more sensitive. The LB films were therefore studied with TERS. After transferring both monomer LB film and irradiated LB film onto Au(111) substrates, their TER spectra were collected. In the case of the monomer film, one would expect to see the band at 1444 cm^{-1}, whereas a band around 960 cm^{-1} would show that a [4+4]-cycloaddition between monomer units had indeed taken place at the air/water interface. The averaged spectra of the LB films are shown in fig. 3.17a. The monomer LB film showed a strong band at 1445 cm^{-1}, as predicted by the calculations and shown in the confocal Raman spectrum of the monomer. In the irradiated LB film, this band was reduced significantly and was barely discernible in the spectrum. On the other hand, a peak at 972 cm^{-1} appeared in the spectrum of the irradiated LB film which had been absent in the monomer LB film. Thus, while the absence of the peak at 1445 cm^{-1} once more confirmed that the tetrafluoroanthracene moieties were consumed during irradiation, the emergence of the peak at 972 cm^{-1} – characteristic for the dimers – showed that the anthracenes reacted to give the corresponding dimer. This peak showed that the chemical bond formed during irradiation and which had conveyed an enhanced mechanical coherence to the irradiated film was indeed the result of a [4+4]-cycloaddition between tetrafluoroanthracenes.

The reaction between anthracenes (or anthracene derivatives) is reversible. In fig. 3.17, a TER spectrum of the monomer monolayer was compared to a polymer monolayer and to spectra obtained after exposing an irradiated film to depolymerization conditions. Exposing the irradiated film to depolymerization conditions, namely, to irradiation at a wavelength of λ = 220 nm for 1 s (corresponds to 16.63 mW/cm^2), led to a disappearance of the peak at 972 cm^{-1} and a re-appearance of the peak at 1445 cm^{-1}. This showed that the polymerization can be reversed to give the monomer film once more and

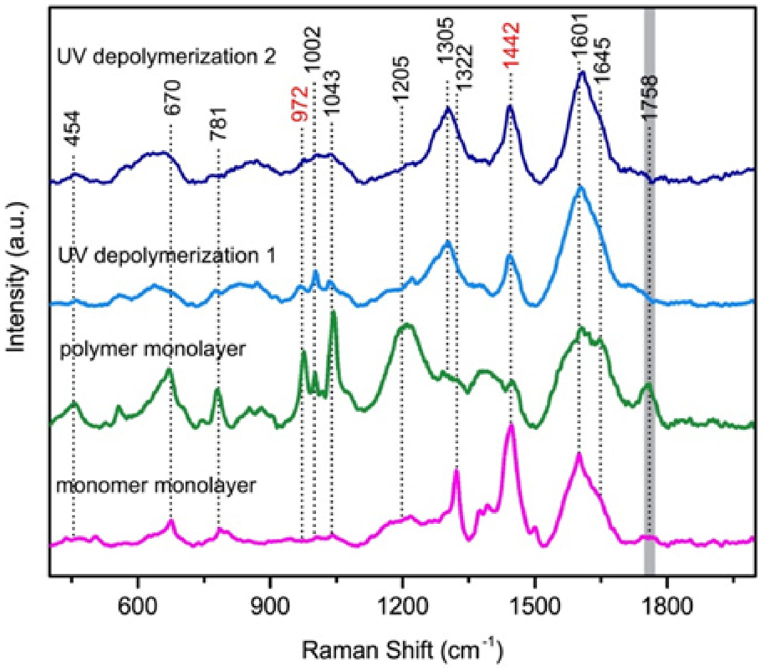

Figure 3.17: From bottom to top: TER spectrum of monomer LB film (pink), TER spectrum of an irradiated LB film (in green). Subjecting an irradiated LB film to depolymerization conditions and remeasuring the TER spectrum gave a spectrum that greatly ressembled the monomer LB film spectrum (light and dark blue spectra).

constitutes further proof for the type of bond formed during irradiation.

TERS also allowed excluding the possibility of oxidation during irradiation at the trough, the most plausible side reaction that could occur during polymerization. By simulating the TER spectra of various oxidation products, it was shown that the anthraquinone, the most plausible oxidation product, would exhibit a strong band at 1714 cm^{-1} (see fig. 3.18a). This band was not observed in the spectrum of the irradiated LB film. On the other hand, during imaging, a new band appeared at 1758 cm^{-1}. The band at 1758 cm^{-1} emerged during the TERS imaging process (after ≈3 hours) and is thought to be an oxidation product that formed due to the imaging conditions. TERS requires laser irradiation, which can lead to heating of the investigated sample. Additionally, the junction between the sample and the tip is subject to strong electromagnetic fields which cause plasma states. Upon prolonged imaging, these conditions can affect the sample. To test this hypothesis, the intensity of the band at 1758 cm^{1} was monitored in a laterally resolved

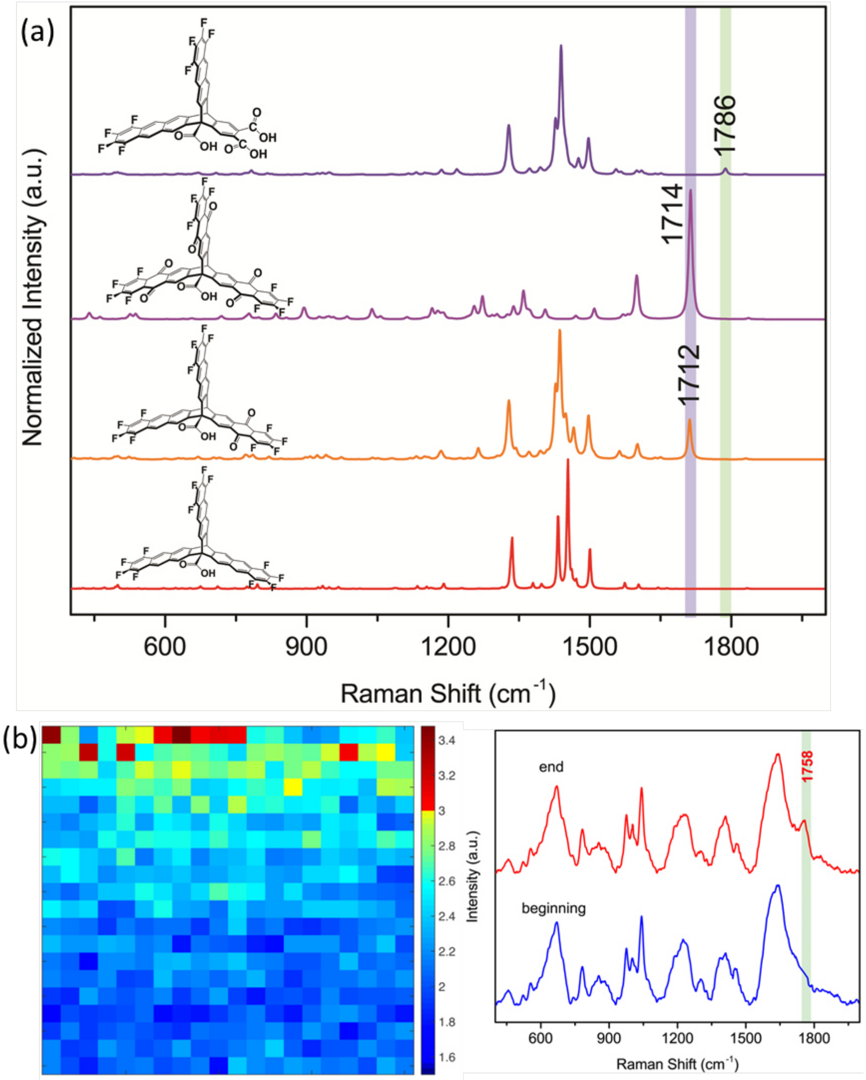

Figure 3.18: (a) Simulated spectra of potential oxidation products. (b) Left: Mapping the band at 1758 cm^1 showed the emergence towards the end of the measurement and right: the extracted spectra showed that only a new band at 1758 cm^1 emerged.

TERS map. The map which was collected over an area of 100 x 100 nm^2 with a resolution of 5 nm/pixel showed the signal-to-noise ratio of the peak at 1758 cm^{-1} (see fig. 3.18b). Only a ratio above three (red pixels) signals the presence of this band. Thus only in the topmost part of the map, which corresponds to the end of the imaging process, could the signal at 1758 cm^{-1} be detected. Furthermore, after subjecting the sample to depolymerization conditions, the sample was imaged once more with a shorter imaging time of one hour and no band at 1758 cm^{-1} was observed. These experiments showed that no oxidation occured during irradiation at the LB trough, but that prolonged imaging during TERS acquisition can lead to oxidation of the sample.

The emergence of the oxidation product does not mean that the entire film breaks down: to show this spectra were extracted from the region where the band at 1758 cm^{-1} can be encountered (red pixels) and compared to a spectrum recorded at the beginning of the measurement (blue pixels). A comparison of these spectra is shown in fig. 3.18b. Apart from the newly formed band at 1758 cm^{-1}, no other new features appeared and the spectra seemed identical. This indicates that the oxidation does not lead to a complete breakdown of the film. The exact nature of this oxidation product was not established but it is thought to bear a carboxylic acid as a functional group, an oxidative degradation product of anthracene upon prolonged UV irradiation treatment that has been reported in the literature.[144] Several potential oxidation products were simulated to account for these changes and are shown in fig. 3.18a. Nevertheless, it was not possible to unequivocally assign this band to a specific oxidation product.

In summary, TERS proved what XPS and UV-vis studies had already indicated: the irradiation at the air/water interface on a LB trough resulted in a [4+4]-cycloaddition of neighboring tetrafluoroanthracene units to give a covalently bonded sheet. Furthermore, this powerful method was able to rule out oxidation to the anthraquinone as a side reaction during irradiation at the air/water interface. Finally, the polymerized film was successfully depolymerized by subjecting it to irradiation at short wavelength (λ = 220 nm). The TER spectrum of the depolymerized film greatly resembled the TER spectrum of the monomer film. All these findings combined are proof that a [4+4]-cycloaddition between tetrafluoroanthracenes takes place at the air/water interface upon irradiation and, by extension, that a covalent two-dimensional sheet can be obtained. Henceforth, the irradiated LB film will be referred to as polymerized LB film or polymerized LB layer.

While the covalent bond between monomer units has been successfully identified as the product of a [4+4]-cycloaddition, the question remains of how the monomers are packed. Evidence has been given for the type of packing adapted by the monomers at the air/water interface which indicated that packing III was most likely, yet it was not clear whether the packing is homogeneous, resulting in a crystalline array, and to what extent domains are formed. It was also of interest to investigate whether several different packings prevailed and whether defects within the film such as holes could be identified. These questions will be addressed in the following section.

3.6 Evidence for Structure

3.6.1 Brewster Angle Microscopy

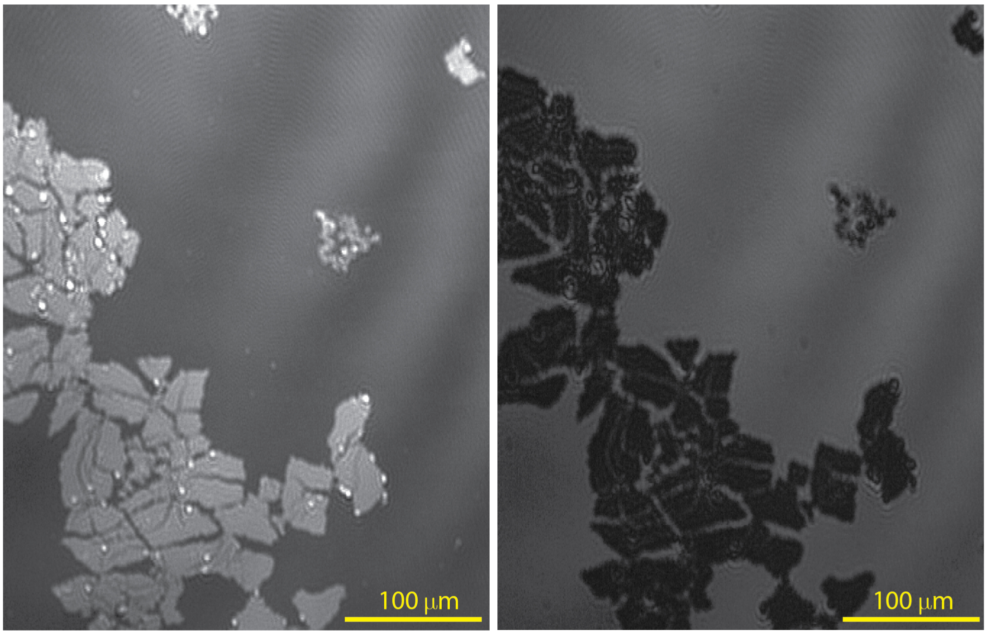

Figure 3.19: Monomer film observed by Brewster angle microscopy. A change of polarization from +2° (left image) to -2° (right image) showed a homogeneous contrast change which indicates the anisotropy of the film.

To learn something about the crystallinity of the monomer film on the water surface, the monomer film was studied with a Brewster angle microscope of high resolution (Nanofilm_ep3 system, Accurion) that allowed to change the polarizer angle. By observing the monolayer at angles other than 0° and by changing the polarizer angle from a positive to a negative value of the same magnitude (or vice versa), conclusions can be drawn with regard to the tilt angle of the molecules and the crystallinity of the domains.

In fig. 3.19, fragments of a monolayer are observed at polarizer angles of opposite sign. Looking at the contrast change of the film pieces upon rotation of the polarizer from +2 (left image) to -2° (right image), it could be observed that the contrast of the domains changed homogeneously. The images revealed several features of the monolayer film. For one, the thickness of the film was the same in all these areas, as indicated by the homogeneity of the grey tone, as well as the uniform contrast change induced by a change of the polarizer angle, which showed that the contrast of the film domains is reversed homogeneously upon polarization change. The sharpness and jagged edges of the domains indicated that the monomer film was in a cohesive, solid-like phase, rather than a liquid-expanded or liquid-crystalline phase. Moreover, the same contrast over a larger area indicated that the orientation of the anisotropy of the refractive index was constant over this area. This meant that the orientation of the molecules at the air/water interface was also the same within these domains. These observations have previously been used as an indication for monocrystallinity of a monolayer.[145–148] It must be noted that due to the resolution of the microscope, one cannot exclude the possibility that the domains are composed of much smaller domains where the molecules have the same orientation, but in different crystalline packings (such as a mixture of packing II and III). This could be an option in the case that the domains' size is smaller than the lateral resolution of the Brewster angle microscope (ca. 1 μm). Within the method's resolution, the domains were monocrystalline, with the exception of bright spots that were trapped between the film edges. These spots are most commonly observed when specks of dust are present at the air/water interface. As the trough cannot be completely shielded from its surroundings, deposition of dust during the experiment cannot be prevented. The homogeneous contrast change upon switching the polarizer angle from a positive to a negative value was a first indicator that crystalline domains are already formed at the air/water interface, most likely due to the π-π stacking and a favorable quadrupole interaction between tetrafluoroanthracenes of neighboring monomer units.

The homogeneity of the domains was also reflected when imaging the fluorescence of the monomer monolayer on solid substrates, such as glass or quartz. In contrast to other monomer systems studied in chapter 5, the fluorescence of the monomer films observed under the fluorescence microscope was completely homogeneous.

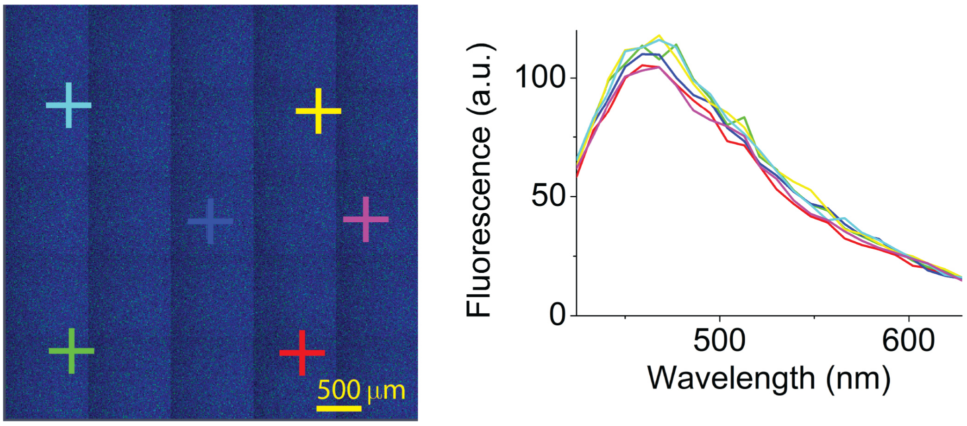

Figure 3.20: A lambda 5 x 5 tile scan, measured with the CLSM and a laser line of 405 nm, reveals the fluorescence of the monomer film on a 4.25x4.25 mm^2 area. The fluorescence is very homogeneous, as can be seen by extracting the spectra in different areas of the film. The colored crosshairs indicate where the spectra were collected.

The image shown in fig. 3.20 was recorded with a confocal laser scanning microscope using a lambda scan. This scan records the fluorescence spectrum for every pixel and the resulting color of the imaged film reflects the fluorescence. A change of orientation or packing between domains would be reflected by a difference in fluorescence. The fluorescence of the monomer film, however, was homogeneous as can be seen by measuring the fluorescence in different areas indicated by the crosshairs. It must be stressed that the homogeneous fluorescence of the film does not mean that the film is crystalline throughout the entire shown area. It could also be attributed to a film that consisted of numerous domains of the same packing, slightly offset to one another. This would not be resolved with the resolution of a confocal laser scanning microscope. Indeed, as the monomer islands exhibit a very rigid behavior when viewed with the Brewster angle microscope, this explanation seems more plausible.

Therefore, the way that the film's contrast changed upon rotation of the polarizer of the Brewster angle microscope was a first indication for the order and crystallinity of the monomer film at the air/water interface.

Upon polymerization, the film's flexibility increases. The increase of flexibility can lead the film to behave like a flexible fishernet during transfer from the LB trough: its pores can expand and be pushed together as it is deposited on the substrate and occasionally covers terraces and imperfections of the substrate. This means that determining the way that the monomers are physically connected and arranged on the substrate can be difficult, as the crystallinity that was encountered at the air/water interface can be lost. Nevertheless, it does not mean that the formed network is not a polymer: it is sufficient that this film is crystalline in a certain conformation. With these things in mind, encountering crystallinity is a safe indicator for order in the film; however, lack of crystallinity does not mean that the polymer cannot form a tesselated, ordered structure which could, for example, be observed upon biaxial stretching of the film.[62]

3.6.2 Estimation of the Conversion

The conversion or extent of polymerization can, in principle, provide information about the crystallinity of the system. In a two-dimensional system with a conversion of 100% the obtained film must be crystalline, according to percolation theory.[69,70] As both monomer and polymerized film gave distinct, characteristic Raman signals, a quantification of the conversion was attempted.

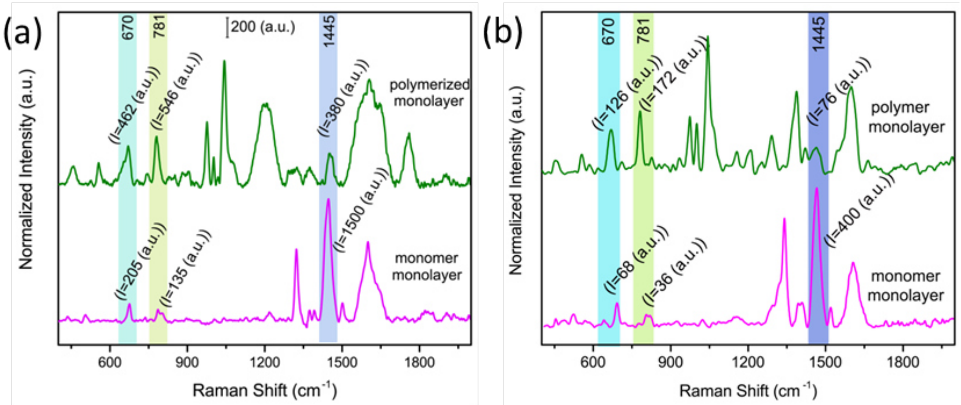

Figure 3.21: Normalized TER spectra of polymerized and monomer LB film of an 100 nm x 100 nm area (a) and an area of 1 μm x 1 μm (b).

In order to estimate a value for the conversion, the results of the TERS study were used.

The TER spectra of monomer LB film and polymerized LB film were subjected to a background correction. Furthermore, to account for the intensity variation between the samples, two peaks at 670 and 781 cm^{-1} were used to normalize the spectra. These peaks were chosen since they were present in both monomer and polymerized film. They arise from a vibration of the triptycene core and are unaffected during polymerization. After having normalized the spectra shown in fig. 3.21a, the ratio of the peak intensities at 1445 cm^{-1} was calculated. According to whether 670 or 781 cm^{-1} was used for normalization, this method resulted in calculated conversions of 89% or 94%, respectively.

For the peak at 670 cm^{-1}:

$$\text{Conversion A} = 1 - \frac{380/462}{1500/205} = 89\% \tag{3.1}$$

For the peak at 781 cm^{-1}:

$$\text{Conversion B} = 1 - \frac{380/546}{1500/135} = 94\% \tag{3.2}$$

This same calculation was carried out for a spectrum obtained from a larger mapping area, namely 1x1 μm^2, shown in fig. 3.21b, and led to very similar results (see below).

For the peak at 670 cm^{-1}:

$$\text{Conversion A-II} = 1 - \frac{76/126}{400/68} = 90\% \tag{3.3}$$

For the peak at 781 cm^{-1}:

$$\text{Conversion B-II} = 1 - \frac{76/172}{400/36} = 96\% \tag{3.4}$$

The conversion for the two-dimensional polymerization obtained by TERS therefore fluctuates between 89–96%. As mentioned previously, the triptycene core may contribute to the vibration at 1445 cm^{-1}. This would mean that even in a perfectly polymerized film, some residual intensity at 1445 cm^{-1} could be encountered and that the values for the conversion may be even higher.

The relative standard deviation for this calculation was estimated to be around 20% by averaging all 400 spectra for monomer and polymer. The fluctuation of the calculated conversions might also be estimated at 20%. This estimate results in a lower threshold for the conversion (69%) that is still higher than the lower threshold of conversion that was determined due to the mechanical coherence of the irradiated films (65%).

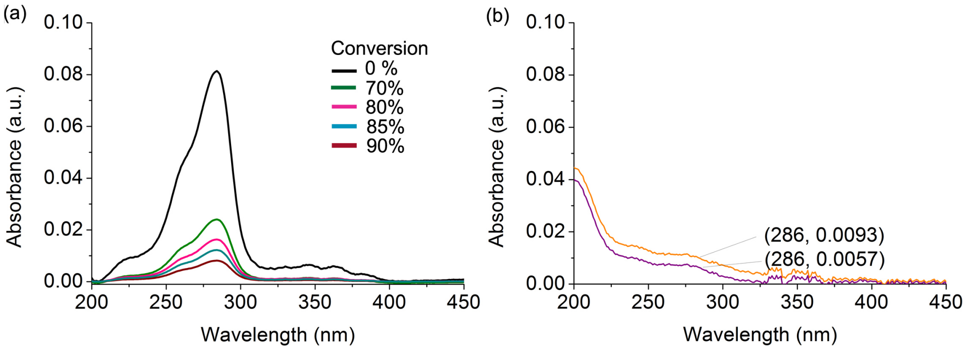

Figure 3.22: (a) Spectrum of the monomer film on quartz (black), subjected to background correction, and simulated curves for different conversions. (b) Spectrum of the polymer film on quartz with the same background correction as the monomer spectrum (orange) and spectrum of the polymer film on quartz with a background correction that accounts for scattering (purple).

The conversion was furthermore determined by UV-vis spectroscopy. In order to do so, the spectrum of the monomer film on quartz was subjected to a background correction. Furthermore, the minimum value of the absorbance was subtracted from the spectrum. Using the corrected spectrum, the absorbance at different conversions was simulated. Peak fitting revealed that the most intense peak has its peak maximum at 286 nm and has a value of 0.080. The spectrum of the polymer film was then corrected in the same way as the monomer spectrum, using the background correction of the spectrum of the monomer film. The absorbance value found at 286 nm was then used to calculate the conversion, which resulted in a conversion of 88%. This procedure gives a conservative estimate, as the polymer spectrum experiences more scattering than the monomer film. If the scattering is accounted for by subtracting a scattering background, the absorbance value at 286 nm results in a conversion of 93%. In both cases, the error of the absorbance at 0.01 amounts to ±2% which gives an error range of ±0.3 in the calculated conversion.[149]

A high conversion suggests that the polymerized LB film must at least have partial order. Furthermore, the high conversion also gave evidence for the packing assumed by the monomers at the air/water interface. As mentioned before, the presence of excimer fluorescence in the monomer film as evidenced by fluorescence spectroscopy did not permit the exclusion of one of the two packings II or III. The high conversion, on the other hand, was only compatible with packing III, as packing II could at best give a conversion of 66%, barely above the percolation threshold. Thus, the estimated conversion allowed drawing conclusions about the packing and, by extension, the structure of the film.

3.6.3 Determining Defects

Whether in a single crystal or in a Langmuir-Blodgett film, the systems are characterized by the formation of domains within the layer(s). These domains could differ in terms of the packing adopted but could also have the same packing and simply be offset from one another such that further growth is prevented. In these cases, it should be possible to find defects within the polymer. During acquisition, the TER spectra are measured in areas of 5 nm x 5 nm over an area of 100 nm x 100 nm. This area of 25 nm^2 corresponded to ≈10 repeat units. Monitoring the peak intensity ratio of the signals at 972 cm^{-1} and 670 cm^{-1} allowed detecting areas where no polymer had been formed (intensity of peak at 972 cm^{-1} = 0), thereby determining defects.

The dark blue areas that are marked with a star in fig. 3.23a show areas where no peak intensity at 972 cm^{-1} could be measured. They represent areas of the film where no polymer was encountered, showing the defects of the film. These dark blue pixels represented around 2–3% of all pixels. These defects could occur at cracks in the film, domain boundaries where no polymerization had taken place or disordered domains. The corresponding spectra resembled the spectrum of monomers.

Red or orange pixels indicated an increased signal intensity during measurements which could be due to random noise in the junction between tip and sample on the substrate, a phenomenon that sometimes occurs in TERS, or due to contamination during the measurement.[150,151] These yellow/orange pixels were rare and accounted for only ≈1% of all counts. The spectra for

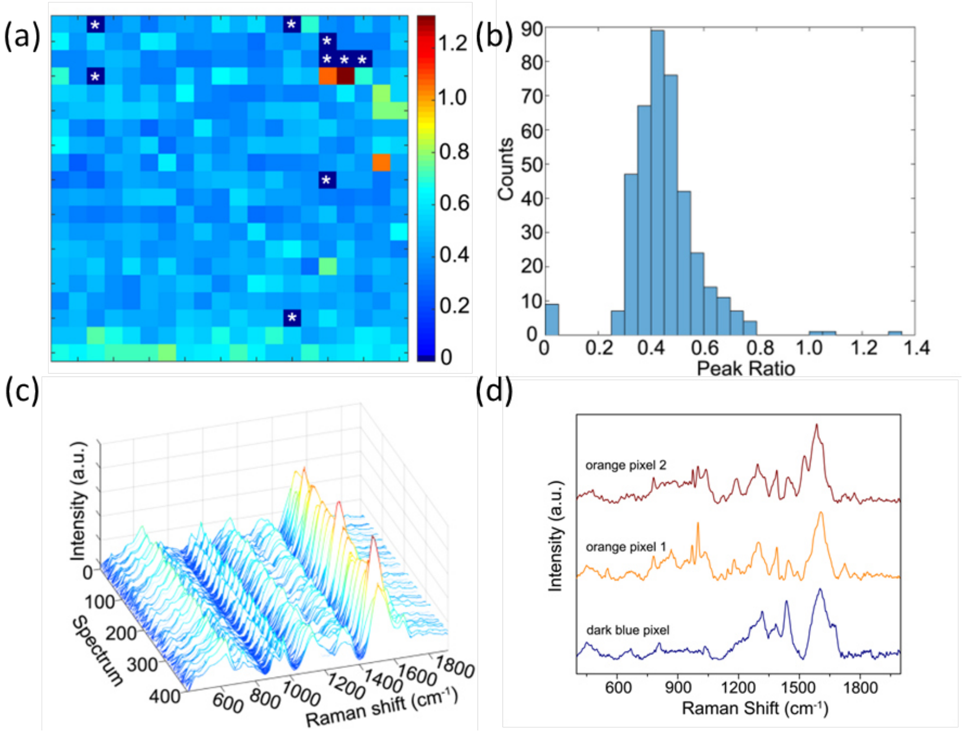

Figure 3.23: (a) Polymer TERS map measured over 100 nm x 100 nm area with a resolution of 5x5 nm^2/pixel based on intensity ratio of the signals at 972 and 670 cm^{-1}. (b) This ratio varies between 0 and 1.2, however, ≈90% of all counts are within the range 0.3–0.6, giving a mean value of 0.455 for the ratio with a relative standard deviation 22%. (c) Waterfall plot of the 400 spectra measured with this map. Each pixel of the map represents one spectrum. (d) Spectra of dark blue and yellow/orange pixels.

these pixels are shown in fig. 3.23d.

The rest of the peak ratios appear more homogeneous and were distributed in the range of 0.3–0.6 (see fig. 3.23b and fig. 3.23c). The slight fluctuations of the ratio indicated that the molecular units in the polymer still encountered thermal diffusion which led them to change their orientation with regard to the substrate. A change in orientation affects the intensity of the band at 670 cm^{-1}, as can be seen in fig. 3.24. While this change in orientation cannot be large since movement of the monomer units is restricted by the covalent bonds that connect them to their neighboring units, some small changes in orientation nevertheless appear to be possible and can be induced by the imaging conditions. Therefore, the variation within the range of 0.3–0.6 is due to thermal fluctuations rather than further defects or domain bound-

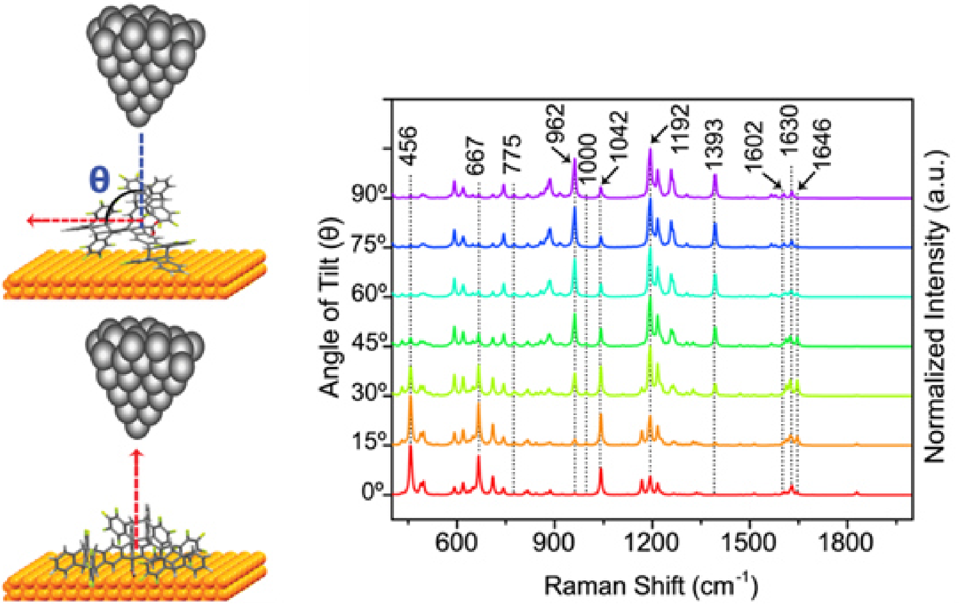

Figure 3.24: Simulation of the change of signal intensities according to orientation of the monomer units to the substrate.

aries and within the range of 0.3–0.6 the polymer film can be considered homogeneous.

The findings outlined here, namely the high conversion and rarity of defects, gave a first indication of the crystallinity, and thereby the order, of the polymerized LB film. It was further investigated by other methods such as HR-AFM (high-resolution atomic force microscopy), STM (scanning tunneling microscopy) and SAED (selected area electron diffraction spectroscopy).

3.6.4 Imaging techniques

Three potential packings for the monomer film at the air/water interface were proposed in fig. 3.3. Irradiation of the film would lead to [4+4]-cycloadditions between neighboring tetrafluoroanthracenes in the case of packing II and packing III. The resulting polymer structures differ from the monomer structures. In fig. 3.25 a comparison of monomer and polymer structures is attempted.

For packing III, the polymer structure can be approximated using the crystal structure of a structurally similar polymer obtained in the single-crystal approach.[45] Upon polymerization, the pore size is reduced by ca. 3–4 Å.

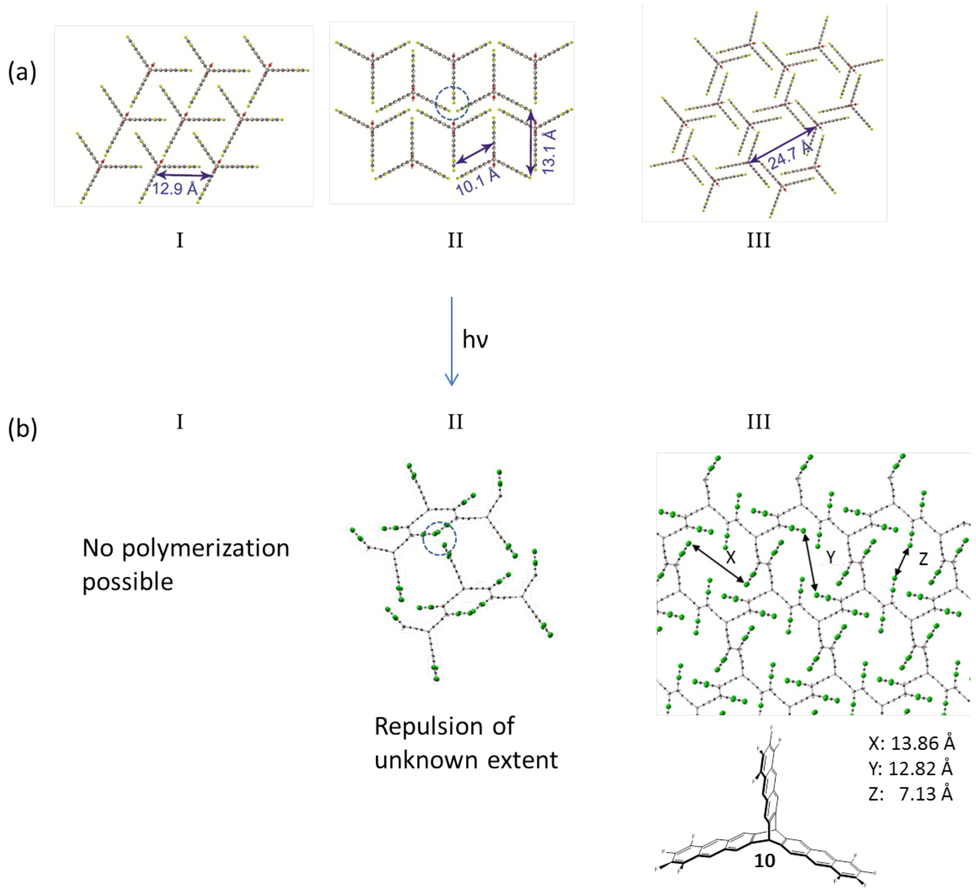
(a)
12.9 Å
10.1 Å
13.1 Å
24.7 Å
I
II
III
hv
(b)
I
II
III
No polymerization possible
Repulsion of unknown extent
X
Y
Z
X: 13.86 Å
Y: 12.82 Å
Z: 7.13 Å
10

Figure 3.25: Change of the monomer packings (a) upon irradiation with UV-vis light (b). In packing I, the monomers cannot react, while in packing II they would form linear polymers. Only packing III would lead to a two-dimensional polymer.

Furthermore, the pore changes from an hexagonal shape in the monomer packing to a more elongated, rectangular shape in the case of the polymer packing.

In the case of packing II, a [4+4]-cycloaddition would result in the formation of ribbons of one-dimensional polymers. The distance between these ribbons would increase compared to the packing II, as the tetrafluoroanthracene dimers would repel the non-reacted monomer (marked by a blue circle, see fig. 3.25). The extent of the repulsion is unknown and difficult to quantify without the crystal structure. The distance between *face-to-face* stacked tetrafluoroanthracenes in the monomer packing is 3.5 Å and as [4+4]-cycloaddition occurs, the distance between the tetrafluoroanthracene bridgeheads decreases to 1.5 Å while the distance between the extremities of the tetrafluoroanthracenes increases to 5 Å. The increase of 1.5 Å (from 3.5 Å to 5 Å) would cause the non-reacted monomer to be displaced by at least this distance – whether it is even more is difficult to predict without theoretical calculations.

High-Resolution Atomic Force Microscopy

For high-resolution AFM, the polymer LB film was transferred onto HOPG and imaged using ScanAsyst high resolution AFM tips in peak force mode.

The AFM images showed that the film covered the HOPG wafers over large areas, without tearing on the HOPG steps (see fig. 3.26a), which revealed that it is flexible. Closer up, some very small tears were revealed (see fig. 3.26b). These tears may be correlated to the fine structures observed within the film islands by Brewster Angle microscope (see fig. 3.19) which means that they already exist at the air/water interface.

When zooming in further, the imaging speed has to be increased and the peak force setpoint decreased to avoid damaging the film during imaging. The imaged structure therefore becomes grainier and while the film is undoubtedly flat, it has a rougher appearance as one zooms in (see fig. 3.26c). On this scale, the film has a porous appearance, but the pores are difficult to discern and do not appear regular.

Occasionally, larger holes were observed in the film (see fig. 3.26d). Measuring the height of the film at these holes confirmed that these holes were part of the film itself, as height values of 0.8–0.9 nm were measured (see fig. 3.26e). Furthermore, it once more confirmed the film height determined by AFM imaging at edges and AFM scratching. The holes were presumably formed at the air/water interface and not during transfer, as tears during transfer usually manifest themselves as long strips that are oriented in a certain fashion, most often horizontally to the dipping direction.

Therefore, while AFM images of higher quality and resolution were obtained, molecular resolution could not be achieved. It was unclear whether this was due to the used imaging settings or because the crystallinity of the film observed at the air/water by BAM was lost upon polymerization and transfer, as illustrated in fig. 1.8. Therefore, high-resolution AFM did not

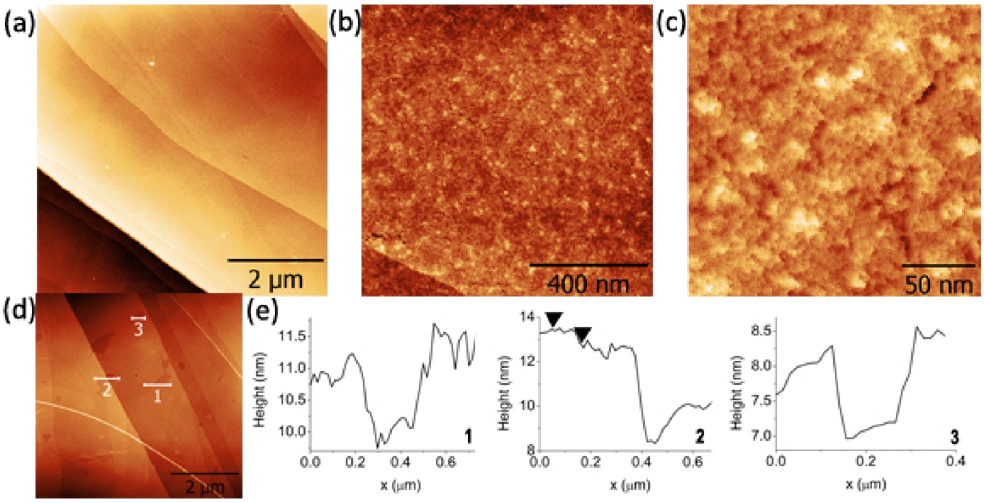

Figure 3.26: AFM images of the polymer film at different scales. The film evenly covers the HOPG substrate over large areas (a). Zooming in further reveals some small cracks (b) and eventually the film exhibits some roughness (c). Occasionally, holes or tears in the film can be observed (d). The step heights measured at the holes were 0.8–0.9 nm. The arrows of profile 2 indicate where the step height was measured and show the HOPG step of ca. 4 nm, which did not lead to tearing of the film.

elucidate the structure of the film. On the other hand, scanning tunneling microscopy provided insight into the structure of the polymerized films.

Scanning Tunneling Microscopy

For STM, polymerized LB films were transferred onto HOPG substrates. The films were imaged *in vacuo* at room temperature from below, while suspended, which caused some issues with the signal stability. The wafers had to be mechanically fastened to prevent this. Despite these difficulties, it was possible to obtain images of the film (see fig. 3.27a).

The image shows one domain of the film that is similar to a distorted fisherman's net: it has pores of different sizes that have an ellipsoid/rectangular shape (see fig. 3.27b). Ellipsoid pores would also be expected in the case of the polymer model (see fig. 3.25b). The variation in size shows that the film is flexible and is distorted when exposed to strain, as encountered during transfer from the air/water interface. Accounting for strain allowed fitting a distorted polymer to the obtained image (for details on the image processing script, see section 9.4).

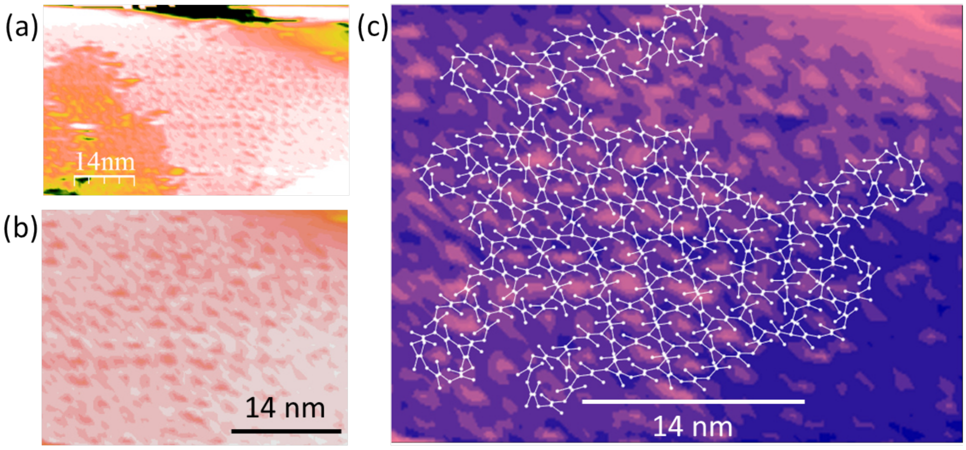

Figure 3.27: (a) STM image (-1.13 V, -1.3 nA) of a structure reminiscent of a fisherman's net. The close-up image (b) showed the area where this structure is most apparent. The proposed model for this region is the two-dimensional polymer, however, the distortion of the film is quite severe which required introducing flexibility into the polymer model in order to create an overlap between the model and the image (c).

The image was direct evidence that the postulated packing III was adopted at least to some extent at the air/water interface. Furthermore, it showed that the [4+4]-cycloaddition proven by TERS led to formation of a two-dimensional polymer. The reason why other methods that relied on crystallinity and long-range order did not reveal the film's structure becomes obvious when looking at the image in fig. 3.27b: all crystallinity is lost as the flexible film distorts.

Furthermore, during polymerization, the pores in the film shrink considerably which makes them harder to discern. In combination with strain, the pores are even less visible. Only imaging methods of the highest resolution would be capable of resolving these structures. Knowing about the distortion of the film, one can go over the HR-AFM images in fig. 3.26b and fig. 3.26c once more. The porous appearance of the film could be due to the pores formed, but the AFM tip does not seem to be sensitive enough to detect these pores. The irregularity of the pores as a direct result of the distortion of the film exacerbates this issue.

A different area of the film shows that a further structure is present. The structure consists of several ribbons that are evenly spaced by 2 nm (see fig. 3.28a,b,c). At first glance, this could be attributed to packing II after [4+4]-cycloaddition of monomers in one dimension had occured, forming one-dimensional polymers (see fig. 3.25). However, upon closer inspection, it becomes clear that this model does not fit the obtained image well. The distance between the ”ribbons” of monomers is 1.3 nm in the monomer model. It is expected to increase upon cycloaddition, as the kink of the reacted tetrafluoroanthracene dimers repulse the unreacted monomers in the neighboring row. Unfortunately, the exact distances between ribbons after polymerization are unknown, as there is no crystal structure that could be used to estimate them. It is, however, unlikely that they would increase by as much as 0.7 nm, which would mean an increase of 54%, and still maintain some molecular interactions that prevents them from being torn apart during transfer from the air/water interface.

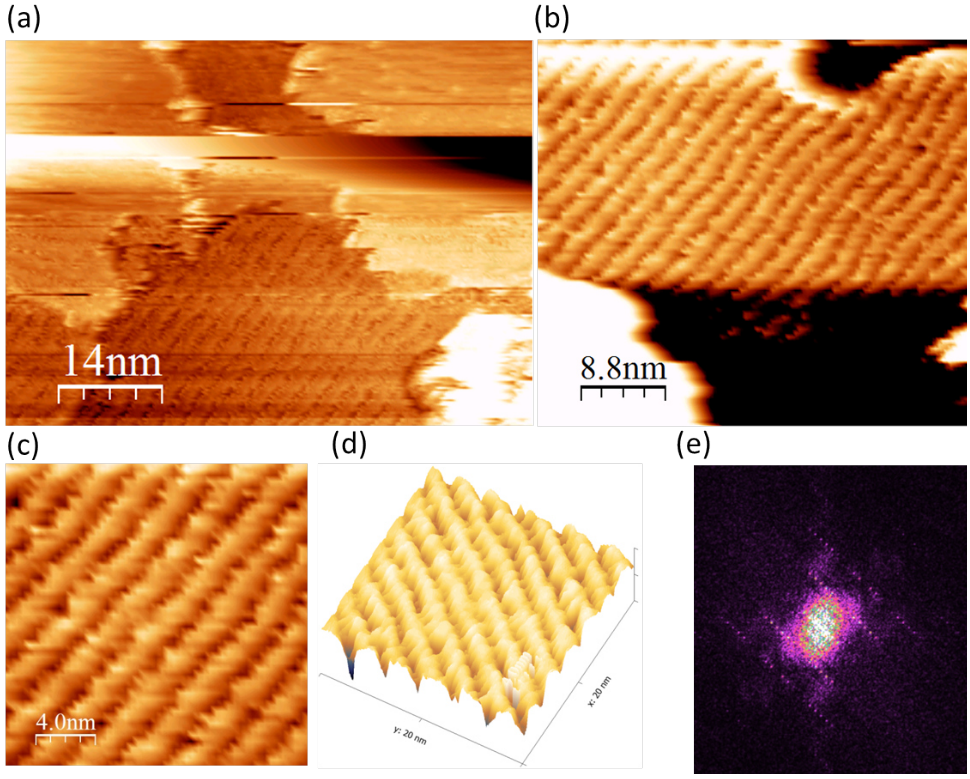

Figure 3.28: STM image of a structure that resembles ribbons (a: -1.13 V, -0.11 nA; b: -1.13 V, -3.3 nA) and a close-up (c). A three-dimensional projection reveals that the ribbons are regularly connected (d), while its Fourier transform reveals crystallinity (e).

Furthermore, a three-dimensional projection of the image showed that the ribbons appeared regularly interconnected (see fig. 3.28d), an observation that was supported by the fourier transform of the image that showed regularity in two dimensions (see fig. 3.28e). When measuring the distances in the fourier transform image, a regular spacing of 2 nm was calculated which corresponded to the distance between the ”ribbons”. This is slightly higher than the 1.8 nm that would be expected. Orthogonally to that direction, a regular spacing of 0.3 nm and 0.5 nm was found. At this point, it is not clear what these values correspond to. Assuming that the ribbons are in fact a two-dimensional structure, what could cause this morphology?

Considering the anticipated polymer structure shown in fig. 3.25 once more, one can see that the pores are not perfectly symmetric, but have an elongated shape. Furthermore, the polymer of the crystal structure shown lacks the carboxylic acid moieties of monomer **1**. If one assumes that these would prop up the polymer, then a scenario such as the one shown in fig. 3.29 could account for the formation of the ribbons, where the longest axis of the pore defines the inter-ribbon distance (marked with arrows) and the carboxylic acids marked with red dots. With a low resolution, the features within the pink rectangles could no longer be resolved (see fig. 3.29b) and would lead to the ribbon-like structure seen with the STM. Unfortunately, without images of higher resolution, this hypothesis cannot be confirmed.

The question of whether the images in fig. 3.27 and fig. 3.28 represent the same kind of polymer subjected to different strains during transfer or whether they represent two different domains of packing II and III, respectively, cannot be answered in a final manner at this point. This also means that the question of domains of different packing (mosaicity) cannot be answered.

What is clear, however, is that the STM images provided the final evidence required to show that a two-dimensional polymer has indeed been synthesized at the air/water interface and that all five criteria of the definition of a two-dimensional polymer have been satisfied.

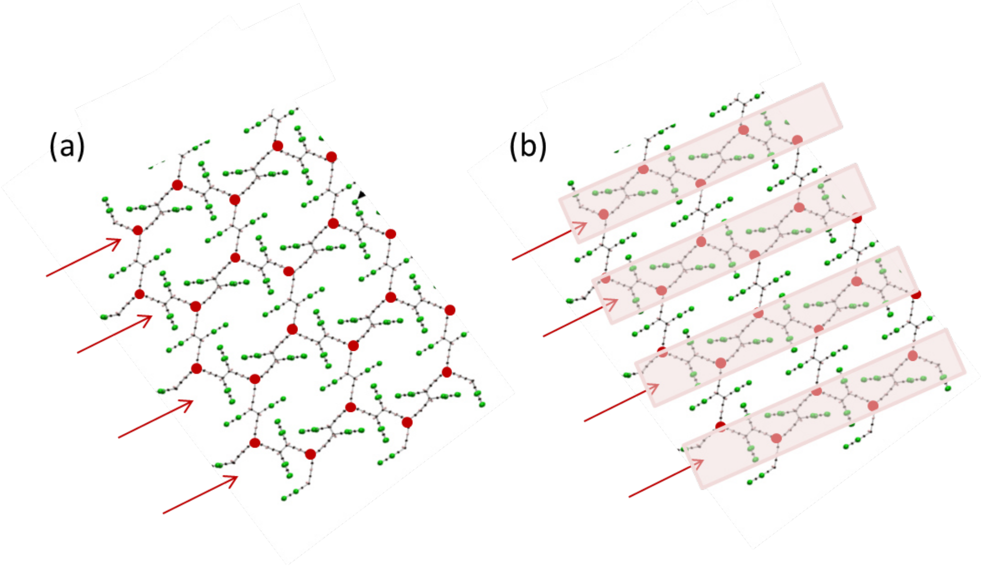

Figure 3.29: (a) Potential explanation of the ribbon structure, taking into account the carboxylic acid moieties missing in the crystal structure (red dots) and the ribbons that may be perceived due to low resolution (b).

Chapter 4

Structure Elucidation of Diazaanthracene-Based Monomer 2

In the previous chapter, the structure elucidation of the two-dimensional polymer synthesized from monomer **1** was achieved. The chemical connectivity and the packing could be proven experimentally. There are other monomers where this analysis was not met with success. One such monomer, which nevertheless proved useful for exploring a potential application, is shown in fig. 4.1a. It was first synthesized by Dr. Ming Li.[152] A structurally very similar monomer is compound **11**, which differs only in terms of reactive moieties used and was synthesized by Dr. Patrick Kissel (see fig. 4.1b).[60,61] Films synthesized from monomer **11** have been thoroughly studied at the air/water interface, both by him and Dr. Payam Payamyar.[62,153] Further work was conducted on synthesizing copolymer LB films using monomers **2** and **11**.[154]

Due to the structural similarity of the two systems, some of the results obtained for monomer **11** can be translated for understanding the behavior of monomer **2**. Films of monomer **2** were investigated in terms of mechanical coherence and film thickness by Dr. Tim Hungerland and further investigated within the scope of this thesis. After describing the monomer's behavior at the air/water interface and on solid substrates, differences to monomer **1** will be discussed, in particular with regard to the question why one monomer system was easier to characterize than the other. In the next chapter, films of this monomer will be investigated for their potential as a miniaturized optical writing device.

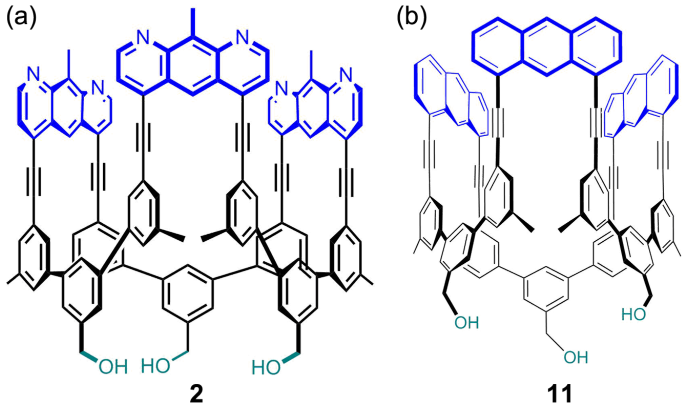

Figure 4.1: Chemical structure of monomers **2** (a) and **11** (b). Their main difference lies in the reactive moieties which are methylated diazaanthracenes in the case of **2** and anthracenes in the case of **11**.

4.1 Characteristics of Monomer 2

Monomer **2** is amphiphilic, bearing three polar hydroxyl groups that help orientate the molecules at an air/water interface as they would be immersed in water whereas the rest of the molecule would stick into the air. As reactive units, it contains three diazaanthracenes (DAA) that can undergo [4+4]-cycloaddition upon irradiation. The reaction is reversible by irradiating at a shorter wavelength or by heating (see fig. 4.2b).

In fig. 4.2c, a top view of a potential packing of the monomers at the air/water interface is shown. In this packing, all diazaanthracenes (in red) would be paired and could, upon irradiation, react with the neighboring diazaanthracenes, according to the reaction shown in fig. 4.2b. Note that the proposed packing was simulated for monomer **11** at the air/water interface and does not take into account defects and domain formation which are highly likely to occur. A follow-up large-scale DFTB molecular dynamics study for monomer **11** showed that the shown packing densifies within 4 ps upon polymerization as the former anthracene moieties deform (see fig. 4.2).[62] This loss of visible order is problematic in terms of structure elucidation and was presumably the reason why structure elucidation by STM or HR-AFM was not met with success. In the following, the behavior of monomer **2** at the air/water interface will first be described and then compared to that of monomer **1**.

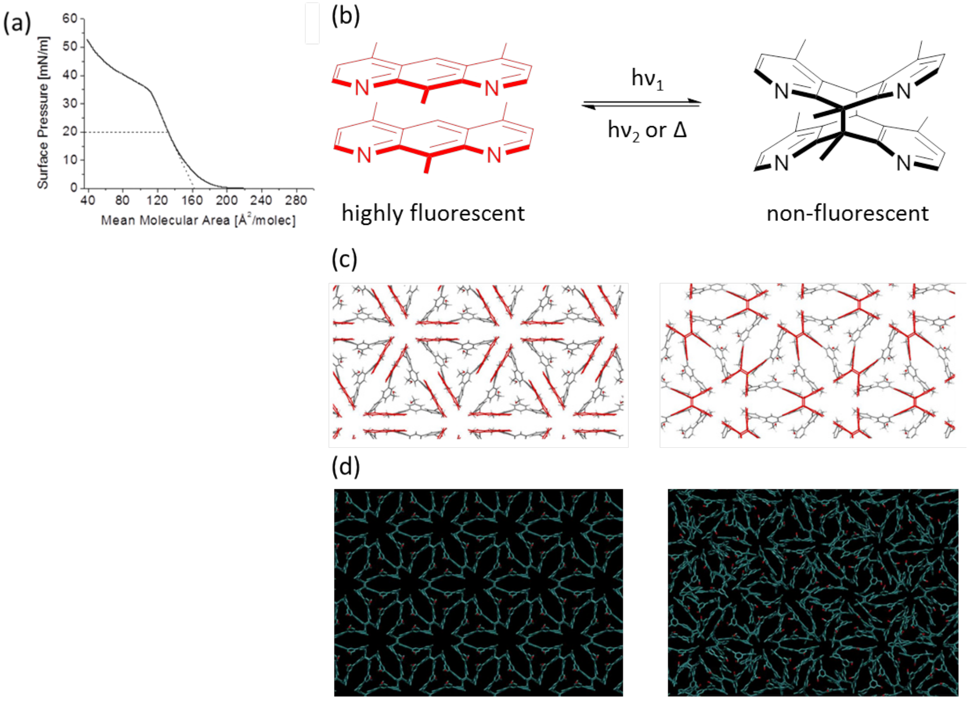

Figure 4.2: (a) Surface pressure versus mean molecular area curve of monomer **2** recorded at the air/water interface. (b) Via a [4+4]-cycloaddition, neighboring diazaanthracene units of monomers undergo dimerizations to give the polymer. This reaction is accompanied by a loss of fluorescence, as the monomers are highly fluorescent, while their corresponding dimers are not. The [4+4]-cycloaddition reaction can be reversed by heating or irradiation at a shorter wavelength. (c) A potential packing of **2** that could be assumed at the air/water interface which would result in all diazaanthracenes (in red) being paired. (d) Upon polymerization, a structural collapse occurs as the flexibility of the system increases (c and d were simulated for monomer **11** and taken from reference [155]).

After spreading a solution of monomer **2** in $CHCl_3$ at the air/water interface on a Langmuir trough, Brewster angle microscopy was used to follow the film formation process during compression of the trough barriers (fig. 4.3). Prior to compression of the barriers, at a low surface pressure of SP = 0.5 mN/m, islands of film were observed which, upon compression, started to merge to form a laterally extended film. At a surface pressure of 20 mN/m, a homogeneous grey tone of the film was observed, indicating a uniform thickness over a macroscopic size range. This surface pressure was chosen for all transfer experiments. Further compression of the barriers to a surface pressure of SP = 45 mN/m led to crease formation in the otherwise uniform film which could indicate the onset of monolayer collapse.

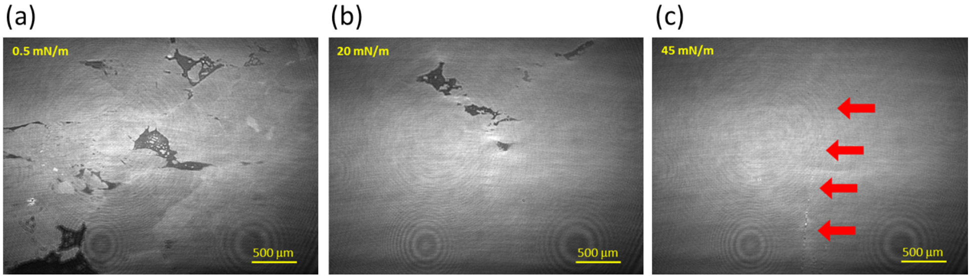

Figure 4.3: BAM images of the film formation at different surface pressures: after deposition of the monomer solution (a), compression to the target surface pressure of 20 mN/m (b) and at high surface pressure, leading to formation of wrinkles due to the onset of monolayer collapse (c).

4.2 Evidence for π-π stacking

At the air/water interface, the monomers are presumed to assume a packing where DAA units of neighbouring monomers stack face-to-face (ftf) (fig. 4.2c). In the case of face-to-face stacking of diazaanthracenes, excimer fluorescence may be observed.[156,157] To confirm this, the fluorescence of the monomer film was investigated at the air/water interface at a surface pressure of SP = 20 mN/m using an excitation source of λ = 373 nm. The monomer layer at the air/water interface exhibited broad excimer fluorescence centered around 560 nm. No monomeric fluorescence was observed at the air/water interface, whereas the fluorescence of the monomer in solution was exclusively monomeric (see fig. 4.4a).

This was a first indication that the diazaanthracenes of the monomer film were paired at the air/water interface. One should note that lone excited diazaanthracenes could be obscured when funneling their energy into excited diazaanthracene pairs.[62,158] Nevertheless, irradiation of the monolayer with an LED of wavelength λ = 373 nm at the air/water interface led to a gradual and complete loss of fluorescence. After irradiation for 24 hours, no residual fluorescence could be measured, as can be seen in fig. 4.4b. At this point, with the excimer emission gone, if the monomeric fluorescence of diazaanthracenes had been obscured by excited diazaanthracene pairs, monomeric fluorescence should have been observable once more. As it was not, the only

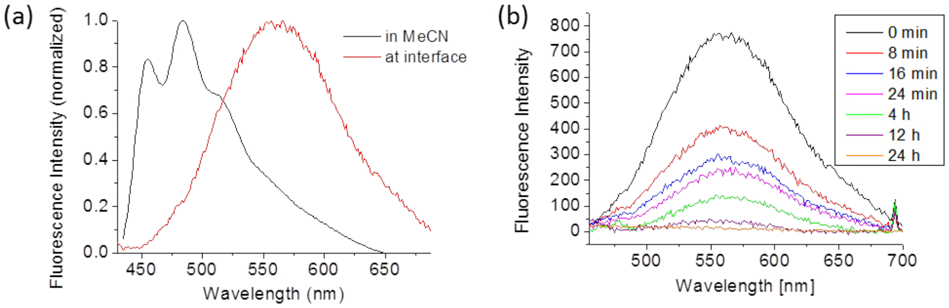

Figure 4.4: (a) Fluorescence of monomer **2** in acetonitrile (in black) compared to the fluorescence of a monomer monolayer at the air/water interface (in red). (b) After compressing the film to a surface pressure of SP = 20 mN/m, irradiation of the monomer monolayer at the air/water interface was carried out which led to a gradual loss of the fluorescence.

other plausible alternative explanation for the observed complete loss of fluorescence (other than all diazaanthracenes being paired) would be oxidation. In the case of the diazaanthracene-based monomer **2**, oxidation would lead to *endo*-peroxides.[159] These *endo*-peroxides are not stable and in the case of anthracenes, usually react to give the corresponding anthraquinones or revert back to the anthracenes. In case of monomer **2**, the follow-up reaction to the diazaanthraquinone is prevented by the presence of a methyl group in the C9-position of the diazaanthracene moieties.[160] One would therefore expect the quenching due to oxidation to be reversible and in equilibrium and thus, the fluorescence should not be quenched completely. The fact that the fluorescence completely disappeared indicates that the loss of fluorescence was due to a more permanent photochemical transformation that had taken place and that there most likely were no single excited diazaanthracenes present. Conversely, the excimer fluorescence and complete quenching of it indicated that all diazaanthracenes were paired, as suggested by the packing in fig. 4.2c. The excimer fluorescence was preserved upon transfer onto solid substrates.

4.3 Absorption and Excitation Spectroscopy

By transferring the films from the air/water interface onto solid substrates, further spectroscopic characterization could be carried out. In order to unequivocally attribute the excimer fluorescence to the monomer and exclude the presence of fluorescent impurities, the excitation spectrum of the monomer layer on quartz was recorded. In the excitation spectrum, the intensity variation of the fluorescence emission at one wavelength is monitored while sweeping the excitation wavelength spectrum. If the observed fluorescence at the monitored wavelength is due to a certain compound, the excitation spectrum will match the absorption spectrum of that compound. If, however, other components contribute to the fluorescence, one would observe an altered absorption spectrum.[129]

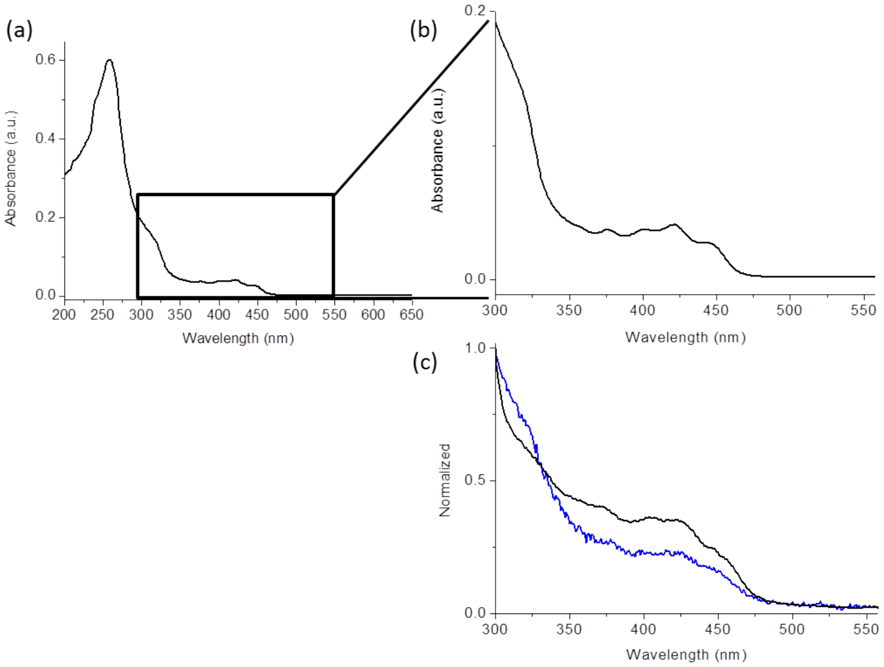

Figure 4.5: (a) Solution UV-vis absorption spectrum of monomer **2** in acetonitrile. (b) A cut-out of the absorption spectrum in solution of the wavelength range relevant for a comparison to the excitation spectrum. (c) Normalized excitation spectrum (black) and normalized absorption spectrum (blue) of the monomer monolayer on quartz.

In fig. 4.5, the absorption spectrum of the monomer in solution is compared to the absorption spectrum of the monomer monolayer on quartz and to the excitation spectrum. The spectra all show the same features, namely the vibrational fine splitting between 350–475 nm that is characteristic of anthracenes in general.[84,161] As fluorescence spectroscopy is more sensitive than UV-vis spectroscopy, the excitation spectrum has less noise than the absorption spectrum. In all cases, the spectra were very similar, indicating that the observed fluorescence can be attributed to emission from the monomer. The similarity of the spectra excluded the possibility of the observed excimer fluorescence at the air/water interface and also on solid substrate (quartz) being due to an impurity and, by extension, confirmed that it was exclusively due to diazaanthracene pairs of the monomers.

4.4 Mechanical Coherence of the Irradiated Film and its Origin

To probe the mechanical coherence of the films and, in particular, to see whether there was a change of the mechanical coherence of the films upon irradiation, the films were transferred onto Cu TEM grids. When transferring a monomer film onto TEM grids, the layer was incapable of spanning the grid holes (see fig. 4.6c), instead falling through the grid holes. In contrast, an irradiated layer was capable of supporting its own weight and spanned the grids over large areas (fig. 4.6a). The enhanced mechanical coherence was most likely due to covalent bonds formed between the monomers during irradiation. Assuming the proposed packing in fig. 4.2c is correct, the increase in mechanical coherence gives a lower threshold for the conversion that must have taken place, which is 65%, according to percolation theory. To investigate the nature of the covalent bonds, XPS experiments were carried out on the irradiated and non-irradiated films.

For this, both monomer layer and irradiated layer were transferred from the air/water interface onto Au/glass substrates. The XPS spectra recorded from the samples appeared quite similar. The C1s spectra of the monomer and the irradiated film can be seen in fig. 4.6b and fig. 4.6d. The C1s peak of monomer and irradiated film resembled each other; deconvolution of the peaks revealed only slight differences. While deconvolution allowed separating the sp^3 component from the other carbons, the sp component could not be differentiated from the sp^2 component. In the case of the irradiated film, an increase of the sp^3 content in the C1s peak was observed. The sp^3 content was on the order of 10% in the spectrum of the monomer film, while it rose to 18% in the spectrum of the irradiated layer, as can be seen in the quantification table (tab. 4.1). In the case of complete polymerization, a rise from 10% to 16% would be expected, as a percentage of the total amount

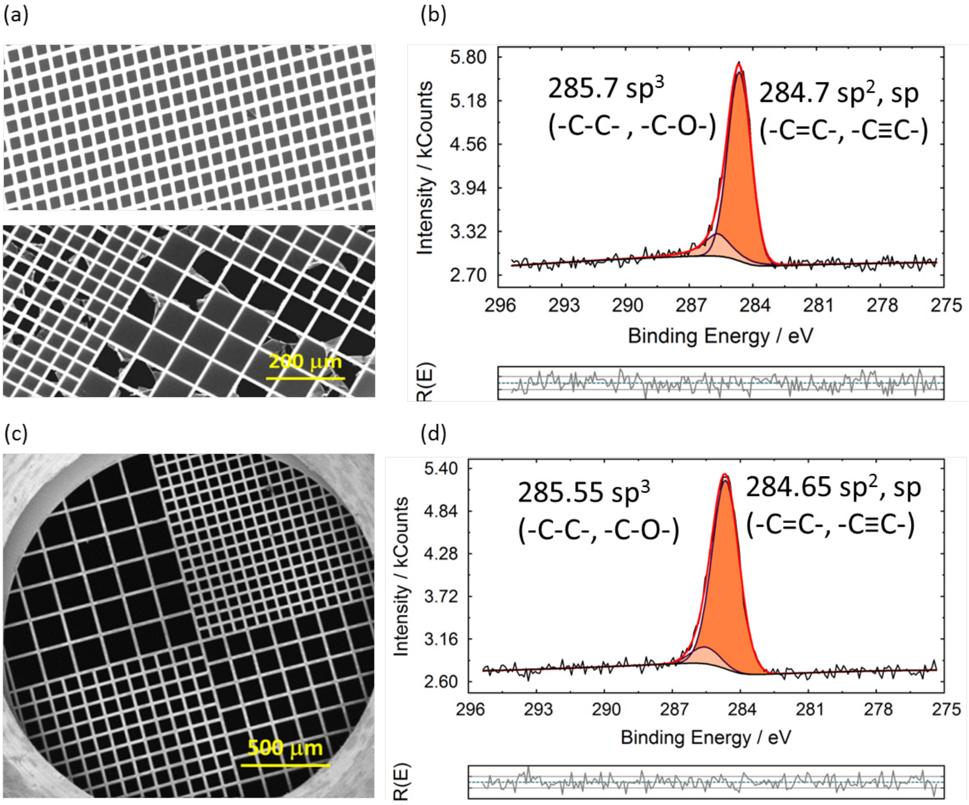

Figure 4.6: (a) Transfer of an irradiated monolayer from the air/water interface onto Cu TEM grids show that it was capable of carrying its own weight. This reflects considerable mechanical coherence which was absent in the case of the monomer film (c). The increase in mechanical coherence could be due to dimerization between neighboring diazaanthracene units. An indication for this was given by XPS which showed an increase of the sp^3 content in case of C 1s spectrum of the irradiated film (b) compared to the C 1s spectrum of the monomer film (d).

of carbon. In general, these values should be taken with a grain of salt, as the peak at 284.7 eV, which corresponds to sp^2-hybridized carbon, is at the same binding energy as carbon-based impurities which may vary between the two samples.

While XPS studies could not unequivocally prove that the monomers polymerize to give a two-dimensional polymer, as suggested by the proposed packing model, the increase of the carbon sp^3 content was consistent with what would be expected upon dimerization of neighboring DAA units. This result, together with the disappearance of excimer fluorescence and the en-

Table 4.1: Quantification table for C1s of the monomer and irradiated film. The areas given are those of the deconvoluted peaks, the normalized areas have been adjusted using the given sensitivity values. Q gives the relative amounts of carbon, while normalized Q gives it in relation to the total amount of carbon for better comparability.

Peak name	Energy (eV)	Area/cps (eV)	Sensitivity factor	Norm. Area	Quantity (Q)	Norm. Q (÷ Σ)
Monomer						
C1s-1	284.65	1836.4647	19.377	94.77549	42.3	0.845
C1s-2	285.7	336.2006	19.367	17.35946	7.75	0.154
Σ					50.05	
Polymer						
C1s-1	284.65	1873.7998	19.377	96.70227	43.17	0.913
C1s-2	285.55	177.20183	19.367	9.14968	4.09	0.086
Σ					47.26	

hanced mechanical coherence of the film upon irradiation, is indicative of a reaction taking place between diazaanthracene units, presumably a [4+4]-cycloaddition. While the evidence for this particular type of reaction is not strong, a sidereaction like a [4+2]-addition between the acetylene and the anthracene moieties was ruled out in a TERS study of monomer **11**.[153] Due to the structural similarity of these two monomers, one can assume that this particular side reaction does not take place with monomer **2** either. The TERS study also showed that there were no characteristic signals of the monomer **11** films or the irradiated film that could be used to provide evidence for polymerization. TERS was therefore not capable of elucidating the type of bond formed in the case of monomer **11** and was therefore not attempted for monomer **2** either.

Finally, a UV-vis spectroscopy study was not feasible due to the lack of an appropriate reference compound that would account for all absorbing functional groups and, upon irradiation, adopt the *syn* orientation achieved in the case of a [4+4]-cycloaddition between monomer diazaanthracenes. As the results do not unequivocally show that a polymer film is formed, the nomenclature of monomer layer and irradiated layer, rather than polymerized layer, will be used for this monomer system.

4.5 Film Thickness Determination by AFM

Both monomer layer and irradiated layer were monolayers. This was shown by transferring the layers onto mica substrates by Langmuir-Schaefer transfer and measuring the film height by AFM (see fig. 4.7). AFM height analysis revealed a thickness of 1.8 and 2.0 nm for the monomer layer and irradiated layer, respectively.

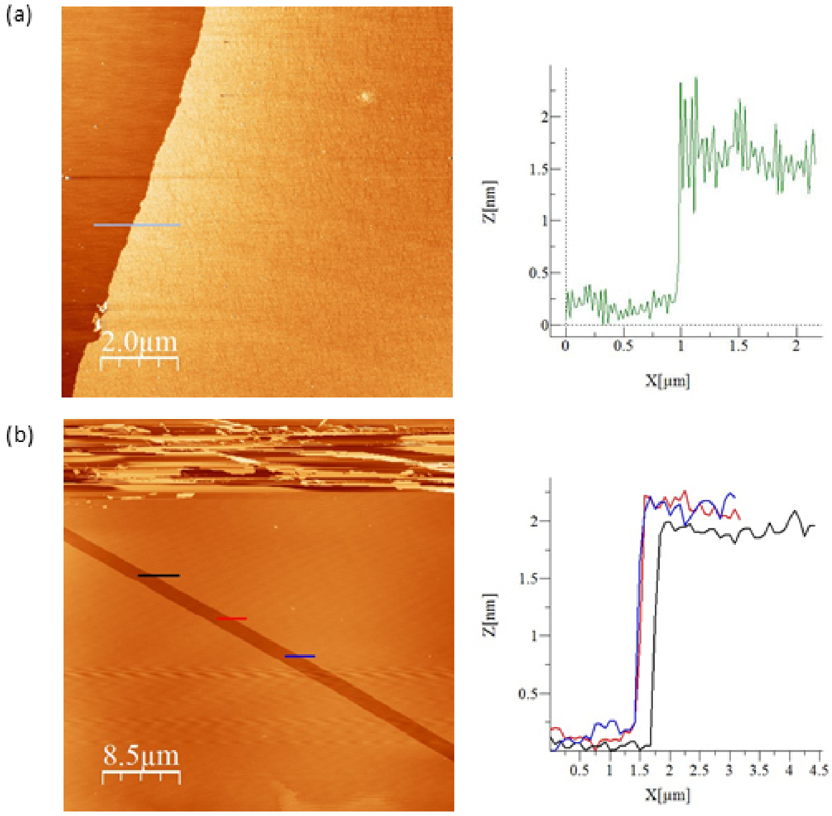

Figure 4.7: (a) AFM height analysis at an edge of the monomer layer on mica. The measured height of 1.8 nm corresponds to a monolayer. (b) AFM height analysis at a crack in the irradiated layer on mica. The measured height of the irradiated layer is 2.0 nm.

These values are in good agreement with the values obtained for monomer **11**.[62] While both values are slightly higher than what was calculated from the molecular model (1.6 nm) they were too small to correspond to double- or even multilayers. The discrepancies between molecular model and measured film height may be due to layers of water trapped between film and substrate. The transfer therefore did not seem to affect the monolayer nature adopted by the amphiphilic molecules at the air/water interface. Furthermore, it showed that the reaction that took place upon irradiation of the monolayer at the air/water interface was confined within a single layer, an aspect that was of particular importance to rule out other exotic mechanisms that could also have accounted for the loss of excimer fluorescence.

In summary, spreading a solution of monomer **2** on the LB trough and compressing to a surface pressure of 20 mN/m led to the formation of a homogeneous film that exhibited exclusively excimeric emission, meaning that the diazaanthracenes were face-to-face stacked. Irradiation of this film led to (1) a disappearance of excimer emission and by extension a consumption of excited diazaanthracene pairs and (2) an increase in mechanical coherence which can be correlated to a minimum conversion of 65%, and (3) an increase of the carbon sp^3 content as measured by XPS. All the while, the film consisted of a monolayer, so that the chemical transformation taking place could only occur in two dimensions (within the layer), between neighbouring monomers. While there was evidence that the suggested polymerization took place, we refrain from postulating it at this point as, contrary to the monomer system **1** studied in the previous chapter, there was no direct spectroscopic proof for the nature of the netpoints formed.

4.6 Comparison of Monomers 1 and 2

Both monomer **1** and **2** are amphiphilic and based on anthracene derivatives as reactive units. The anticipated connection reaction in both cases was the photoinduced [4+4]-cycloaddition of anthracenes of neighboring monomers which was chosen due to its high yield (in the single crystal) and its reversibility.

LB films of monomer **1** and monomer **2** were fluorescent due to their anthracene-derived reactive units and exhibited excimer emission in the fluorescence spectra on solid substrates, a sign that their π systems are interacting in the closely packed monomer films. On the other hand, in solution, the monomers only exhibited monomeric emission. In both cases, the excimer fluorescence could unequivocally be attributed to the proximity of the reactive units of the monomers to one another by excitation spectroscopy. The excimer emission was lost in the case of the polymerized films derived from both monomers. In the case of monomer **2**, the loss of excimer fluorescence during irradiation could be monitored at the air/water interface. This experiment could not be performed with films of monomer **1** as the set-up uses an excitation source of wavelength λ = 373 nm. At this wavelength, monomer **1** absorbs so weakly that it was not possible to record a fluorescence response.

The height analysis of the films synthesized from monomer **1** and **2** indicated the height of a monolayer, regardless of whether the monomer film or the polymerized film were measured. In both cases, the presence of water in the AFM height analyses led to a slightly larger height than predicted by the molecular models, but nevertheless the heights were in good agreement with those of single layers in all cases.

For both monomer **1** and **2**, irradiation of the film at the air/water interface led to an enhancement of the mechanical coherence of the films. In case of the polymerized films, spanning of Cu TEM grids was observed by SEM while this was not the case for the monomer film. The enhanced mechanical coherence indicates that covalent bonds were formed between monomer units upon irradiation. In the case of polymerized LB films of monomer **1**, spanning occured over larger areas. It was not clear whether this could reflect a higher conversion, as the amount of spanning also naturally varies from sample batch.

In both cases, XPS showed an increase of the sp^3-hybridized carbon content for the irradiated films but it was not precise enough to estimate the conversion or account for all observed changes. In particular, the different chemical environment of the carbons of monomer **1** allowed distinguishing them well, while in the case of monomer **2** there was only one peak for carbon that had to be deconvoluted and even then did not allow for distinction between carbon sp^2 and carbon sp.

There are several differences in the monomer structures that affect the monomers' behavior at the air/water interface and thus the obtained polymerized film. Most importantly, they influenced the capability of elucidating the structure of the polymerized films.

In contrast to monomer **1**, monomer **2** has greater flexibility. This was reflected in the study of the films by Brewster angle microscopy, where the domains formed by monomer **2** at the air/water interface coalesced over time and exhibited a very homogeneous grey tone. In contrast, monomer **1** formed domains that did not merge, but exhibited a rather rigid behaviour, even tearing when compressed into another by the barriers rather than merging together. The flexibility also leads to a loss of visible order upon polymerization of monomer **2**, as shown by DFT simulation using monomer **11**.

Monomer **2** is structurally much more complex than monomer **1** and this made structure elucidation much more challenging due to several reasons. First, the abundance of functional groups in monomer **2** made it necessary to rule out side reactions, such as the [4+2]-cycloaddition between acetylene and anthracene which had been observed before in the single-crystal approach,[42] but ruled out at the air/water interface in the case of monomer **11**.[153] Furthermore, in the case of monomer **1**, it was possible to synthesize reference compounds for a UV-vis study, as it was the tetrafluoroanthracenes that contributed to the absorption spectrum, while for monomer **2** the multitude of absorbing functional groups (phenyls, acetylenes, diazaanthracenes) did not allow to rationally choose a simple reference compound that would reflect all changes encountered during polymerization and adopt the required *syn* conformation that the diazaanthracenes have in the monomer film. Successful AFM/STM imaging requires that the pores of the polymer are still visible and the high flexibility of monomer **2** was detrimental in this regard, while the more rigid films of monomer **1** were successfully imaged using these techniques.

In the case of monomer **1**, TERS enabled the chemical connectivity to be elucidated and the conversion of this reaction to be estimated (90%), as well as defects within the film to be visualized. This is possible since both monomer and polymerized LB film exhibited a characteristic signal in the Raman spectrum. TERS of monomer **11** had not shown a characteristic band for the polymerization product and therefore it was not suitable for investigating the polymerization product of monomer **2**. As mentioned before, no simple reference compound could be used to elucidate the polymerization product by UV-vis spectroscopy. While these methods were highly useful in the case of monomer **1**, they did not allow to elucidate the exact nature of the covalent bonds formed between the diazaanthracenes. The unsuccessful characterization of films formed from monomer **2** can therefore be attributed to a combination of factors, most notably the chemical complexity of this system, the flexibility and the lack of characteristic signals in Raman spectroscopy.

The spectroscopic methods that were suitable for elucidating the chemical connectivity of the polymer composed of monomer **1** did not lead to a successful structure elucidation which shows that sensitivity of the method is not the only factor that has to be considered for the characterization of two-dimensional polymers.

In the case of monomer **1**, evidence for the crystallinity of the monomer film at the air/water interface was provided by high-resolution Brewster angle microscopy. This experiment was not carried out with monomer **2**, as the instrument was in a different facility.

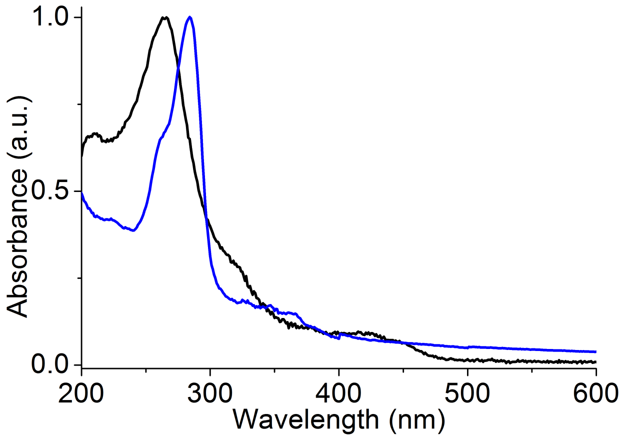

Figure 4.8: Comparison of normalized absorption spectra of monomer **1** film (blue) and **2** film (black) on quartz.

The extended conjugation of monomer **2** has a direct effect on its absorption spectrum, which extends to longer wavelengths, well into the visible region, compared to the absorption spectrum of monomer **1** (see fig. 4.8). This aspect is of particular interest with regard to the topic of the next chapter.

Chapter 5

Towards Applications: Molecular Paper

For centuries, the way to preserve and store information was by writing or drawing onto walls, papyrus or cellulose paper with some sort of ink. In the digitalization age, information is encoded in basic units of information (bits) of 0 and 1. 0/1 can stand for true/false, on/off or yes/no. This binarisation of information has expanded the means for writing and information storage. A few examples include magnetic writing,[162] optical writing,[163] and, even more recently, qubit storage[164–166] and storage using DNA.[167] Common to these techniques is the desire to miniaturize the writing as much as possible, in order to cope with the ever-increasing amounts of data that have to be stored.

One potential application of two-dimensional polymers already mentioned in the introduction could be as miniaturized optical devices. In the case of anthracene-based monomers, irradiation is accompanied by a measurable optical change, namely the loss of excimer fluorescence. This is due to the fact that anthracene-based monomers are fluorescent, while their corresponding dimers and thus the two-dimensional polymer, are not. This reaction is reversible. If it turned out that polymerization could be carried out on solid substrates and that this polymerization could be confined to the irradiated areas, a loss of fluorescence can be induced in specific areas of the monomer film. The change in fluorescence can be considered as a binary on/off state, such that the loss of fluorescence in the film could be used for data storage in optical recording devices as a molecular paper.

For the films to be suitable as optical recording devices, they would have to fulfill several criteria:

1. Transfer of monomer layers preserves the excimer fluorescence observed at the air/water interface, leading to strongly fluorescing monolayers.
2. The fluorescent monomer layers show reasonable lateral extension, allowing them to be incorporated into an optical device.
3. Irradiation of a predetermined area leads to a measurable optical change which is durable and not subject to ageing.
4. This optical change can be reversed.

The aspect of on-substrate polymerization was also of interest with regard to a different issue encountered in the Langmuir approach. Conducting polymerization directly on solid substrates, post-transfer, instead of at the air/water interface (pre-transfer) was of particular interest in view of obtaining laterally extended polymer films: A big advantage of the air/water interface approach is the large lateral size of the sheets that can be obtained, which is in theory only restricted by the size of the Langmuir trough and by the lateral extension of the irradiation. However, the issue of domains within the film also plays a role at the air/water interface, limiting polymer size. Even disregarding the limitation of lateral size due to domain formation within the film, the area of the film that can be polymerized at the air/water interface is limited by irradiation time. This is because extended irradiation leads to evaporation of the aqueous subphase which causes the film to leak outside the barriers and to a loss of control over film formation. It would therefore be of advantage to be capable of performing the polymerization post-transfer, directly on solid substrates. While this would not prevent the formation of domains that limit the lateral size of the film, at least irradiation could be carried out without limitations. This would reinforce the main advantage that this approach has over the single-crystal approach whose major drawback is the limited sheet size of the obtained two-dimensional polymers. The sheet sizes are limited in size by the dimensions of the crystal - depending on the orientation of the lamellar structure within the crystal and the exfoliation conditions, the obtained sheets are on the order of a few hundred micrometers at best.[64] It was with these considerations in mind that the on-substrate polymerization was investigated.

5.1 Choice of Monomer

In principle, all monomers that fulfil the above criteria could be considered for this project. Apart from monomers **1** and **2** which were introduced in the previous chapters, a third monomer was also considered, monomer **3** (see fig. 5.4a). This monomer carries anthracenes as reactive units and is orientated at the air/water interface due to the hydrophilic diethylene glycol chains attached to one of the central benzene rings. Monomer **3** was synthesized and its films were characterized in terms of spanning, film height and presence of excimer fluorescence by Dr. Marco Servalli. It exhibited excimer fluorescence at the air/water interface, a film height corresponding to a monolayer and the capability of spanning TEM grids after having been irradiated at the air/water interface (unpublished results).

All monomers **1**, **2**, and **3** have reactive units that are anthracene-derived and thus their corresponding monomer films are fluorescent. From the point of view of structure elucidation, monomer **1** is surely the most thoroughly studied and best characterized system of the three. However, monomer **2** is more flexible which may lead to less brittle films and, by extension, presumably to more extended domains. More importantly, the absorption spectrum of monomer **2** showed that the monomer absorbed up to a wavelength of λ = 475 nm, whereas monomer **1** did not absorb above the wavelength of λ = 390 nm (see fig. 4.8). The absorption range of the monomer is of particular importance, as it allowed switching from an UV irradiation source to an irradiation source that operated in the visible range. This was relevant, since the fluorescence microscope which was used in this study did not allow for UV irradiation. Both monomer **2** and monomer **3** absorb in the visible range. Furthermore, monomer **3** had exhibited a particularly intense fluorescence which also made it an interesting candidate. In the end, monomers **2** and **3** were investigated in terms of their suitability in optical recording films.

5.2 Molecular Paper

5.2.1 Monomer 2

The behavior and properties of monomer **2** were explored in the previous chapter. As mentioned before, transferring a monomer monolayer of monomer **2** onto quartz did not lead to a loss of the excimer fluorescence observed at the air/water interface and thus the layer presumably retained its packing adopted at the air/water interface. This was not to be taken for granted, as there are several forces during transfer – shear, drying, adsorption amongst others – that could disrupt the packing assumed at the air/water interface. The fluorescence remained unchanged not only upon transfer onto quartz but also upon transfer onto various other non-flexible substrates.

The transferred fluorescent monomer layers were visualized in a confocal laser scanning microscope (CLSM) using a laser line of λ = 458 nm. At this wavelength, the monomers absorb only slightly as it is at the very edge of their absorption spectrum (see fig. 4.5). The emission spectra of the monomer monolayer on different substrates were recorded with the CLSM (see fig. 5.1).

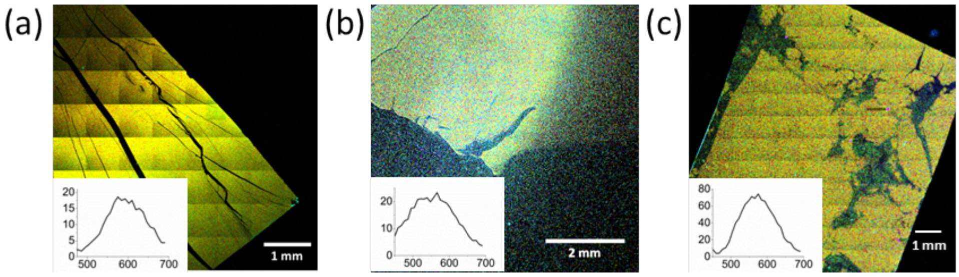

Figure 5.1: (a) The image was composed of 8x8 850 μm x 850 μm images, showing the monomer layer on C_{18}-SAM modified SiO_2/Si wafer and the excimer emission recorded with the CLSM using a laser line of 458 nm. (b) An image of the monomer layer on polystyrene and its excimer emission recorded with the CLSM. As the substrate was quite rough it was difficult to focus over large areas. (c) The image was composed of 10x10 850 μm x 850 μm images, showing the monomer layer on SiO_2/Si and its excimer emission recorded with the CLSM.

For all substrates, the monomer layer exhibited homogeneous excimer fluorescence over large areas, exhibiting occasional cracks or gaps. These gaps had also been observed directly at the air/water interface (see fig. 4.3) while the cracks may have formed during transfer. The fact that the fluorescence is nevertheless homogeneous over large areas of the substrate showed that intermolecular forces must exist that retain the packing. In fig. 5.1, the fluorescence images of the monomer layer on three different substrates are shown. These substrates varied in roughness (rough polystyrene, smooth Si wafers) and hydrophobicity (hydrophilic SiO_2/Si, hydrophobic polystyrene and C_{18}-SAM modified silicon wafer).

Using a laser line of λ = 405 nm, it was indeed possible to irradiate designated areas of the film with a spatially confined loss of fluorescence.

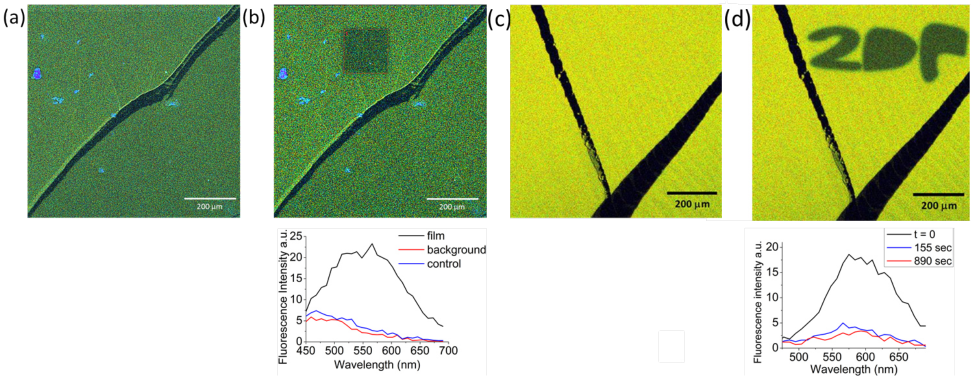

Figure 5.2: Writing a rectangle on the film on a PS substrate (a, b) and "2DP" on a C_{18}-SAM substrate (c, d). The writing is accompanied by a loss of excimer fluorescence (b, d).

The loss of fluorescence had two important implications:

1) It might indeed be possible to carry out irradiation post-transfer. It was therefore of interest to show that the loss of fluorescence was due to polymerization.

2) This loss of fluorescence and its restriction to certain areas allow the creation of arbitrary patterns on the monolayer, therefore enabling writing on a single-molecule thin film.

Henceforth, the term "molecular paper"will be used for the monomer layer when used for writing purposes, as it is a single-layer thin film composed of molecules which can be written on in a controlled fashion and, theoretically, with a precision that is on the length scale of a few molecules.[18] Furthermore, the spatially confined irradiation at a wavelength of λ = 405 nm that leads to loss of fluorescence in this area will be called writing in order to distinguish the actual writing process from images that were recorded using a longer wavelength (458 nm), which nevertheless entails an irradiation, but with the purpose of visualizing the fluorescence of the film.

Writing was possible on several substrates (for examples, see fig. 5.2): glass, quartz, SiO_2/Si, polystyrene (PS), and C_{18}-SAM. The only two substrates where writing was not successful were gold (Au) and cyclic olefin copolymer (COC) film. In the case of Au, this may be due to the reflectivity that the metal has in the visible range.[168] In the case of COC, a thin, flexible material, removing the COC substrate from the dipping stage after film transfer without bending the substrate was impossible. Therefore, the bending of the substrate may have affected the film.

Interestingly, it was possible to reverse or 'erase' the writing by heating the samples to 200 °C for two hours (see fig. 5.3). To prevent oxidation of the film during heating, this process was carried out under N_2. This restored the fluorescence completely, regardless of the substrate used. Some substrates were not suitable for this treatment and were therefore not subjected to it, for example polystyrene which would melt at such high temperatures. Initially, a heating time of 4 hours was used, but after a systematic investigation of the heating time it was established that heating for 2 hours was sufficient to restore the fluorescence.

While heating the samples to 200 °C led to a recovery of the excimer fluorescence in the formerly bleached part, it was not possible to re-write onto the layer after the heat treatment. Irradiating areas of the sample after heat treatment did not lead to a loss of fluorescence, regardless of whether the irradiation was carried out in the area that had formerly been irradiated or in a new area. The heat treatment, while not destroying the fluorescence or other features of the film on a macroscopic scale, nevertheless seemed to have affected the packing of the monomers on a molecular scale. Plausible explanations could be slight changes in the packing of the monomer due to the heat or an onset of monomer desorption from the substrate at this temperature. No experiments were carried out that would allow to rule out one or the other.

However, it was attempted to circumvent this problem by using a different approach for the erasing of the writing. For this approach, the quartz slides were irradiated at a wavelength of $\lambda = 220$ nm under N_2. At this wavelength, the monomers do not absorb but the [4+4]-cycloaddition product does. It is therefore plausible that the [4+4]-cycloaddition of diazaanthracenes could be reversed using this treatment. A number of irradiation conditions were

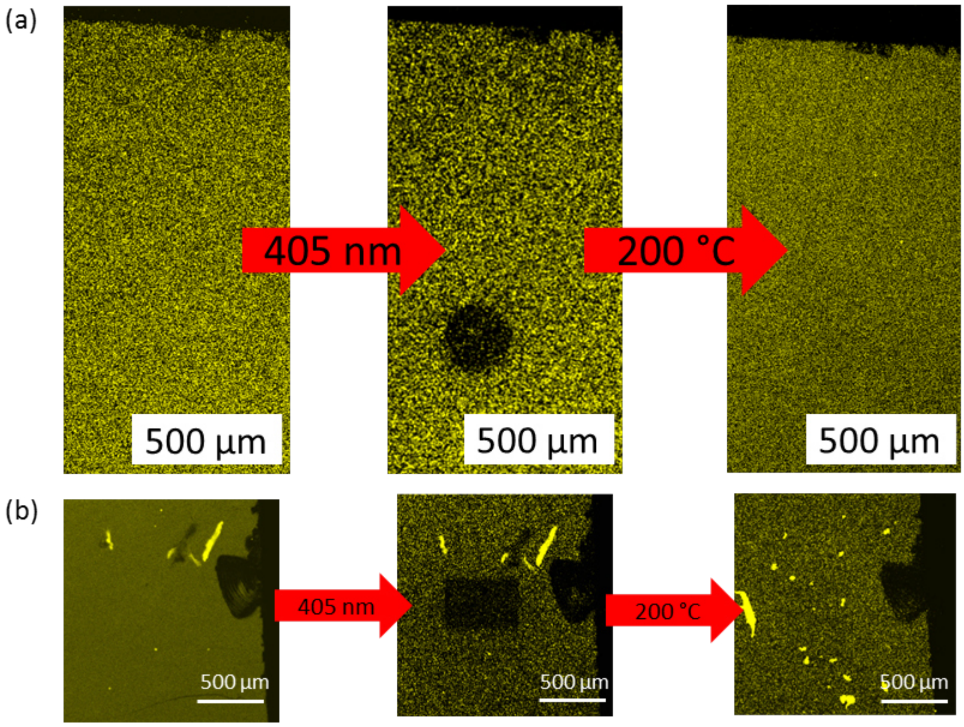

Figure 5.3: (a) Writing of a circle on the molecular paper on SiO_2/Si using a laser line of λ = 405 nm, then erasing by heating to 200 °C for two hours. (b) Writing of a rectangle into the molecular paper on SiO_2/Si using a laser line of λ = 405 nm, then erasing by heating to 200 °C for two hours.

tested. As the *ex-situ* irradiation of the substrates required them to be removed from the microscope slides, the samples grew increasingly dirtier with each irradiation cycle. None of them succeeded in erasing the writing (see tab. 5.1). In the case of monomer **1** an irradiation time of 2 s using this irradiation set-up was sufficient to induce the reversion reaction of the polymer. While it is possible that monomer **2** has entirely different reaction kinetics, one would expect to see the onset of a reversion reaction after 5 minutes. However, this was not the case.

From the point of view of applications, this implies that the molecular papers could only be used for non-rewritable optical devices and thus permanent data storage.

Films composed of monomer **2** therefore fulfilled all four criteria stated at the beginning of the chapter: The monomer films exhibited excimer fluorescence after transfer onto solid substrates, the films showed considerable

Table 5.1: Irradiation conditions tested on different substrates. The irradiation time was gradually increased, the irradiation length indicated is the cumulated irradiation time.

Sample number	Substrate	Irradiation Length (Cumulative)	Outcome
1	quartz	2 s	no change
		4 s	no change
		64 s	no change
		364 s	slight lessening of fluorescence
2	quartz	30 s	no change
		330 s	no change
3	SiO_2/Si	10 s	no change
		310 s	no change

lateral extension, and irradiation within a specified area of the film led to an optical change (disappearance of the fluorescence) which could be reversed by heating. Using the CLSM, it was possible to write and erase writing down to a scale of about 30 μm. If the writing and erasing was due to [4+4]-cycloaddition and reversion, respectively, the writing could theoretically be performed on the nanometer scale, at monomer level. This is provided that an irradiation source can be focussed well enough to achieve these length scales – a molecular pen, in a manner of speaking. It was envisioned to do this with the help of a metalens, however, calculations showed that the required metalens, that allows focussing at the necessary excitation wavelength, could not be constructed.

Before going into the possible mechanisms responsible for the writing, the films of monomer **3**, a further potential candidate will be investigated.

5.2.2 Monomer 3

In order to gain more understanding of the optospectroscopic characteristics of monomer **3**, LB films formed from **3** were characterized in terms of their optical spectroscopic behavior. For this, the monomer film was transferred onto quartz from the air/water interface at a surface pressure of 20 mN/m. The absorption and emission spectra of the monomer film on quartz were measured.

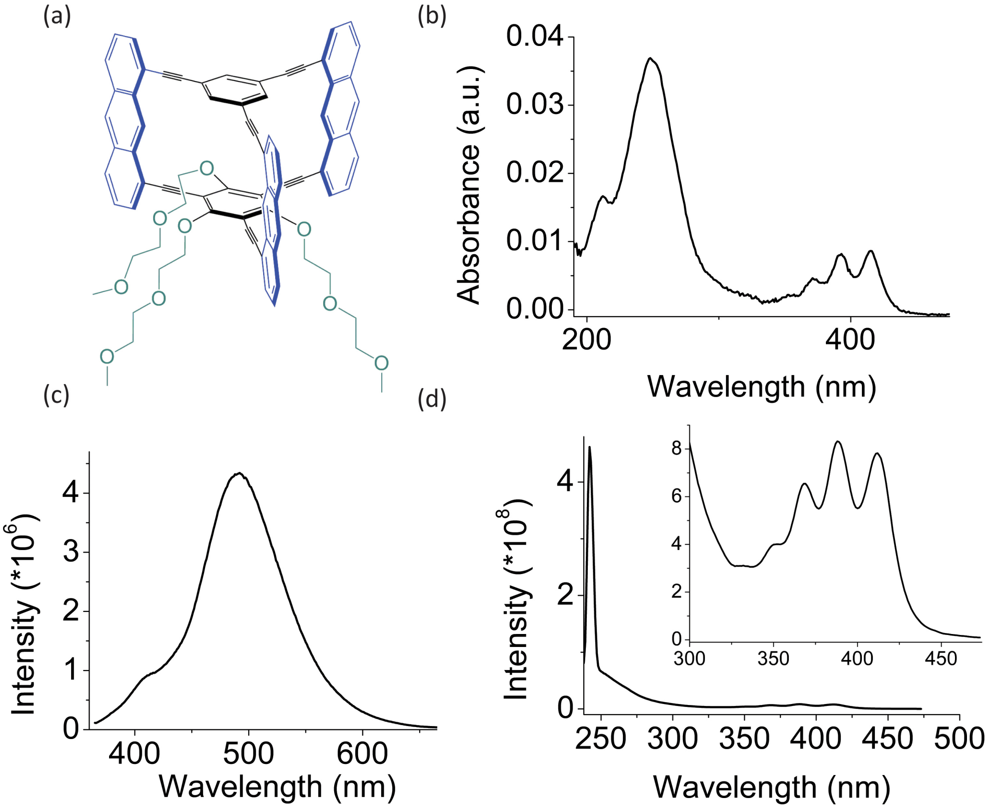

Figure 5.4: (a) Structure of monomer **3**. Absorption spectrum (b), fluorescence spectrum (c) and excitation spectrum (d) of a monomer **3** LB film on quartz.

Furthermore, its excitation spectrum was recorded. The results are shown in fig. 5.4. Even as a monolayer, the absorption spectrum showed strong absorption well into the visible region. The characteristic absorption signature of anthracenes dominated the spectrum with a particularly well-defined vibrational fine structure. The well-resolved fine structure was a direct result of the fact that unsubstituted anthracenes were used. The expansion of the absorption into the visible domain of the spectrum was a consequence of the extended conjugation of the molecule via the acetylene bridges. As mentioned above, the absorption above a wavelength of λ = 400 nm was a prerequisite for the monomer to be of interest in this project.

The emission spectrum of the monomer film on quartz showed unstructured excimer fluorescence centered around λ = 490 nm which was a first sign that the monomer units experience face-to-face packing. This excimer emission had also been observed at the air/water interface, indicating that film transfer did not disrupt the assumed packing. Thus, it met the first requirement mentioned above.

The excitation spectrum of the monomer LB film on quartz was recorded by monitoring the fluorescence at its maximum while sweeping the excitation wavelength range. The excitation spectrum confirmed that the observed excimer fluorescence exclusively stemmed from the monomers, as it was superimposable with the absorption spectrum of the monomer film and showed no additional bands that would have indicated a fluorescent impurity.

Investigation of the monomer film using the confocal laser scanning microscope revealed a laterally extended film with few cracks. These cracks may have been caused during transfer from the air/water interface or could be a result of the way the monomers arrange themselves at the air/water interface. The former is more likely and the fact that the films still showed excimer fluorescence is an indicator that some molecular interactions had to exist between neighboring monomers in order to preserve *face-to-face* stacking. The packing itself was not completely homogeneous. A lambda scan, a scan that records the specific fluorescence in each pixel, showed different types of excimer fluorescence, visualized by cyan and dark blue areas of the film (see fig. 5.5a,b). The colors recorded during a λ scan reflect differences in the fluorescence of these areas and small shifts in the excimer fluorescence are represented by a change of color. Some of the dark blue areas exhibited an intense fluorescence, such that saturation of the detector occured as can be seen from the cropped appearance of the curve (see fig. 5.5c). A second fluorescence measurement in a less intensely dark blue area revealed that in the dark blue areas, the maximum of the excimer fluorescence is hypsochromically shifted to approximately 450 nm. The cyan fluorescence, on the other hand, is centered around 500 nm (see fig. 5.5c). As films in these images were deposited on quartz, the fluorescence was exclusively due to the monomer and the substrate did not contribute to the fluorescence, as quartz does not absorb above a wavelength of 190 nm. These differences in fluorescence cannot be measured with a conventional emission spectrum which averages over a larger area. The differences in fluorescence could be due to different packings of the monomer within the film. Unfortunately, it was not possible to determine which emission corresponded to which packing. It was, however, only possible to write within the cyan area of the film. Attempting to write on the dark blue areas of the film left the fluorescence completely unaffected. These findings indicated that the packing found within the dark blue region is one that does not permit anthracene dimerizations with neighboring monomer units. This point will be further discussed in the next section that deals with the origin of the writing.

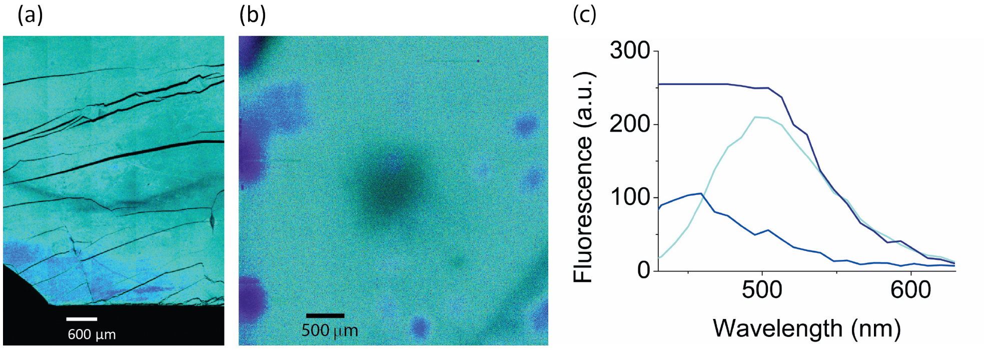

Figure 5.5: (a) Fluorescence of the monomer film of **3** on quartz recorded with a lambda scan. (b) The dark blue and cyan areas of the film correspond to a difference in fluorescence. The corresponding color-coded fluorescence spectra are shown in (c).

Writing into the monomer film in the cyan areas led to a significant loss of fluorescence in that area. As in the case of monomer **2**, films of monomer **3** can be used as molecular paper. Attempting to reverse the writing led to an interesting observation: the fluorescence of the film changed once more. This change, which occured upon heating of the substrate to 200 °C for two hours, but which was also observed to appear over time at room temperature, led to a drastic bathochromic shift of the excimer fluorescence maximum by approximately 100 nm. The shift was not restricted to certain areas (for example, only to areas of the film exhibiting cyan fluorescence) but was observed over the entire substrate (see fig. 5.6b). Writing into films of this changed fluorescence was still possible (see fig. 5.7a).

While the change of fluorescence could in principle be due to evaporation of residual water, it would be quite a significant shift for a mere change of environment. A different reason could be that the monomer film underwent a structural reordering of the film over time, presumably to a packing that is thermodynamically more favored on solid substrates. Furthermore,

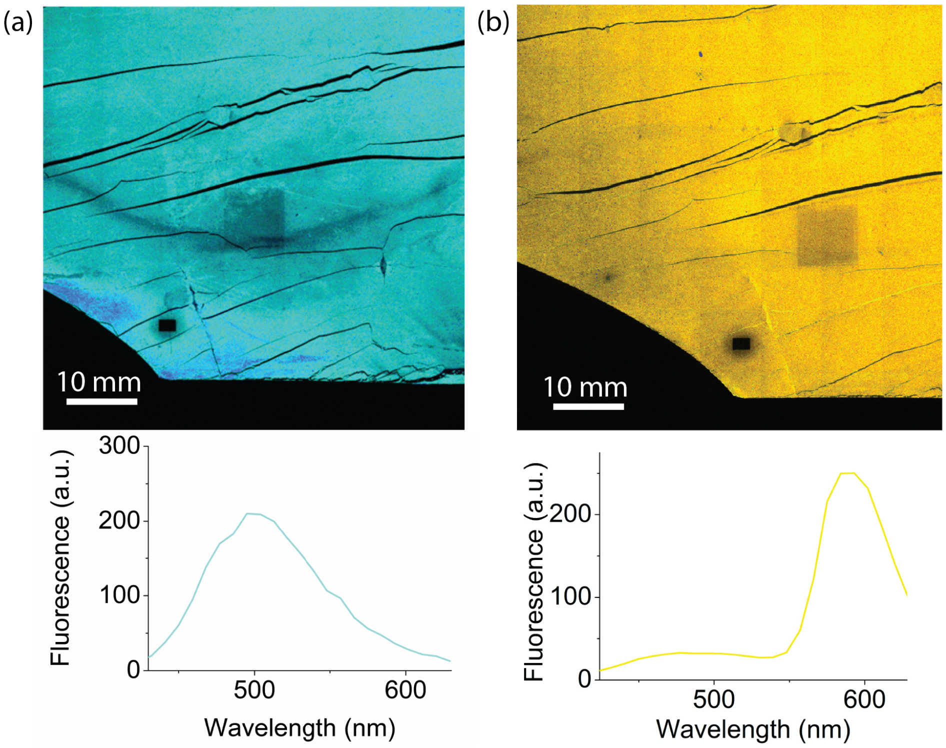

Figure 5.6: (a) Image of the fluorescent monomer film of **3** on quartz recorded with a lambda scan. Below it, the fluorescence that corresponds to the cyan color is shown. (b) After heating, this same sample showed a completely different fluorescence. The fluorescence was bathochromically shifted to 600 nm, as can be seen in the fluorescence curve extracted from the image.

one could observe that writing was not reversed by heating to 200 °C for two hours. Heating for a further two hours also did not lead to a reversal of writing. Whether different reaction conditions, such as higher reaction temperatures, would be required for erasure could not be ruled out.

After the change of the fluorescence, the type of excimer fluorescence of the film did not change further, but remained stable over a long period of time. Even after a year, the fluorescence exhibited the same maximum and the writing was still clearly visible. It was, however, possible to see a decrease of the fluorescence intensity in general, which was attributed to ageing (see fig. 5.7b).

Once more, it was not possible to correlate the observed fluorescence with a specific packing. As mentioned in the introduction, Kato's work found

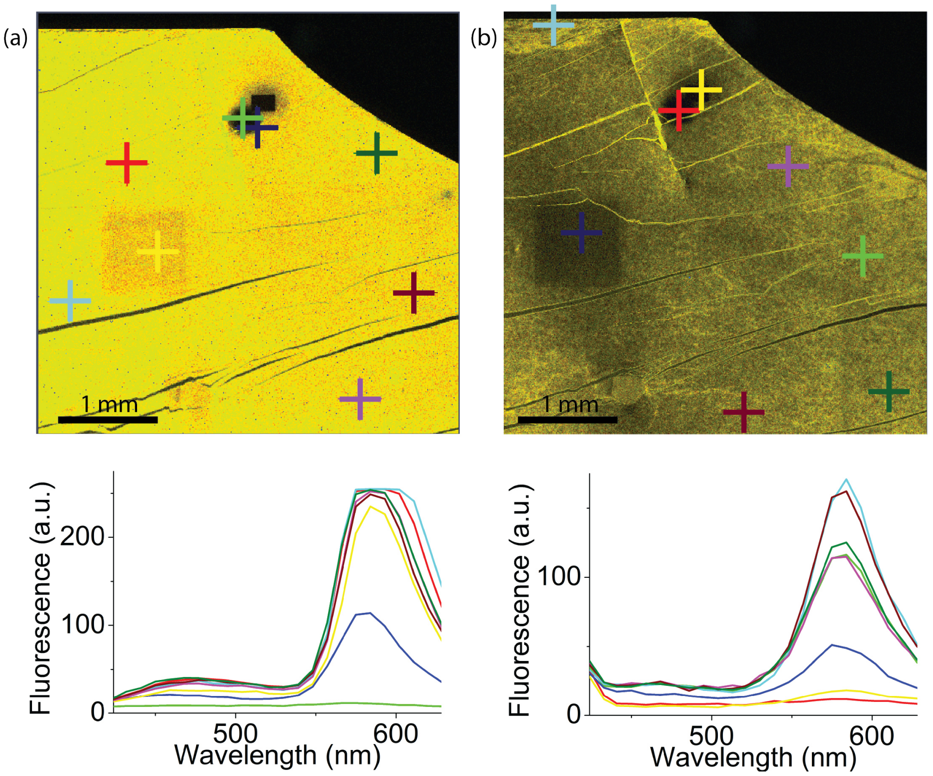

Figure 5.7: (a) Image of the fluorescence of the monomer film of **3** on quartz recorded with a lambda scan after heating to 200 °C. Below it, the fluorescence curves extracted from different areas of the image indicated by crosshairs are shown. The circle was bleached onto the layer after it had already changed its fluorescence. (b) The same sample after one year. The fluorescence is the same, as can be seen in the fluorescence curves extracted from areas of the image indicated by crosshairs, but the film showed signs of ageing. The bleached regions remained unchanged.

a correlation between extent of *face-to-face* stacking of the anthracene π systems and the maximum and FWHM of their excimer fluorescence. Applying these findings to the observed excimer fluorescence, one could tentatively assign the yellow excimer fluorescence to a full overlap of the anthracene moieties at an optimal distance (ca. 3.5 nm). The cyan fluorescence could correspond to a packing where the anthracenes' π-π systems have enough overlap to react but where either the distance between anthracenes is greater or there was slipping from the full overlap. For a definite answer to this question, theoretical calculations of the excimer fluorescence would be required. As writing was possible in regions of cyan or yellow fluorescence, but not in regions of dark blue fluorescence, it is assumed that dark blue fluorescence is presumably exhibited by a packing of unknown nature where reaction between monomers cannot take place. The consequences of this observation for the mechanism behind writing and erasing will be further discussed in the following section.

Therefore, while films of monomer **3** showed excimer fluorescence over large areas, they also exhibited what was most likely different packings within one film and therefore the existence of domains of different packing, something that has not been observed in films composed of monomer **1** (see section 3.6.1) or monomer **2**, which did not exhibit domains of different fluorescence within the microscope's resolution. Furthermore, films of monomer **3** showed a change of fluorescence over time which might be an indicator that the initial packing is not stable but subject to rearrangement. Finally, the writing in molecular paper composed by monomer **3** was not reversible. With these results in hand, it became obvious that monomer **2** was the better candidate for molecular paper. It was therefore with this monomer that further investigations into the origin of writing were conducted.

5.3 Origin of Writing

The loss of excimer fluorescence upon irradiation with a laser line of λ = 405 nm and its recovery by heating to 200 °C could be due to various distinct processes. The three most probable ones are shown in fig. 5.8.

Quenching (and thereby irreversible destruction) of the fluorophore might occur under intense UV irradiation. This phenomenon is used in fluorescence recovery after photobleaching (FRAP) where the migration of fluorophores into a photobleached region is monitored to assess certain diffusion kinetic parameters.[169] The photobleached fluorophores are irreversibly destroyed and fluorescence in the bleached region can only be recovered by migration of fluorophores into the area (process 1).

Oxidation of the diazaanthracenes would also result in loss of fluorescence. Usually, oxidation of anthracenes and their derivatives leads to anthraquinone formation via the intermediate *endo*-peroxides.[170] As the C9 position of the diazaanthracenes is blocked by a methyl group, oxidation would stop at the stage of *endo*-peroxides (process 2). Oxidation of anthracenes can occur in the presence of oxygen under UV irradiation and in the case of a reaction in solution, is concentration dependent. If a packing existed that had all anthracene reactive units poised to react with their neighbor, it is unlikely that oxidation could compete. Nevertheless, this needed to be ruled out.

Finally, dimerization of neighbouring DAA units and thus polymerization would also lead to a loss of fluorescence (process 3).

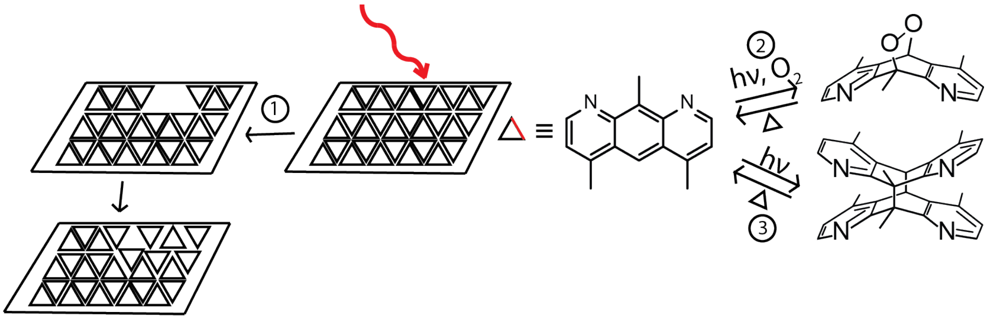

Figure 5.8: Possible mechanisms behind disappearance and recovery of fluorescence.

In order to identify the underlying phenomenon and rule out the other potential pathways, several control experiments were carried out. In the case of both oxidation and polymerization, the loss of fluorescence is reversible by heating, while in the case of bleaching, the fluorophores are destroyed permanently and irreversibly. This means that once the fluorophores have been destroyed, the fluorescence cannot be recovered unless fluorescent monomers diffuse into the bleached areas. Monitoring the samples over a time period of three months showed that the non-fluorescent areas remained unchanged and the borders of the bleached regions stayed sharp. Heating the samples for 2 hours to 100 °C, a temperature that is still well below the temperature that leads to cycloreversion,[171–173] had no effect on the fluorescence of the samples either (see fig. 5.10). If the recovery of fluorescence was only due to migration of fluorophores into the bleached regions, one would expect to see the onset of this process, either by heating to 100 °C or by monitoring the sample over a longer time period. Likewise, one would expect the fluorescent monomers to diffuse into the cracks between the films. Finally, one would expect the recovered fluorescence to be different from the initial one: since the packing of the monomers would be more loose, one would expect to see the emergence of monomeric fluorescence, although it must be said that the microscope's resolution may simply not be powerful enough to detect these changes. None of these three phenomena were observed. These findings do not support the mechanism of process 1.

As mentioned above, the fluorescence of the sheet was successfully recovered by heating the sample to 200 °C. This temperature is in the range required for the reversal of anthracene dimerization as it is reported in the literature. Both oxidation (process 2) and polymerization (process 3) are reversible.

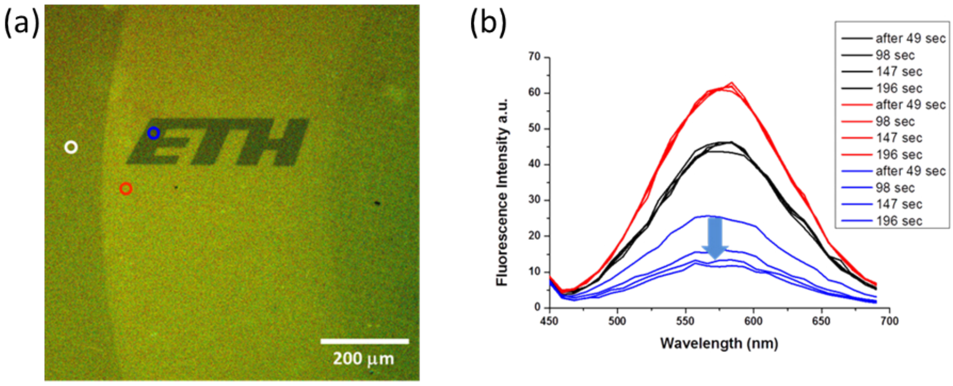

Figure 5.9: (a) Writing on monolayer of **2** on SiO_2/Si under reduced oxygen conditions: A TEM grid served as a mask for writing in a quartz cuvette under N_2 with an LED of 400 nm. This was followed by writing of "ETH" with the CLSM using a laser line of 405 nm. The fluorescence intensity decay in three different spots of the image is shown during writing at the CLSM. The fluorescence spectra recorded at the red, blue, and white circle are shown as red, blue, and black spectra, respectively.

To rule out oxidation as an underlying mechanism, the irradiation was performed under oxygen-reduced conditions (see fig. 5.9). To start with, the irradiation was carried out in an external irradiation set-up in a quartz cuvette that was continuously flooded with argon. This set-up lowered the residual oxygen content to 35 ppm and allowed making an imprint of a TEM grid on the film. Afterwards, the irradiation was carried out inside the CLSM with a nitrogen-flooded flow cell, which had a residual oxygen content of 1000 ppm. There, the letters "ETH" were written onto the film in a region formerly covered by the TEM grid. With both irradiation set-ups, writing into the monomer layers was still possible. The irradiation set-up used outside the CLSM was less powerful than the laser of the CLSM, which explains why the imprint of the TEM grid is less distinct than the ”ETH” pattern. The loss of fluorescence in different parts of the film was monitored (see fig. 5.9b). The fluorescence recorded during the writing process in the blue, red, and white circle is visualized by the blue, red, and black spectra, respectively. The fact that writing is also possible under oxygen-reduced conditions made it less likely that process 2 is the underlying mechanism for fluorescence disappearance and recovery. However, in both experimental set-ups, the oxygen content is not quite low enough to completely rule out oxidation.

One further aspect that should be considered is the fact that irradiation at the air/water interface led to the formation of mechanically coherent films. If the process occuring at the air/water interface and on solid substrate during irradiation was the same, oxidation could not account for this increase in mechanical coherence, as a mere oxidation of monomers would not increase the mechanical coherence of the film. This observation provided indirect evidence for the irradiation on solid substrate.

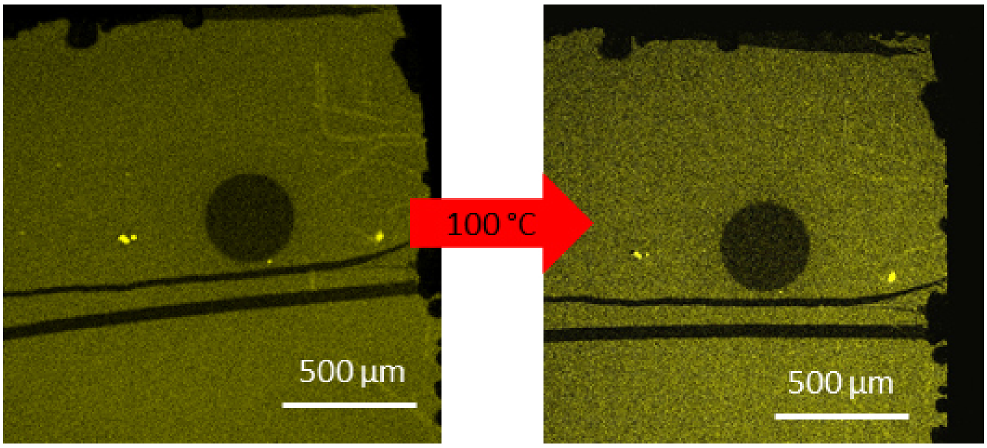

Figure 5.10: Left: SiO_2/Si wafer with a circle bleached into the film. Heating the wafer to 100 °C did not affect the writing (right).

Finally, the packing of the monomers in the film is only relevant for mechanism 3. Therefore, the fact that writing was not successful on a substrate that had been bent after LB film transfer (monomer **2** on COC), as well as the observation that bleaching was only possible in areas of a certain fluorescence in the case of monomer **3** was a strong argument for the polymerization mechanism. While bleaching in areas of ”yellow” and ”cyan” fluorescence was possible, it was not successful in areas of "dark blue" fluorescence, as mentioned before. However, the type of fluorescence, which reflects the packing of the monomers, should be irrelevant in the case of oxidation of monomers or in the case of the irreversible destruction of fluorophores, as these proceed regardless of how the monomers are arranged with respect to one another. A loss of fluorescence due to polymerization is the only mechanism where the packing of the monomers is of relevance. The observation that the type of fluorescence played a role in the writing therefore indicates that process 3 takes place, assuming that the same mechanism took place in both films of monomer **2** and monomer **3**. The observation that the writing was not reversible in the case of films composed of monomer **3** does not support process 3, however, one cannot rule out that different reaction conditions are required or that a different process is taking place in the case of this monomer.

While ruling out the other two mechanisms does not mean that one can unambiguously attribute the phenomenon to process 3, it seems nevertheless plausible that the loss of excimer fluorescence due to irradiation and its recovery by heating are due to [4+4]-cycloaddition and cycloreversion of neighboring monomer units, respectively. It also shows that monomer **2** fulfills all the conditions required for optical recording, as listed above. For incorporation into an optical recording device, the question of the exact mechanism behind writing and the reversal of writing is not essential – even in the case of oxidation, the writing could be restricted to a molecular scale. However, from the point of view of structure elucidation, these findings were of great interest. Contrary to monomer **1** discussed in the previous chapter, the complex molecular structure and the flexibility of monomer **2** did not allow to elucidate the exact structure of the polymerized film obtained at the air/water interface. In the absence of hard spectroscopic evidence, the finding that the effects of irradiation - namely, loss of fluorescence - could be reversed and the excimer fluorescence recovered strongly indicate that a packing is adopted where monomers are packed in a way that they can undergo [4+4]-cycloadditions, as would be the case in the postulated packing (see fig. 4.2c). Furthermore, it showed that polymerization may indeed be possible post-transfer, on solid substrates.

The monomer films of monomer **2** and **3** can both be used as molecular paper - but only on films of monomer **2** can writing and erasing both occur.

The writing in the shown examples is on the scale of tens of micrometers and a further miniaturization would be desirable with regard to applications such as data storage. Assuming that the proposed mechanism is correct, the further miniaturization is dependent on the irradiation source or ″pen″, not the monomer film. All techniques that aim at focusing light below its diffraction limit are of interest. One approach – using metalenses – was briefly explored but failed due to the short wavelength required for polymerization which was impossible to implement in the available metalenses.

Part III

Conclusion and Outlook

Chapter 6

Conclusion

Two amphiphilic monomers were studied at the air/water interface and on solid substrates in order to elucidate the structures of their corresponding polymer films and to explore potential applications. Both monomers were based on anthracene derivatives as reactive units, but they differed significantly in terms of rigidity and structural complexity. These differences were of relevance when it came to the challenging structure elucidation of the synthesized monolayers. In case of monomer **1**, due to its rigidity and structural simplicity, structure elucidation was more successful than in the case of the flexible and structurally complex monomer **2**.

For monomer **1**, all five criteria of the structure of two-dimensional polymers were investigated: It was shown by tapping-mode atomic force microscopy and by AFM scratching that the synthesized films had the thickness of a monolayer. The films were capable of carrying their own weight, as evidenced by transfer onto Cu TEM grids and analysis by scanning electron microscopy. These findings were the first indicators that the monomer units were connected by covalent bonds. The exact nature of these covalent bonds was shown subsequently. The [4+4]-cycloaddition occuring between tetrafluoroanthracene blades of monomers was proven by tip-enhanced Raman spectroscopy and corroborated by X-ray photoelectron spectroscopy and UV-vis spectroscopy. Moreover, a conversion of 90% was estimated based on these results. Oxidation of anthracene moieties to the corresponding anthraquinones during irradiation at the air/water interface was shown not to occur, thereby eliminating the most likely side reaction that could take place during synthesis at the Langmuir trough.

Indirect evidence for the type of packing most likely assumed at the air/water interface was given. Of the three types of packing considered, packing III was the most likely, as it fitted well with the value for the mean molecular area, the occurence of excimer fluorescence, the evidence of π-π stacking found in a combined DFT-TERS study of the monomer layer, and the observed mechanical coherence. The value for the conversion obtained by TERS makes it unlikely that the two other proposed packings play an important role. Furthermore, images of the polymer film were obtained by STM, which showed that the polymer synthesis is successful and that transfer from the air/water interface leads to deformation of the polymer film that results in the loss of long-range crystallinity.

The occurrence of defects was investigated using tip-enhanced Raman spectroscopy. Regions in the film were found where no reaction had taken place between monomers. These accounted for 2–3%, which confirmed that the conversion was high, as mentioned above. The investigation of the domains in the monomer film by fluorescence microscopy did not show different domains within the resolution of the method. However, it may be possible that domains that show the same packing are offset by a few degrees to one another which cannot be shown using the confocal laser scanning microscope. Assuming that the structure of the monomer film reflects the situation at the air/water interface, one could conclude that in fact there were several domains of similar packing within the LB film. This was indicated by the high-resolution BAM images obtained from the air/water interface which exhibited a homogeneous contrast change upon rotation of the polarizer, indicating monocrystallinity within the method's resolution. STM could not provide a definite answer to this question, as two packing scenarios could not be distinguished with the resolution of the images obtained.

These findings lead to the conclusion that the criteria for a two-dimensional polymer were met by this particular monomer system. It must be stressed that this is the first time that a monomer system used for two-dimensional polymerization at the air/water interface has been investigated this thoroughly and also the first time that the chemical transformation taking place between monomers could be proven and quantified, marking a breakthrough for two-dimensional polymerizations at the air/water interface.

Although many useful techniques have been identified that are of relevance for the investigation of these extremely thin films, there is no ”standard” recipe that could be followed. At this point, it is only possible to characterize the films on different length scales using different solid substrates and assuming that the found results can be correlated to one another and that the nature of the substrate does not change the structure of the film during transfer from the air/water interface. In particular, the evidence for the bond formation between monomers required identifying spectroscopic techniques where the reactive units were known to have characteristic signatures. Even then, many analytical techniques failed to deliver unambiguous results.

Structural investigation of two-dimensional polymers synthesized at the air/water interface remains challenging, a fact that is highlighted by the case of monomer **2**, where only indirect evidence for the formation of a two-dimensional polymer could be found. The difficulties that arise are a direct consequence of the design of the monomer: a large variety of functional groups, a multitude of carbon atoms of similar chemical environment, and the general complexity of the system impeded studies that rely on UV-vis or X-ray photoelectron spectroscopy. Furthermore, a characteristic Raman signal to distinguish and identify polymer and monomer, which proved so useful in the case of monomer **1**, was not present for monomer **2**. All these factors combined were the reason why the characterization of the chemical connectivity was not successful. There were further features in the design which turned out to be a liability when it came to structural characterization: the high flexibility of the monomers, which further increased upon polymerization, leads to a collapse of the regular monomer film structure, thereby reducing the pore size of the irradiated film which are not particularly large to start with, in their initial monomer film packing. As a consequence, no visible order is detectable and no molecular resolution can be achieved using STM or AFM imaging techniques.

This work also provided some insight into how monomers behave at the air/water interface depending on their rigidity and their propensity to arrange themselves in a particular fashion. From these observations and the lessons learned due to the characterization of monomer **2**, one could derive some guidelines for the monomer design and characteristics a monomer should possess in order to

1. facilitate structural characterization as much as possible and

2. obtain a maximally laterally extended two-dimensional polymer with a low amount of defects.

For the structure elucidation (1), a monomer should be rigid and its reactive units should favor a specific arrangement at the air/water interface. These two properties increase the chances of obtaining a crystalline film at the air/water interface which can subsequently be analyzed by imaging techniques (STM, AFM, TEM) but also by techniques that rely on diffraction (SAED, LEED). In particular for diffraction-based techniques, heavy atoms are desirable. For XPS, having carbons that differ dramatically in terms of their chemical environment is beneficial for characterization of the thin films. In the case of anthracenes, their Raman signal is maximized when their long axis is perpendicular to the air/water interface and the substrate. This also holds true for the case that they are polymerized and form the anthracene dimers, as the dimers, too, have a maximized characteristic signal in this orientation. In order to not compromise the reaction between anthracene moieties, the 9- and 10- positions of the anthracenes should not be substituted. Finally, the monomer has to be asymmetric, with one side exhibiting a higher propensity to be in the water to help orientate the monomer at the air/water interface.

On the other hand, if the two factors *rigidity* and *propensity to pack in a certain way* are maximized, it is at the expense of objective (2). These monomers behave in a very rigid fashion at the air/water interface and once deposited no longer coalesce or merge to increase domain size and correct for defects. Thus, these factors favor a higher amount of small domains and the synthesis parameters at the trough have to be optimized even more carefully. On the other hand, a more flexible monomer leads to a film with laterally more extended domains, but its flexibility has a detrimental effect on the film in terms of crystallinity and thus on the elucidation of its structure. It is thus with great care that a compromise between the two criteria should be found during monomer design.

Despite the lack of structure elucidation in the case of monomer **2**, it nevertheless proved useful when it came to taking first steps towards applications. It was chosen for the study of post-transfer polymerization over monomer **1** due to its absorption spectrum which extended well into the visible range, such that polymerization could be carried out using a visible light source.

Furthermore, its flexibility was of advantage when it came to producing films of extended domain sizes. This became particularly clear when contrasting the appearance of its films to the films produced by monomer **3**, a more rigid monomer, which showed distinct regions of different packing.

The irradiation on solid substrates proved successful in the cases of both monomer **2** and monomer **3** films. Due to the fluorescent nature of the films, the spatially confined irradiation led to a disappearance of the fluorescence in the affected areas and to the creation of patterns on the fluorescent films. The writing was reversible by heating to 200 °C in the case of monomer **2**. It was hypothesized that the observed writing and its erasing could be due to the [4+4]-cycloaddition and its reversion, respectively, of monomer units. This finding was of particular interest as it may allow for the synthesis of laterally more extended two-dimensional polymers, compared to the polymerization at the air/water interface.

Efforts were made to rule out alternative pathways for the disappearance of fluorescence, such as oxidation or photobleaching with subsequent fluorescence recovery. While these control experiments indicated that polymerization and depolymerization were likely the causes of writing and erasing, it was not possible to unequivocally prove that it was indeed this reaction that was taking place.

Regardless of the mechanism behind writing and erasing, it was shown that the monomer films could be suitable for incorporation into a miniaturized optical recording device, in particular in the domain of permanent data storage. The miniaturization step of the writing is dependent on the irradiation source, or ″pen″ that is used for writing. One potential candidate as a pen could be a metalens that enables focussing the laser beam below its Rayleigh diffraction limit. The attempt to incorporate the monomer film into a metalens was abandoned at an early stage, as no metalens was available that could focus light at a wavelength below λ = 500 nm.

Chapter 7

Outlook

As mentioned in the conclusion, there is a trade-off between designing a monomer that can be easily characterized due to its rigidity and simplicity and a monomer that is flexible enough to re-adjust at the Langmuir trough, thereby correcting defects between domain boundaries which favors large, defect-free domains. With the appropriate analytical techniques in hand, this choice may no longer have to be made and tuning the synthesis parameters at the Langmuir trough in order to achieve large lateral two-dimensional polymers would become possible.

In principle, there are two approaches to this goal: either, one works with flexible monomers that lead to fewer domains which requires more advanced characterization methods or one uses monomers that are rigid and tries to increase the domain sizes.

In the first approach, the characterization techniques play a central role. In order to further advance the structure elucidation of two-dimensional polymers, new characterization methods have to be chosen that also enable characterizing polymers made of flexible, more complex monomers.

For structure elucidation, it would be desirable to have techniques that can be used on a variety of substrates and that provide information on different length scales simultaneously, rather than having to combine information from molecular, domain, and macroscopic levels.

Of all techniques, tip-enhanced Raman spectroscopy and atomic force microscopy-IR seem like the most promising techniques, as they combine sensitive spectroscopic analysis with a high lateral resolution on the order of nanometers. They do not rely on the rigidity or crystallinity of the monomer systems, which means that they are also suitable for polymers synthesized from less rigid monomers. On the other hand, they too suffer when the monomer system becomes too complex as the interpretation of the obtained spectra usually relies on DFT calculations. Furthermore, they are limited when it comes to the choice of substrate to substrates that promote the TER effect.

Any other technique that would combine sensitive spectroscopic analysis (ellipsometry, UV-vis, fluorescence) with nanometer resolution (by coupling with an AFM or STM) would also be of particular interest.

Fluorescence microscopy may also be of use, as it allows visualizing both domain extent and the arrangement of the monomers, provided a comprehensive computational study is carried out to understand how the fluorescence of the systems change according to the orientation of the monomers in order to correctly identify and interpret the fluorescence spectra obtained. There is hope that conducting these calculations for one anthracene system facilitates calculating or at least estimating it for another. Furthermore, advances in fluorescence microscopy have led to ever-increasing resolutions, which could mean that at some point even small changes in packing could be readily visualized by this technique.

Furthermore, the loss of order that ensues upon irradiation of the monomer film may not be as detrimental to structure elucidation if the packing of the monomers could be determined directly at the air/water interface using methods such as grazing-incidence small angle X-ray scattering (GISAXS) or grazing-incidence wide angle X-ray scattering.

In the second approach, increasing the domain size and decreasing the number of domains is vital to achieving large polymer sizes. The deposition and irradiation parameters would have to be optimized: using low concentrations in the monomer stock solution, as well as irradiation sources where the rate of polymerization is kept low in order to facilitate defect corrections during polymerization. Another plausible approach could be to heat up the water subphase to attempt to anneal the monomer film and thereby correct defects.

Whichever approach is chosen, the synthetic parameters will have to be optimized in order to obtain extended films with few domains and defects before further applications of these systems can be explored.

The exact nature of the applications are not fully established. Achieving a large lateral extension of packing III for monomer **1** may allow to test its suitability as a gas separation membrane. The application for optical storage outlined within this thesis also relies on having laterally extended, defect-free films. With recent further advances in the field of metalenses,[174,175] the films of monomer **2**, which were shown to be suitable for optical writing, could be combined with a metalens to achieve optical writing on the nanometer scale. This is of particular interest in order to use the films in optical recording and data storage.

Part IV

Experimental

Chapter 8

Sample preparation

8.1 Langmuir trough

A KSV 2000 System 2 and a KSV minitrough were used for all film transfer experiments. Both are equipped with a platinum Wilhelmy plate and a dipper. The troughs are made from teflon and the barriers from Delrin. Prior to experiments the trough was cleaned successively with millipore H_2O, $CHCl_3$, EtOH, $CHCl_3$, millipore H_2O, wiping them dry using dust-free paper towels (Kimtech Science Precision Wipes, Kimberly-Clark Professional, Woodbridge, Ontario, Canada) after every solvent, followed by a final rinse with millipore H_2O. The barriers were cleaned with millipore H_2O, EtOH and then millipore H_2O, wiped off with Kimtech Precision Wipes after each solvent and given a final rinse with millipore H_2O. The Wilhelmy plate was cleaned by heating with a Bunsen burner, then rinsing with millipore H_2O. The stage for the substrates was cleaned with EtOH and millipore H_2O. The stage carrying the substrate was immersed in the water prior to deposition of the monomer solution (transfer from below). Solutions of monomer were applied using a 100 μL glass microsyringe. After a time lag of 30 minutes that allowed for evaporation of the solvent, the barriers were compressed to a surface pressure specific to the monomer. The barriers moved with a speed of 2 mm/min and 3 mm/min for the minitrough and the KSV 2000, respectively.

Parameters used for monomer **1**: a stock solution of concentration 0.2 mg/mL in $CHCl_3$ with 5% iPrOH was used. For the small LB trough, 20–25 μL were applied. A target surface pressure of 2 mN/m was used for transfer experiments.

Parameters used for monomer **2**: a stock solution of concentration 1 mg/mL in $CHCl_3$ with 10% MeOH was used. For the small LB trough, 20–25 μL were applied. The monomer was occasionally purified by rGPC in pure $CHCl_3$. A target surface pressure of 20 mN/m was used for transfer experiments.

Parameters used for monomer **3**: a stock solution of concentration 0.25 mg/mL in $CHCl_3$/cyclohexane (1:1). For the small LB trough, 20–25 μL were applied. A target surface of 20 mN/m was used for transfer experiments.

8.2 Preparation of Substrates

Silicon (SiO_2/Si, Thermo, 300 nm) and quartz substrates were cleaned with Piranha solution (H_2SO_4, H_2O_2 3:1) under sonication for 15 minutes, followed by sonication in millipore H_2O (3 x 15 min). In the case of SiO_2/Si, this was done to remove a coating of photoresist (10 μm of AZ9260, Merck Performance Materials GmbH, Germany). They were then stored under millipore H_2O. Prior to use they were rinsed with EtOH, then millipore water.

TEM grids were used as provided by the manufacturer (PLANO GmbH, Wetzlar, 35578 Germany).

Au substrates for TERS and XPS (Au grown on glass and glued to a silicon slide, as described in [176]) were removed from the silicon slide protecting them, rinsed with EtOH and then millipore H_2O.

All other substrates (polystyrene, COC) were rinsed with millipore H_2O.

Polystyrene supports were prepared using polystyrene beads (158 K, BASF Ludwigshafen) that were dissolved in chloroform (10w%) and poured into a Petri dish. After evaporation of the solvent under ambient conditions (2–3 days), the formed films were further dried in a vacuum oven for one day at 40 °C.

C_{18}-SAMs were prepared following a literature procedure.[177] SiO_2/Si wafers were cleaned with Piranha solution, then by oxygen-plasma treatment. Subsequently, they were immersed for 2 h in a solution of octadecyltrichlorosilane (OTCS) in dry decalin (cis/trans mixture; approx. 3 μM). The contact angle was determined to be 105°, which is in accordance with the reported value for the self-assembled ML.

Highly ordered pyrolitic graphite (HOPG SPI-2 ZYB, SPI supplies, Westchester, PA, USA) and mica substrates (PLANO GmbH, Wetzlar, 35578 Germany) were exfoliated with scotch tape and rinsed with millipore H_2O prior to use.

8.3 Polymerization and Film Transfer

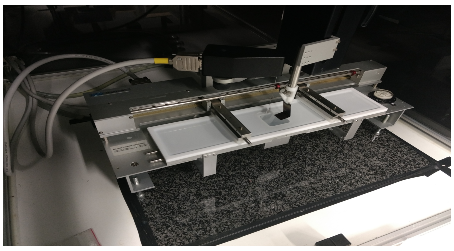

Figure 8.1: Compressed film on Langmuir trough.

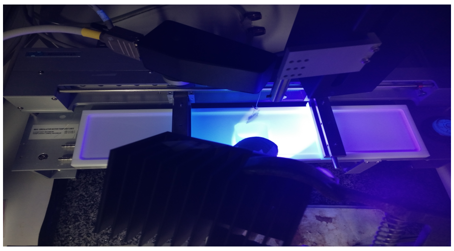

Figure 8.2: Langmuir trough during irradiation of the film.

Polymerization on the LB trough was carried out using LEDs of wavelength $\lambda = 365$ nm (Omicron Laser LEDMOD365.250.OEM) after the film had been kept at the target surface pressure for one hour. Film transfer was achieved by raising the stage carrying the substrate. This stage had been mounted underneath the water surface prior to monomer deposition. The stages used were horizontal or had a tilt angle of 45°. The lifting speed of the dipper was 0.5 mm/min. In the case of film transfer onto TEM grids, the copper grids with a mesh size of 1000 (PLANO, G2780C, Wetzlar, Germany) or mixed mesh (PLANO G2770C, Wetzlar, Germany) were deposited onto the film with tweezers. A piece of writing paper was then placed onto the grids and, upon adsorption of the grids to the paper, peeled of the water surface and dried in a covered petri dish in the dark.

Chapter 9

Analytical techniques

9.1 Brewster Angle Microscope (BAM)

The used BAM was a KSV MicroBAM (KSV NIMA, Finland) which was incorporated within the KSV 2000 system 2. The BAM operated with a 659 nm laser.

For BAM images of a higher resolution, a Nanofilm_ep3 BAM (Accurion, Göttingen, Germany) was used equipped with an internal solid-state laser of a wavelength λ = 658 nm. A CCD camera (768 x 562 pixels) and a 10x objective were used to record the images. The lateral resolution was 1 μm.

9.2 Scanning Electron Microscopy (SEM)

The TEM grids used were placed on a holder (PLANO, G3662, Wetzlar, Germany) and imaged with FEG-SEM (Zeiss LEO Gemini 1530, Germany) microscope with an in-lens detector.

9.3 Atomic Force Microscopy (AFM)

Height analyses of the film were carried out using OMCL-AC160TS silicon tips (Olympus, Shinjuku, Japan) were used for imaging with a resonance frequency between 200 and 400 kHz and a spring constant of about 26 N/m. The microscope was a Bruker Dimension Icon (Bruker, Billerica, MA, USA) used in tapping mode. The substrates used most commonly were SiO_2/Si, HOPG and mica. The film heights were measured at film edges created by placing a strip of mica on the substrate prior to film transfer which was removed after transfer from the LB trough to reveal the bare substrate. Removal of the mica strip afforded a clearly defined edge of the film, however, mica residues (bright specks in AFM image) remained and occasionally, removal of a mica strip led to the monomer film covering the mica strip to glide in part onto the substrate.

Film scratching was carried out using a peak force setpoint of 4 V and a Bruker Nanoscope-Multimode-AFM (Bruker, Billerica, MA, USA) in peak force tapping mode.

A molecular model of the monomer giving the theoretical height was obtained using a MM2 geometry optimization in Chem3D 16.0 (ChemOffice 2016, PerkinElmer, Waltham, MA, USA).

For high-resolution AFM imaging, a Bruker Nanoscope-Multimode AFM was used in peak force tapping mode with ScanAsyst-air-hr nitride cantilevers (Bruker, Billerica, MA, USA).

AFM images were processed with the software Gwyddion.[178]

9.4 Scanning Tunneling Microscopy

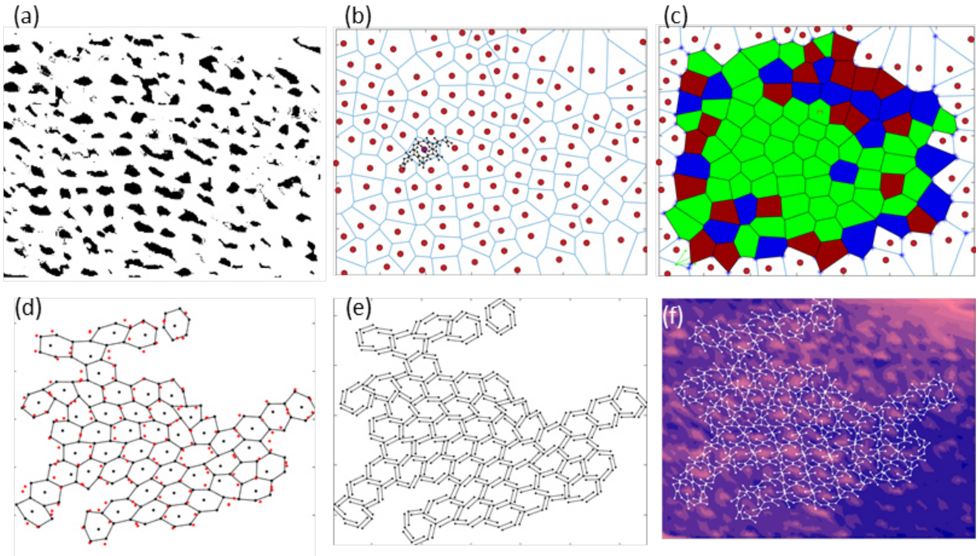

Figure 9.1: Step-by-step procedure used to fit the contorted polymer to the image.

The microscope is a SPECS SPM Aarhus 150 with a SPC 260 Control System (Specs, Berlin, Germany). All of the STM measurements were performed *in vacuo* at room temperature in constant current mode using Pt-Ir tips (90% Pt, 10% Ir) prepared by mechanical cutting and cleaned by in-situ sputtering. The STM images were processed using the WSxM software.

To fit the model of the polymer with the image of the contorted film, an algorithm was used that used the following steps: the image was first binarized (fig. 9.1a) and the centers of the pores were defined (red dots). Then, the pores were parted into equal pieces by lines at the middle of the center-center distances (fig. 9.1b,c). Only pores of a certain size and with a certain number of sides were considered (fig. 9.1d) and in those, the monomers were plotted (fig. 9.1e,f).

9.5 Confocal and Tip-enhanced Raman Spectroscopy

All confocal Raman and TER spectra were acquired on a combined STM/Raman microscope (Ntegra Spectra, NT-MDT, Zelenograd, Russia).[179,180]

Confocal Raman spectra were obtained by averaging 5 accumulations with an acquisition time of 10 s each, using a 632.8 nm HeNe laser at an incident power of 0.5 mW for excitation.

For TERS imaging, an exposure time of 5 s and 4 accumulations was used for all pixels. A 632.8 nm HeNe laser at an incident power of 0.3 mW was used as the excitation source. Based on the diameter of the laser focus, which is around 1.0 μm, the laser fluence was estimated to be 6.4 x 10^3 mW/cm^2. During measurements, the bias voltage was set to 0.2 V and the tunneling current was kept at 0.1 nA. All TERS images were obtained after overnight measurements to minimize the drift of the system. The instrument was equipped with an electron multiplying charge-coupled device (EMCCD, Newton 971 UVB, Andor, Belfast, UK).

The TERS imaging data were fed into MatLab (R2015a, MathWorks, USA) for plotting peak intensity ratio maps. The background was subtracted by an automatically applied MatLab function (msbackadj) to each individual spectrum, followed by gently smoothing with another MatLab function (rloess). Cosmic rays on individual CCD pixels were using custom-made MatLab codes. Peak heights were determined by means of the automatic peak finder

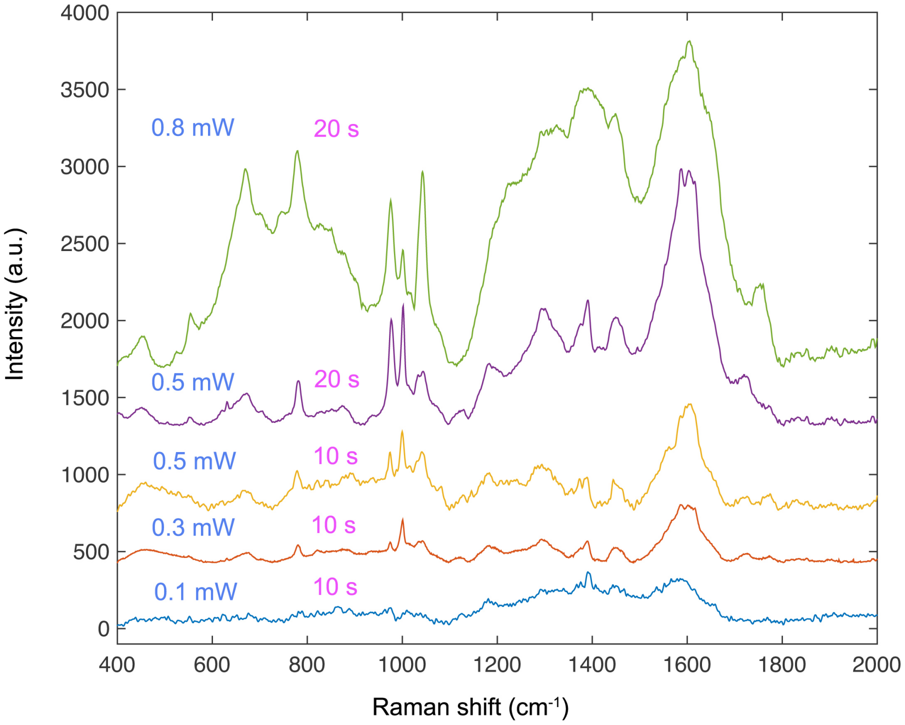

Figure 9.2: TER spectra obtained of the polymer monolayers synthesized from monomer **1** when varying acquisition time and excitation power to find the optimal imaging conditions.

based on MatLab, and the individual threshold (signal-to-noise ratio $\geq$3) was calculated for each spectrum (after aforementioned preprocessing) at every position of the maps.

9.6 DFT calculations

Theoretical Raman spectra were calculated using Gaussian 09 (Gaussian, Wallingford, USA) by means of DFT. All calculations, including full geometry optimizations and frequency predictions, were performed using B3LYP/ 6-31G(d) basis. The keyword Integral = (Grid=UltraFine, Acc2E=11) was used to increase the two-electron integral accuracy when SCF calculations failed to converge using default run parameters. Molecular orientation dependence calculations based on the dipole approximation was carried out as described in [181, 182]. Briefly, a Raman tensor α was extracted from the DFT calculation results. By assuming that the local vertical field (ZZ axis) provides the primary plasmon enhancement, only the vertical component of the Raman tensor (αZZ) and polarization were taken into account. Molecular bending and twisting was ruled out from the orientation dependent calculation. All calculated frequencies were scaled with a factor of 0.977. The optimized geometry and the calculated vibrational modes were visualized using the Gaussview 5 package.

9.7 UV-Vis spectroscopy

The spectra were recorded on a JASCO V-660 UV-VIS-NIR Spectrophotometer (Jasco Inc., Tokyo, Japan). The scanning speed was 400 nm/min. The spectral resolution was 1 nm. The substrates used were Suprasil quartz (Suprasil 1, 0.5 mm thick, Heraeus, Hanau, Germany). In the case of solution UV-Vis spectroscopy, quartz cuvettes (0.6 mL, light path 2 mm) were used. The solvents of choice were $CHCl_3$, cyclopentane or CH_3CN.

9.8 Fluorescence and excitation spectroscopy

The fluorimeter used for recording the excitation and emission spectra of the film on quartz was a Fluorolog 3 fluorimeter (Horiba Jobin Yvon, Kyoto, Japan). A sample holder for solid substrates was used and the probing mode was set to front-facing (FF). The side entrance slit, side exit slit and first intermediate slit were set to 5 nm bandpass. The integration time was 0.1 sec. For the excitation spectrum, the monitoring wavelength was set to 578 nm and the excitation was swept between 300 and 558 nm, taking care to avoid 289 nm in order to prevent Rayleigh scattering. The data were processed in Origin.

9.9 X-Ray Photoelectron Spectroscopy (XPS)

XPS spectra were collected using SPECS Analyzer Phoibos 150, with a monochromatic AlK_α source (energy of 1486.6 eV, power 400 W). The base pressure in the spectrometer was 10^{-11} mbar. Data acquisition was controlled using SpecsLab2 software, while analysis was done using Unifit2013 software. The binding energy (BE) scale was referenced by setting BE of $Au4f_{7/2}$ peak from the substrate to 84.0 eV.

9.10 Confocal Laser Scanning Microscope (CLSM)

A Zeiss LSM 880 upright laser scanning confocal microscope (Zeiss, Oberkochen, Germany) was used. The system comprises a motorized X-Y stage (135 cm x 80 cm), a tunable chameleon multi photon laser, two conventional PMTs and a highly sensitive GaAsP detector. Images were recorded using a laser line of 458 nm (diode) for fluorescence images or 633 nm (HeNe) for phase contrast images and a 10x 0.3NA EC Plan-Neofluar Ph1 M27 objective.

Furthermore, Zeiss LSM 780 inverted laser scanning confocal microscope (Zeiss, Oberkochen, Germany) was used in order to record lambda-scans. It features a motorized X-Y stage (Märzhäuserstage Scan 120x100 IM), a piezo stage that enables fast focussing, two Quasar PMTs, 1.32 PMT GaAsP detector, a transmission PMT and two APDs. Images were recorded using a laser line of 633 nm (HeNe), 458 nm (Argon) or 405 nm (diode) and a 10x 0.3NA EC Plan-Neofluar objective.

Image processing was done using *Zen Black 2012* software (Zeiss, Oberkochen, Germany) and *Fiji* (U.S. National Institutes of Health, Bethesda, Maryland, USA).

9.11 Photoreaction

The photoreaction for solid substrates was carried out under N_2 in an in-house built quartz reactor (see fig. 9.3). The longer metal tube was the inlet for N_2, while the shorter one served as an outlet. N_2 was continuously blown through the tube for five minutes prior to start of the irradiation and during the irradiation experiment. The photoreactor used was an RMR-600 (Rayonet, Branford, CT, USA) equipped with 6 lamps (λ = 350 nm, 4 W each). For the reversion of the cycloaddition, an ABM deep UV mask aligner (ABM-USA, Inc. San Jose, CA, USA) was used with a laser line of λ = 220 nm and a 1000 W Hg light source. A second of irradiation corresponds to 16.4 mW/cm^2 or 33 mJ. The quartz cell was kept under N_2 for the entire irradiation time.

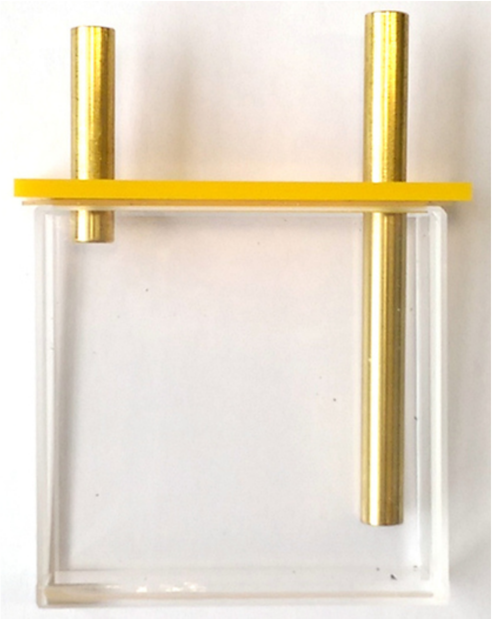

Figure 9.3: Quartz photoreaction cell

Chapter 10

Synthetic Procedures

Reagents and solvents were purchased at reagent grade from commercial suppliers and used without further purification unless otherwise stated. Solvents (hexane, EtOAc, CH_2Cl_2) for extraction and chromatography were obtained in technical grade and distilled before use. Unless otherwise stated, all reactions were performed under an inert atmosphere by applying a positive pressure of N_2 or Ar. Reaction monitoring was achieved by NMR or by thin layer chromatography. The photoreactor used was a RMR-600 (Rayonet, Branford, CT, USA) equipped with 8 lamps (λ = 350 nm, 4 W each).

Flash column chromatography (FC): Carried out with SiO_2 60 (particle size 0.040–0.063 mm, 230–400 mesh ASTM; Fluka).

Thin layer chromatography (TLC): Conducted on aluminium sheets coated with SiO_2 60 F254 (Merck). Visualization occured by UV light (254 nm or 366 nm).

^{1}H-, ^{13}C-, ^{19}F-NMR spectra: Measured on a Varian Mercury 300, a Bruker DRX 400 or on a Bruker Avance 500 spectrometer. Chemical shifts are reported in ppm relative to the signal of $SiMe_4$. Residual solvent signals in the ^{1}H and ^{13}C NMR spectra were used as an internal reference. Coupling constants (*J*) are given in Hz. The resonance multiplicity is described as s (singlet), d (doublet), t (triplet), q (quartet), m (multiplet), and br. (broad).

Mass spectrometry (HR-MS): Performed by the MS-service of the Laboratory for Organic Chemistry, ETH Zurich. High resolution matrix-assisted laser desorption/ionization (HR-MALDI) spectra were measured on a Varian Ionspec FT-ICR spectrometer using *trans*-2-[3-(4-*tert*-butylphenyl)-2-methyl-

2-propenylidene]malonitrile (DCTB) (for compound **4**) and DCTB+Ag (for compounds **3** and **5**) as matrices.

10.1 1,2,3,4-Tetrafluoroanthracene 4

1,2,3,4-Tetrafluoroanthracene was synthesized via a three-step synthesis that had been adapted from two procedures previously reported in the literature.[139, 140]

2-methyl-2*H*-isoindole 8

THF (24 mL) was cooled to 0 °C, LAH (60 mmol, 2.4 M in THF, 25 mL) was added, then a solution of MeOH (4 mL) in THF (24 mL) was added dropwise over 15 min. The mixture was cooled to -78 °C and *N*-methylphthalimide (3.30 g, 20 mmol) was added portionwise. The resulting colorless mixture was stirred for 60 min at -78 °C, then at 0 °C. After 1 h, TLC indicated two products, one which corresponded to the isoindole and the other to the partially reduced phthalimide. After 2.5 hours, TLC of the yellow solution indicated only one product. Sat. aq. Na_2SO_4 (12 mL) was added, the mixture filtered and the residue washed with acetone. The filtrate was dried ($MgSO_4$) and concentrated to give **8** as a pale green solid (2.2 g, 8.6 mmol, 83%) which was pure judging by NMR spectroscopy and due to its instability was used as such in the next reaction step.
^{1}H NMR (300 MHz, $CDCl_3$) δ in ppm: 7.50 (dd, J = 6.5, 3.1 Hz, 2H), 7.04 (s, 2H), 6.91 (dd, J = 6.6, 3.0 Hz, 2H), 3.99 (s, 3H, N-*Me*).
^{13}C NMR (76 MHz, $CDCl_3$) δ in ppm: 124.73 (qC), 120.73, 119.45, 111.82 (*CH*-N), 37.66 (N-*Me*).

1,2,3,4-tetrafluoro-11-methyl-9,10-dihydro-9,10-epiminoanthracene 9

n-BuLi (10.5 mL, 1.6 M in hexane) was added dropwise over 2 min to chloropentafluorobenzene (2.16 mL, 16 mmol) in Et_2O (9 mL) at -78 °C and then stirred for 30 min. **8** (2.2 g, 8 mmol) in Et_2O (9 mL) was added dropwise over 5 min and the resulting yellow-green suspension was allowed to warm to RT. After 18.5 h, the brown solution was poured onto dist. H_2O, the org. phase was separated and the aq. phase extracted with CH_2Cl_2 (2x). The comb. org. portions were dried ($MgSO_4$), filtered and concentrated to give **9** as a brown solid (3.43 g), exhibiting peaks at 2.26 and 5.23 ppm ascribed to

N-Me and the bridgehead protons, respectively. Approximately 45% starting material remained, as determined by comparison of the N-Me peaks of starting material and product in the ^{1}H NMR. The crude was used as such in the next step.

1,2,3,4-Tetrafluoroanthracene 4

9 (3.43 g, 16 mmol) was dissolved in $CHCl_3$ (60 mL), cooled to 0 °C and mCPBA (5.506 g, 24.56 mmol) was added. The resulting mixture was stirred at 0 °C for 3 h, allowed to warm to RT and stirred for 18 h. The mixture was filtered, the residue washed with CH_2Cl_2, the org. portions washed with sat. aq. Na_2CO_3, dried ($MgSO_4$), filtered and concentrated to give a brown oil. CC (100% hexane) afforded **4** as a pale yellow solid (135 mg, 6% over two steps).
^{1}H NMR (300 MHz, $CDCl_3$) δ in ppm: 8.55 (s, 2H), 8.01 (dd, J = 6.5, 3.3 Hz, 2H), 7.56 (dd, J = 6.6, 3.2 Hz, 2H).
^{13}C NMR (76 MHz, $CDCl_3$) δ in ppm: 144.27–139.61 (m), 132.01, 128.34, 127.25, 119.58 (p, J = 3.0 Hz), 118.97-117.75 (m).
^{19}F NMR (282 MHz, $CDCl_3$) δ in ppm: -150.74, -159.47.
HR-MALDI-MS: *m/z*: 250.03996 ($[M]^+$, calcd for $C_{14}H_6F_4{}^+$: 250.04001).

10.2 Tetrafluoroanthracene Dimer 5

4 (56 mg, 0.2 mmol) was dissolved in deoxygenated benzene (2.5 mL) in a 10 mL Schlenk tube and irradiated in a Rayonet photoreactor at a wavelength of λ = 350 nm for 12 h. The yellow supernatant was pipetted off, the solid washed with benzene and dried to give spectroscopically pure **5** (100 mg, 89%) as colorless crystals. Recrystallization (and heating to 60 °C) resulted in the dimers reverting back to the tetrafluoroanthracenes. Subjecting these dissolved crystals to a further photoreaction gave a mixture of *anti*- and *syn*-dimer (**5a**, **5b**) at a ratio of 2:1. Even though a HOESY NMR was measured to assign the two stereoisomers, it was not possible to unambiguously do so. However, due to the difference in the shifts in the ^{19}F NMR spectra it was possible to assign all peaks to the corresponding isomer.

Due to its low solubility and stability, it was not possible to obtain a ^{13}C NMR spectrum where the peaks of carbons connected to or α to fluorines were visible. Nevertheless, two-dimensional ^{19}F-^{13}C NMR correlation spectroscopy, HSQC and HMBC allowed assignment of the chemical shifts of all carbon peaks for both isomers.

Major component ^{1}H NMR (500 MHz, benzene-d$_6$) δ in ppm: 6.66 (dd, J = 5.5, 3.2 Hz, 4H), 6.56 (dd, J = 5.4, 3.3 Hz, 4H), 4.55 (s, 4H).
^{13}C NMR (500 MHz, benzene-d$_6$) δ in ppm determined from HSQC and HMBC: 143.57 (C-F, inner), 140.44 (qC), 138.35 (C-F, outer), 127.48 (C-H), 126.90 (C-H), 126.24 (qC$_\alpha$-CF), 44.64 (bridgehead C-H).
^{19}F NMR (500 MHz,benzene-d$_6$) δ in ppm: -146.02 (m, J = 20.3 Hz), -157.62 (m, J = 20.3 Hz).

Minor component ^{1}H NMR (500 MHz, benzene-d$_6$) δ in ppm determined from HSQC and HMBC: 6.69 (dd, J = 5.4, 3.3 Hz, 4H), 6.63 (dd, J = 5.5, 3.2 Hz, 4H), 4.54 (s, 4H).
^{13}C NMR (400 MHz, benzene-d$_6$) δ in ppm: 143.51 (C-F, inner), 140.44 (qC), 138.15 (C-F, outer), 127.01 (C-H), 127.46 (C-H), 125.91 (qC$_\alpha$-CF), 44.70 (bridgehead C-H).
^{19}F NMR (500 MHz, benzene-d$_6$) δ in ppm: -145.36 (m, J = 20.4 Hz), -159.15 (m, J = 20.4 Hz).

HR-MALDI-MS: *m/z*: 606.98561 ([*M*+Ag]$^+$, calcd for $C_{28}H_{12}AgF_8^+$: 606.98567).

10.3 Dianthracene 7

Anthracene **6** (300 mg, 5.61 mmol) was dissolved in deoxygenated benzene (70 mL) and irradiated at λ = 350 nm for 24 h at room temperature in a rayonet reactor. The precipitated solid was washed with benzene, recrystallized in EtOH and **7** was obtained as white crystals (540 mg, 90%).
^{1}H NMR ($C_2D_2Cl_4$, 300 MHz): 6.94 (dd, J = 5.4, 3.3 Hz, 8 H), 6.81 (dd, J = 5.4, 3.3 Hz, 8H), 4.54 (s, 4 H) ppm.
^{13}C NMR ($C_2D_2Cl_4$, 76 MHz): 143.24, 127.08, 125.46, 53.23 ppm.
HR-MALDI-MS: *m/z*(%): 463.0610 ([*M*+Ag]$^+$, calcd for $C_{28}H_{20}Ag^+$: 463.0616).

Chapter 11

NMR Spectra

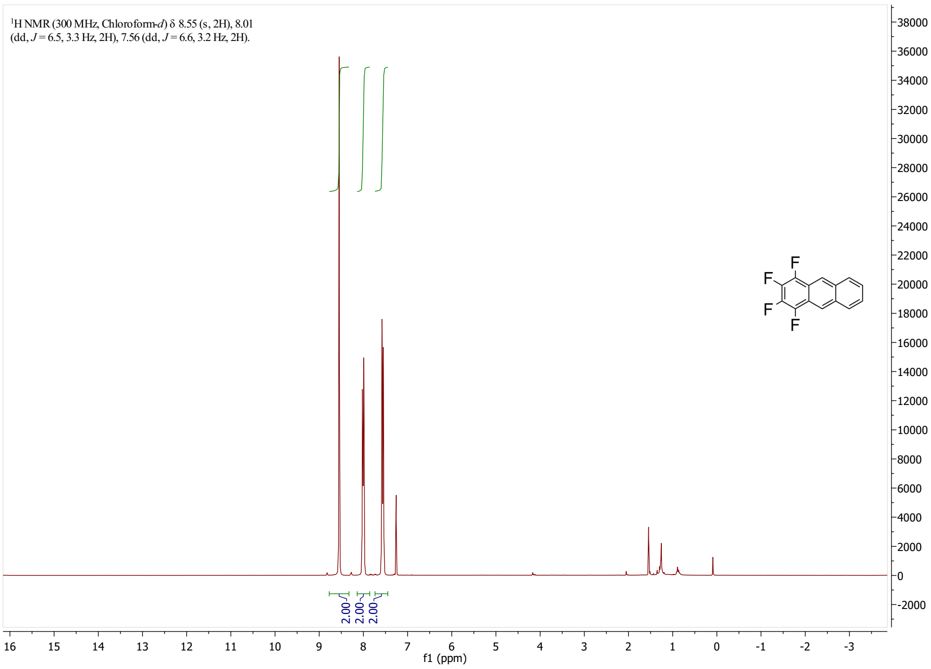

^{1}H NMR (300 MHz, Chloroform-*d*) δ 8.55 (s, 2H), 8.01 (dd, *J* = 6.5, 3.3 Hz, 2H), 7.56 (dd, *J* = 6.6, 3.2 Hz, 2H).

Figure 11.1: ^{1}H NMR spectrum of compound **4** in chloroform-*d*.

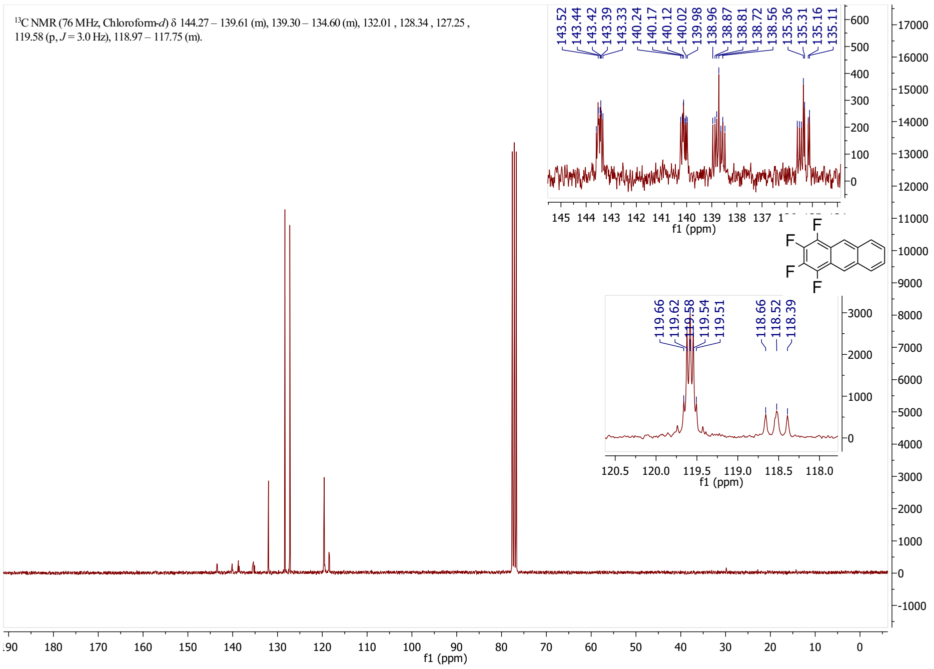

^{13}C NMR (76 MHz, Chloroform-*d*) δ 144.27 – 139.61 (m), 139.30 – 134.60 (m), 132.01 , 128.34 , 127.25 , 119.58 (p, *J* = 3.0 Hz), 118.97 – 117.75 (m).

Figure 11.2: ^{13}C NMR spectrum of compound **4** in chloroform-*d*.

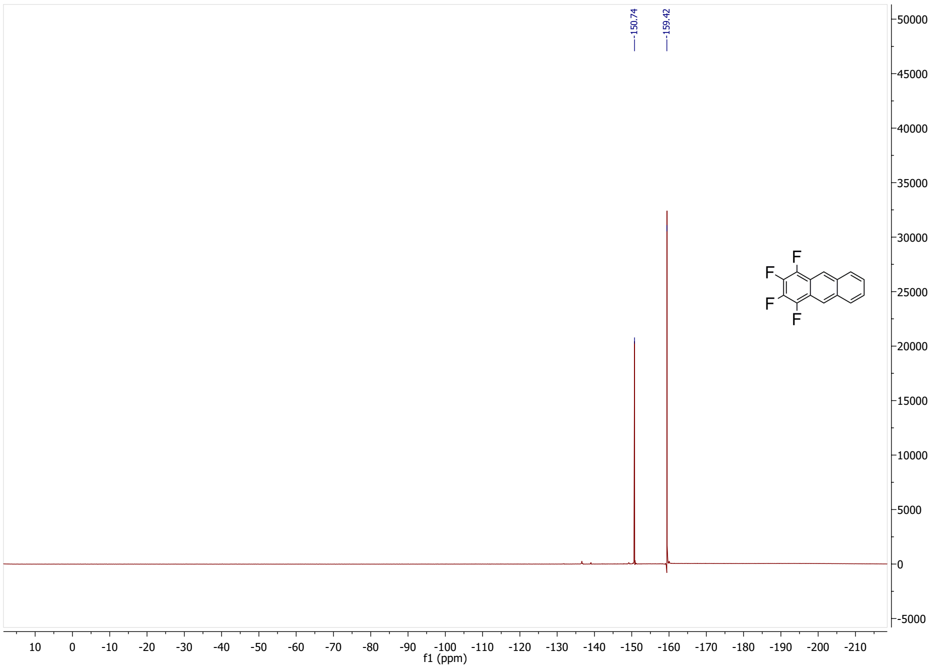

Figure 11.3: ^{19}F NMR spectrum of compound **4** in chloroform-*d*.

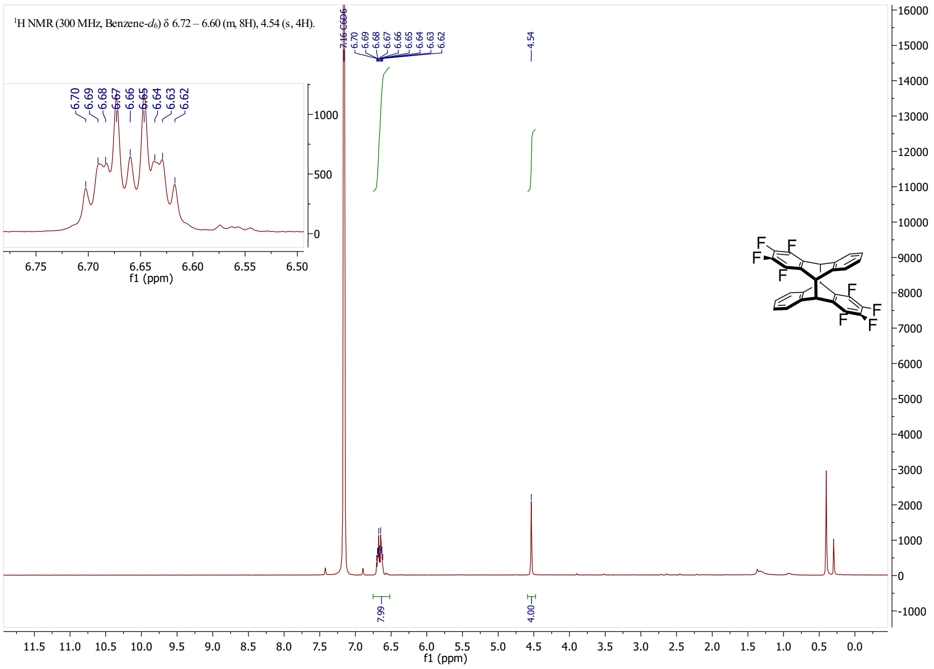

^{1}H NMR (300 MHz, Benzene-d_6) δ 6.72 – 6.60 (m, 8H), 4.54 (s, 4H).

Figure 11.4: ^{1}H NMR spectrum of compound **5** in benzene-*d6*, prior to recrystallization. Only one isomer is present.

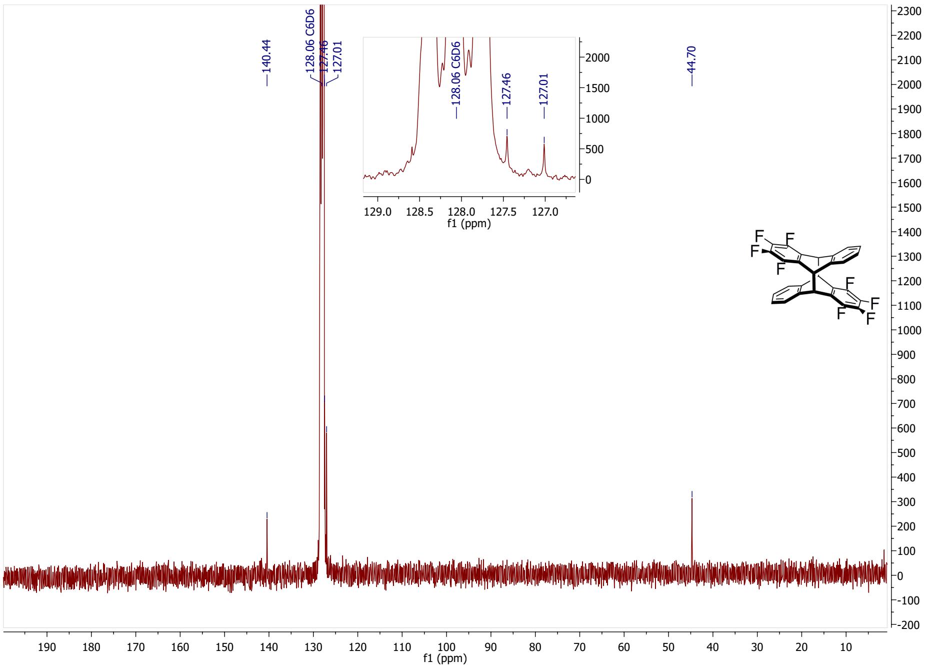

Figure 11.5: ^{13}C NMR spectrum of compound **5** in benzene-*d6*, prior to recrystallization. Only one isomer is present. The carbons bearing fluorines or α to carbons bearing fluorines cannot be discerned due to coupling which decreases the signal intensity significantly.

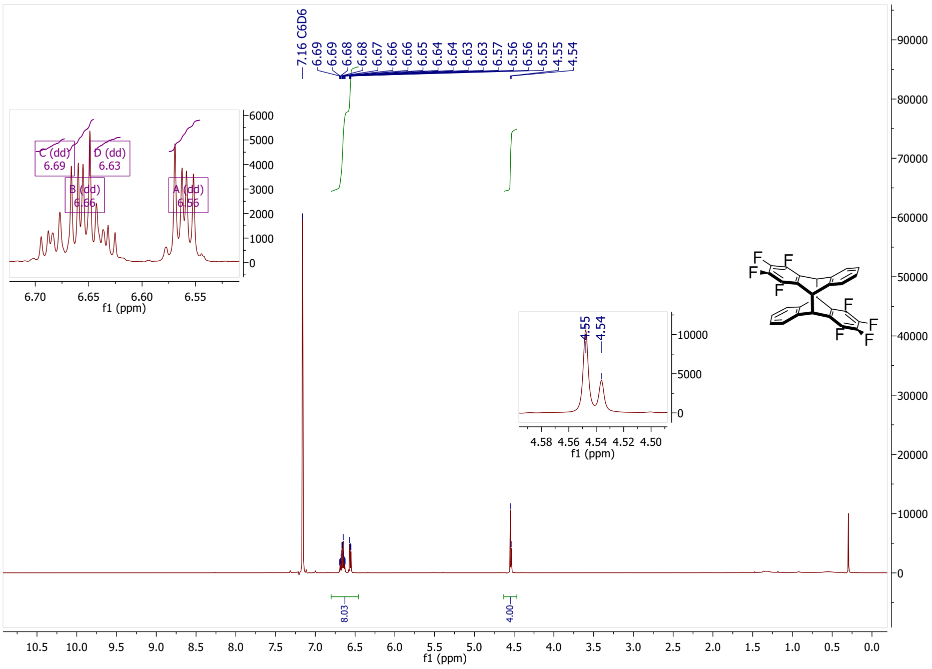

Figure 11.6: ^{1}H NMR spectrum of compound **5** in benzene-*d6*, after recrystallization that led to reversion and a further photoreaction. Two isomers **5a** and **5b** are now present with a ration of 2:1, as determined by integration of the peaks at 4.54 and 4.55 ppm. These peaks and the peak at δ = 6.56 ppm were also used in the HMBC spectrum in order to determine which proton peaks belong to which isomer. After identification of the protons, the corresponding carbon peaks were assigned using the HSQC spectrum.

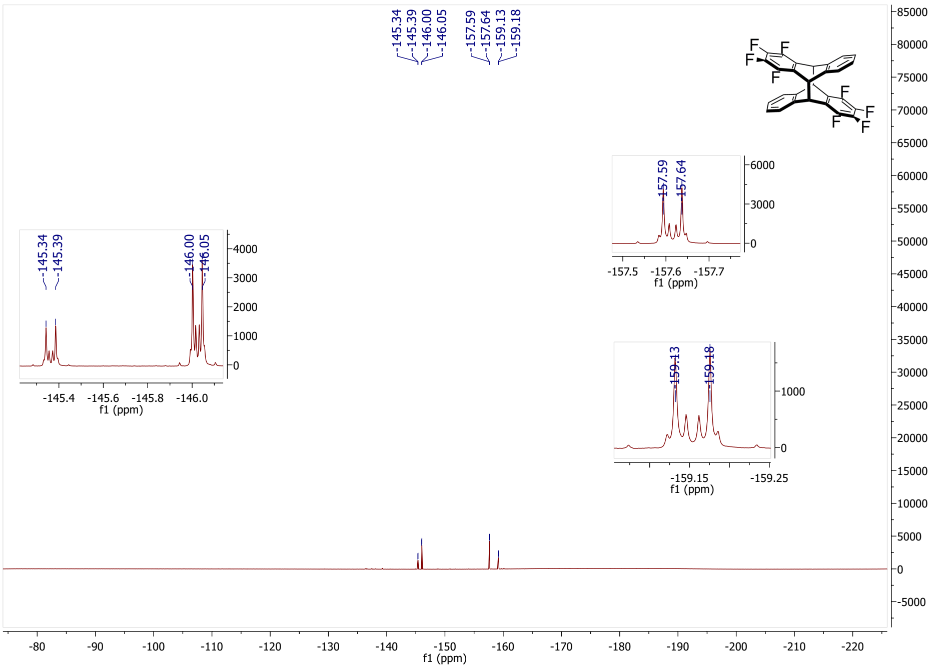

Figure 11.7: ^{19}F NMR spectrum of compound **5** in benzene-*d6*, after recrystallization that led to reversion and a further photoreaction. Two isomers **5a** and **5b** are now present.

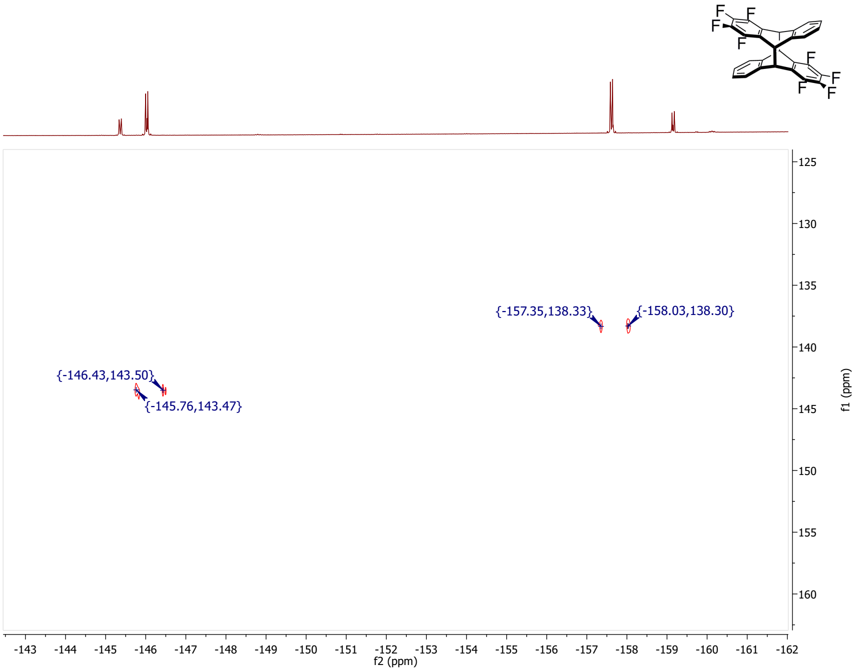

Figure 11.8: ^{19}F-^{13}C NMR correlation spectrum in benzene-*d6* showing ^{1}J coupling of compounds **5a** and **5b**. The spectrum permits the identification of the fluorine-bearing carbons of both isomers.

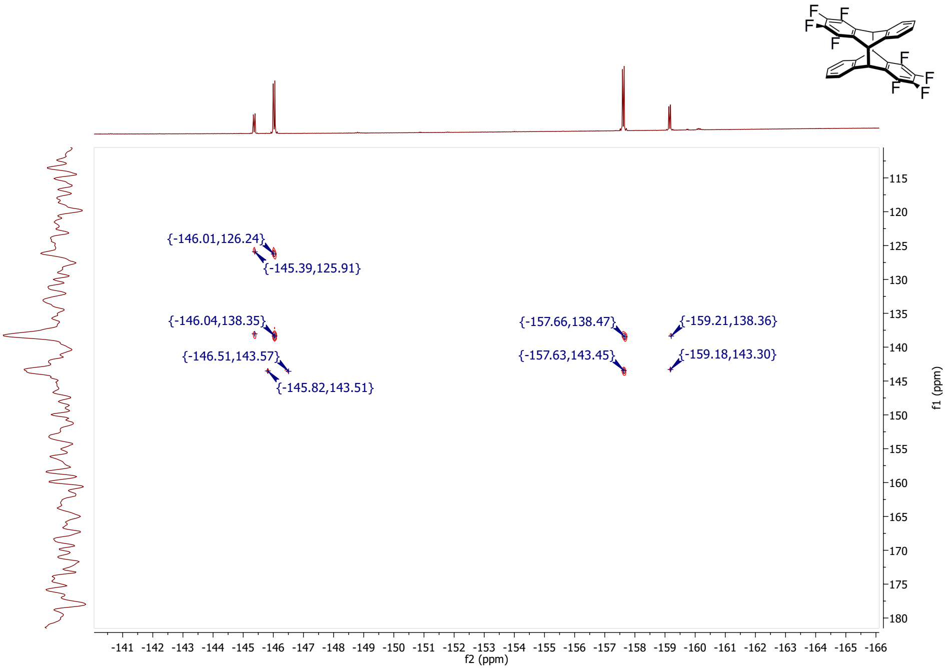

Figure 11.9: ^{19}F-^{13}C NMR correlation spectrum in benzene-*d6* showing ^{2}J coupling of compounds **5a** and **5b**. The spectrum allows the identification of the carbon α to the fluorine-bearing carbons of both components.

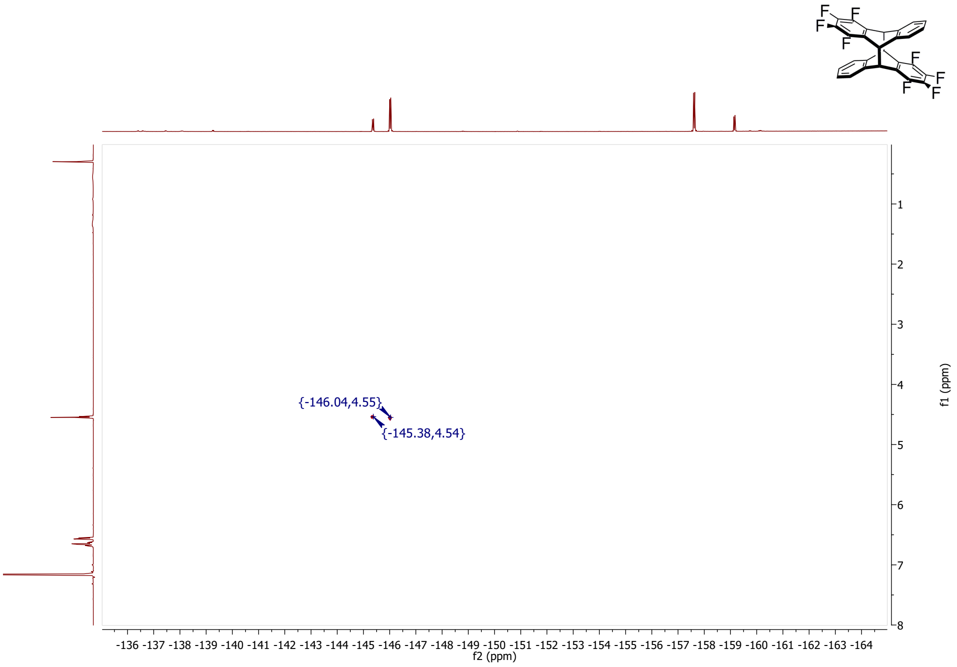

Figure 11.10: HOESY spectrum of **5** in benzene-*d6*: ^{19}F-^{13}C NMR correlation spectra showing the heteronuclear NOE connectivity of compounds **5a** and **5b**. The spectrum reveals the proximity of the bridge bicyclic core protons to the inner fluorines (fluorines closer to the center of the molecules). In theory, this experiment would allow for a differentiation between the two isomers, as only one of the two should show a cross peak to the aromatic protons. During acquisition, the level of noise increases significantly. Varying the mixing time did not circumvent this problem, and so the relevant cross peaks could not be observed.

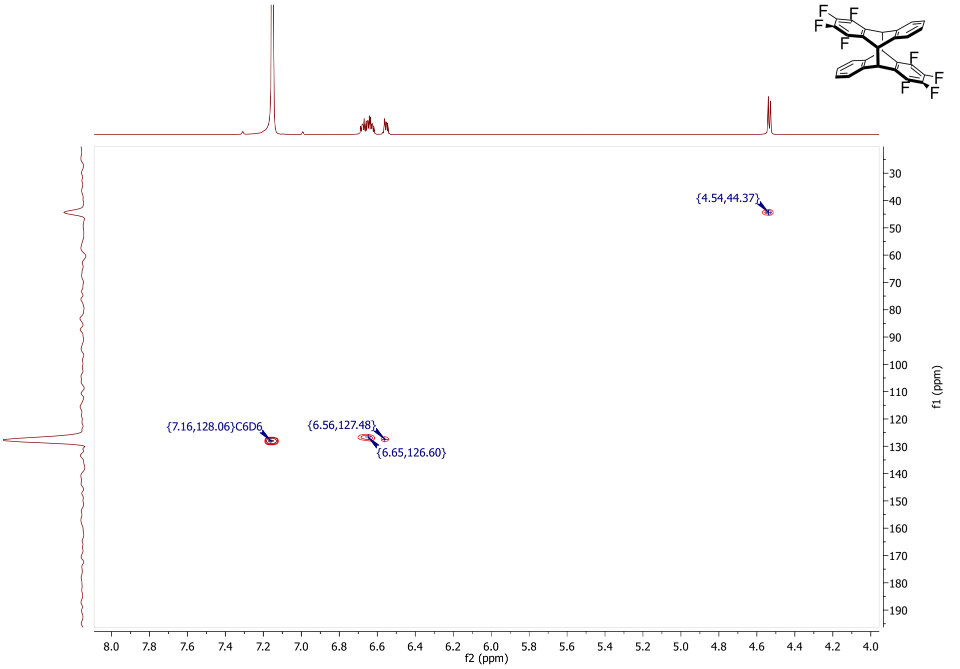

Figure 11.11: HSQC NMR spectrum of **5a** and **5b** in benzene-*d6*. The spectrum permitted the identification of the carbon connected to the proton at δ = 6.56 ppm.

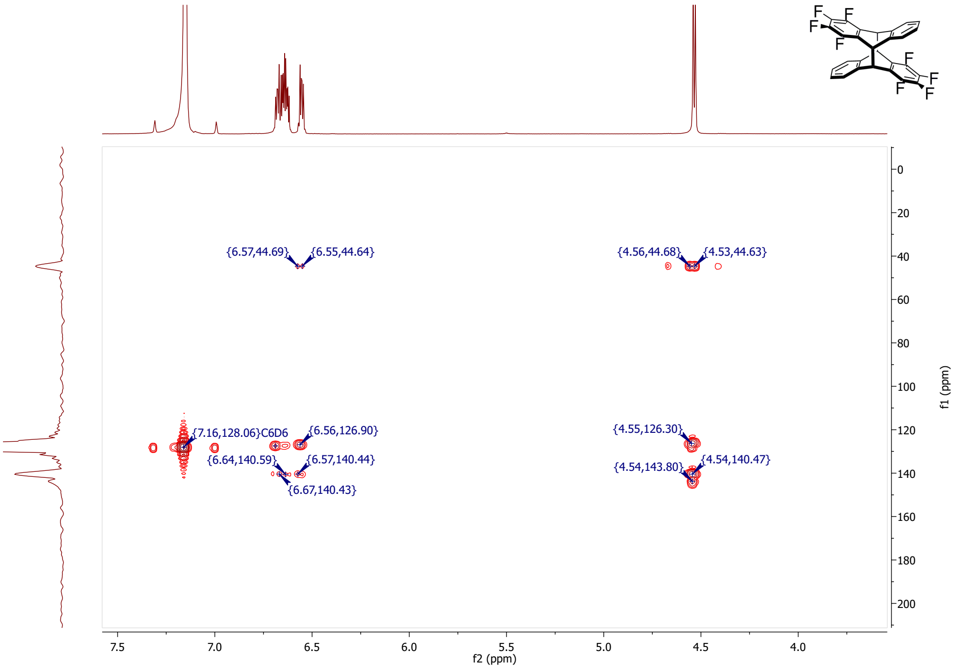

Figure 11.12: HMBC NMR spectrum of **5a** and **5b** in benzene-*d6*. Using the proton peak at δ = 6.56 ppm, it was possible to assign all carbons of this isomer (not bearing fluorines or α to fluorines).

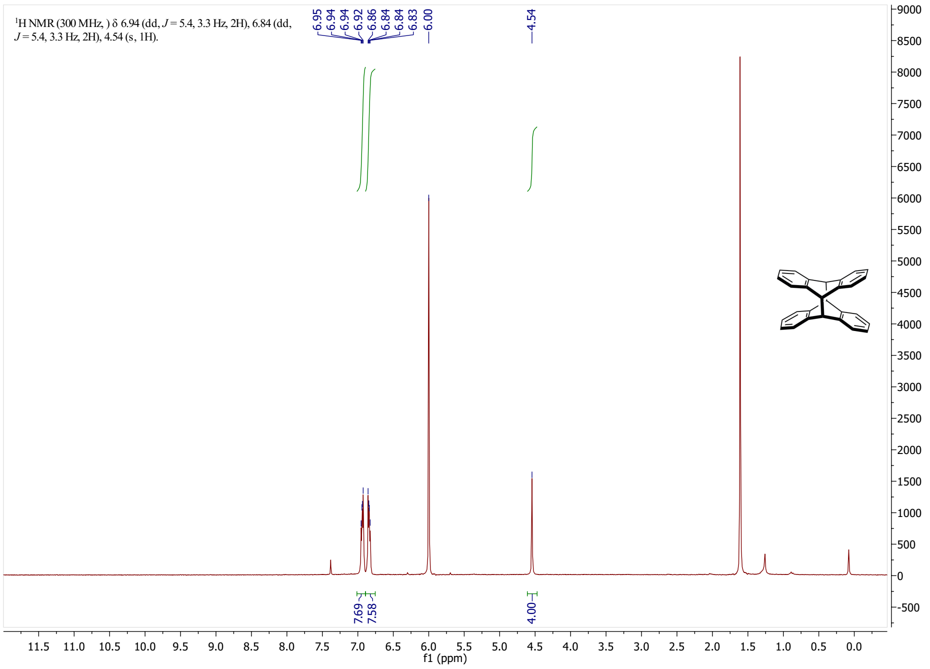

Figure 11.13: ^{1}H NMR spectrum of **7** in tetrachloroethane-*d2*.

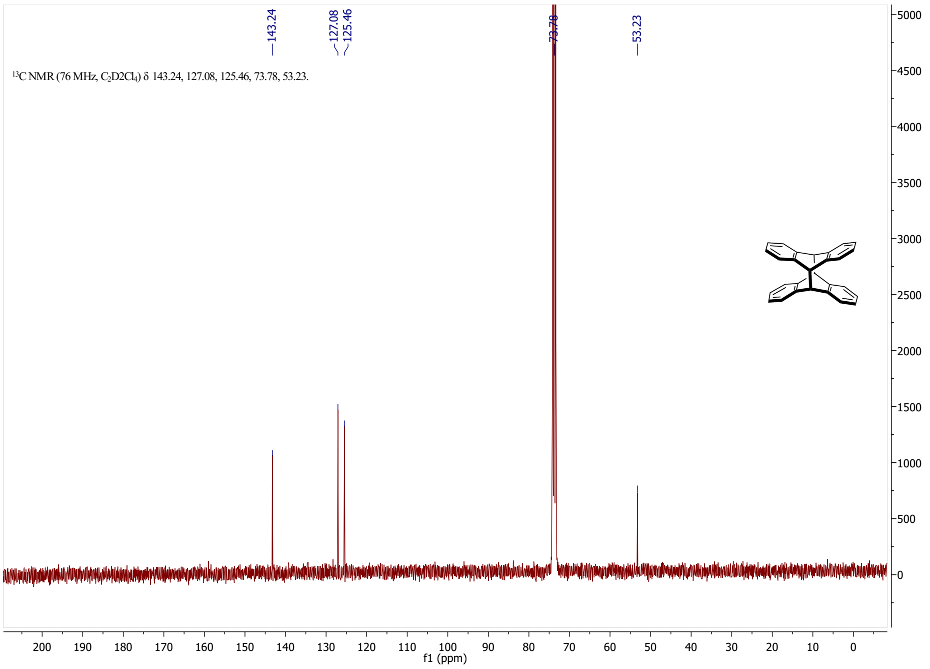

Figure 11.14: ^{13}C NMR spectrum of **7** in tetrachloroethane-*d2*.

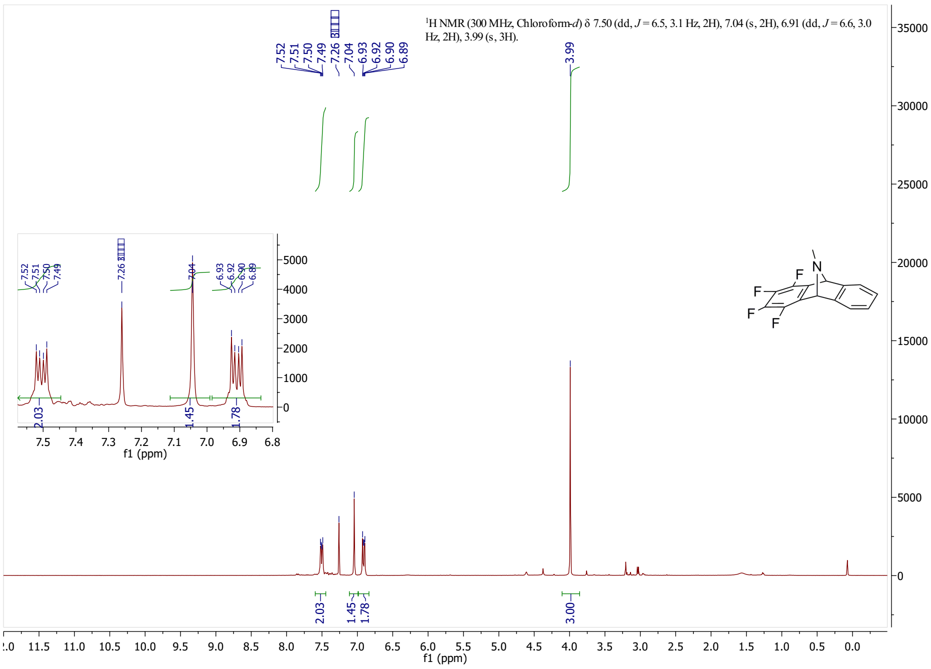

^{1}H NMR (300 MHz, Chloroform-*d*) δ 7.50 (dd, *J* = 6.5, 3.1 Hz, 2H), 7.04 (s, 2H), 6.91 (dd, *J* = 6.6, 3.0 Hz, 2H), 3.99 (s, 3H).

Figure 11.15: ^{1}H NMR spectrum of **9** in chloroform-*d*.

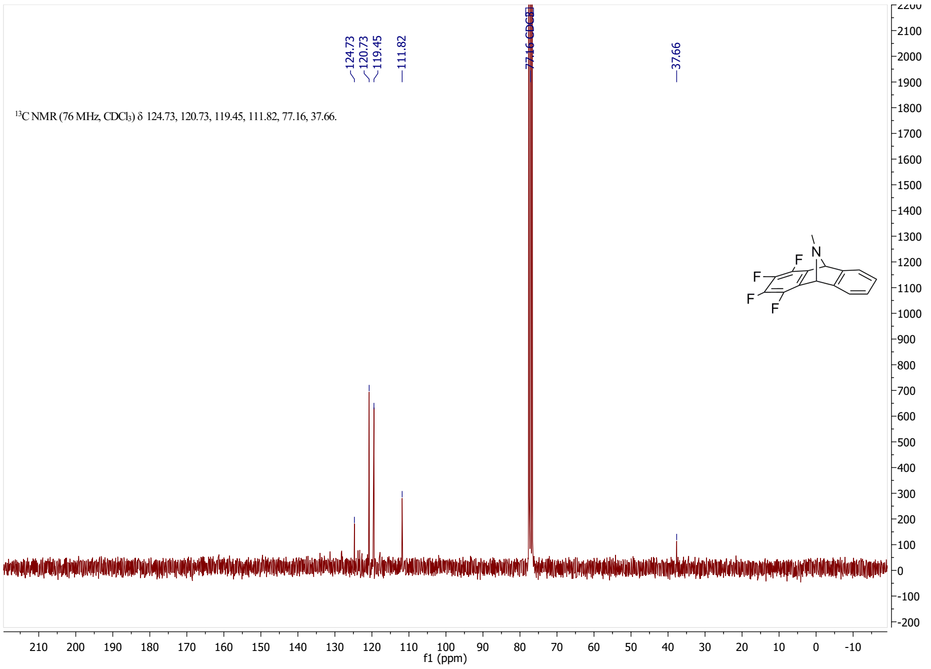

^{13}C NMR (76 MHz, $CDCl_3$) δ 124.73, 120.73, 119.45, 111.82, 77.16, 37.66.

Figure 11.16: ^{13}C NMR spectrum of **9** in chloroform-*d*.

Bibliography

[1] J.-S. Wang, K. Matyjaszewski, *J. Am. Chem. Soc.* **1995**, *117*, 5614–5615.

[2] G. Moad, E. Rizzardo, D. H. Solomon, *J. Macromol. Sci. Part A - Chem.* **1982**, *17*, 51–59.

[3] E. Rizzardo, D. H. Solomon, *Polym. Bull.* **1979**, *1*, 529–534.

[4] P. G. Griffiths, E. Rizzardo, D. H. Solomon, *J. Macromol. Sci. Part A - Chem.* **1982**, *17*, 45–50.

[5] A. D. Schlüter, A. Halperin, M. Kröger, D. Vlassopoulos, G. Wegner, B. Zhang, *ACS Macro Lett.* **2014**, *3*, 991–998.

[6] J. M. Ren, T. G. McKenzie, Q. Fu, E. H. H. Wong, J. Xu, Z. An, S. Shanmugam, T. P. Davis, C. Boyer, G. G. Qiao, *Chem. Rev.* **2016**, *116*, 6743–6836.

[7] A. C. Grimsdale, K. Müllen in *Des. Synth. Conjug. Polym.* Wiley-VCH Verlag GmbH & Co. KGaA, Weinheim, Germany, **2010**, pp. 227–245.

[8] V. Gupta, S. K. Nayak, *J. Appl. Pharm. Sci.* **2015**, *5*, 117–122.

[9] G. Polymeropoulos, G. Zapsas, K. Ntetsikas, P. Bilalis, Y. Gnanou, N. Hadjichristidis, *Macromolecules* **2017**, *50*, 1253–1290.

[10] G. Gee, *Proc. R. Soc. London A Math. Phys. Eng. Sci.* **1935**, *153*, 129–141.

[11] G. Gee, *Trans. Faraday Soc.* **1936**, *32*, 187–195.

[12] K. S. Novoselov, A. K. Geim, S. V. Morozov, D Jiang, Y Zhang, S. V. Dubonos, I. V. Grigorieva, A. A. Firsov, *Sci.* **2004**, *306*, 666–669.

[13] L. Wang, Y. Zhu, J.-Q. Wang, F. Liu, J. Huang, X. Meng, J.-M. Basset, Y. Han, F.-S. Xiao, *Nat. Commun.* **2015**, *6*, 6957.

[14] X. Huang, P. Sheng, Z. Tu, F. Zhang, J. Wang, H. Geng, Y. Zou, C.-a. Di, Y. Yi, Y. Sun, W. Xu, D. Zhu, *Nat. Commun.* **2015**, *6*, 7408.

[15] S.-C. Lu, J.-P. Leburton, *Nanoscale Res. Lett.* **2014**, *9*, 2413.

[16] J. Sakamoto, J. van Heijst, O. Lukin, A. D. Schlüter, *Angew. Chem. Int. Ed. Engl.* **2009**, *48*, 1030–69.

[17] K. Celebi, J. Buchheim, R. M. Wyss, A. Droudian, P. Gasser, I. Shorubalko, J.-I. Kye, C. Lee, H. G. Park, *Science (80-.).* **2014**, *344*, 289–292.

[18] V. Müller, T. Hungerland, M. Baljozovic, T. Jung, N. D. Spencer, H. Eghlidi, P. Payamyar, A. D. Schlüter, *Adv. Mater.* **2017**, *29*, 1701220.

[19] J. W. Colson, W. R. Dichtel, *Nat. Chem.* **2013**, *5*, 453–465.

[20] G. H. Gunasekar, K. Park, V. Ganesan, K. Lee, N.-K. Kim, K.-D. Jung, S. Yoon, *Chem. Mater.* **2017**, acs.chemmater.7b01539.

[21] W. Liu, Q. Su, P. Ju, B. Guo, H. Zhou, G. Li, Q. Wu, *ChemSusChem* **2017**, *10*, 664–669.

[22] A. V. Bavykina, A. I. Olivos Suarez, D. Osadchii, R. Valecha, R. Franz, M. Makkee, F. Kapteijn, J. Gascon, *ACS Appl. Mater. Interfaces* **2017**, acsami.7b07339.

[23] C. R. Mulzer, L. Shen, R. P. Bisbey, J. R. McKone, N. Zhang, H. D. Abruña, W. R. Dichtel, *ACS Cent. Sci.* **2016**, *2*, 667–673.

[24] D. D. Medina, M. L. Petrus, A. N. Jumabekov, J. T. Margraf, S. Weinberger, J. M. Rotter, T. Clark, T. Bein, *ACS Nano* **2017**, *11*, 2706–2713.

[25] D. Er, L. Dong, V. B. Shenoy, *J. Phys. Chem. C* **2016**, *120*, 174–178.

[26] S. B. Alahakoon, C. M. Thompson, G. Occhialini, R. A. Smaldone, *ChemSusChem* **2017**, *10*, 2116–2129.

[27] S. Dey, A. Bhunia, I. Boldog, C. Janiak, *Microporous Mesoporous Mater.* **2017**, *241*, 303–315.

[28] K. Wang, Y. Tang, Q. Jiang, Y. Lan, H. Huang, D. Liu, C. Zhong, *J. Energy Chem.* **2017**, *26*, 902–908.

[29] S. N. Talapaneni, J. H. Lee, S. H. Je, O. Buyukcakir, T.-w. Kwon, K. Polychronopoulou, J. W. Choi, A. Coskun, *Adv. Funct. Mater.* **2017**, *27*, 1604658.

[30] A. P. Côté, A. I. Benin, N. W. Ockwig, M. O'Keeffe, A. J. Matzger, O. M. Yaghi, *Science (80-.).* **2005**, *310*, 1166–1170.

[31] K. T. Jackson, T. E. Reich, H. M. El-Kaderi, T. Terao, M. Mitone, C. Tang, C. Zhi, M. W. Ambrogio, Y. Y. Botros, X. F. Duan, S. Seki, J. F. Stoddart, O. M. Yaghi, *Chem. Commun.* **2012**, *48*, 8823–8825.

[32] B. T. Koo, W. R. Dichtel, P. Clancy, Y. Olivier, R. Silbey, J.-L. Brédas, M. G. Spencer, J. Park, W. R. Dichtel, *J. Mater. Chem.* **2012**, *22*, 17460–17469.

[33] K. T. Jackson, M. G. Rabbani, T. E. Reich, H. M. El-Kaderi, *Polym. Chem.* **2011**, *2*, 2775–2577.

[34] H. Wang, B. He, F. Liu, C. Stevens, M. A. Brady, S. Cai, C. Wang, T. P. Russell, T. Tan, Y. Liu, *J. Mater. Chem. C* **2017**, *5*, 5090–5095.

[35] Y. X. Ma, Z. J. Li, L. Wei, S. Y. Ding, Y. B. Zhang, W. Wang, *J. Am. Chem. Soc.* **2017**, *139*, 4995–4998.

[36] M. Matsumoto, R. R. Dasari, W. Ji, C. H. Feriante, T. C. Parker, S. R. Marder, W. R. Dichtel, *J. Am. Chem. Soc.* **2017**, *139*, 4999–5002.

[37] S. B. Alahakoon, G. T. McCandless, A. A. K. Karunathilake, C. M. Thompson, R. A. Smaldone, *Chem. - A Eur. J.* **2017**, *23*, 4255–4259.

[38] S.-Q. Xu, R.-R. Liang, T.-G. Zhan, Q.-Y. Qi, X. Zhao, J. Rouquérol, T. Siemieniewska, S. Qiu, Y. Yan, D. Trauner, A. Hartschuh, T. Bein, *Chem. Commun.* **2017**, *53*, 2431–2434.

[39] P. Kuhn, M. Antonietti, A. Thomas, *Angew. Chemie Int. Ed.* **2008**, *47*, 3450–3453.

[40] J. Roeser, K. Kailasam, A. Thomas, *ChemSusChem* **2012**, *5*, 1793–1799.

[41] O. Buyukcakir, S. H. Je, S. N. Talapaneni, D. Kim, A. Coskun, *ACS Appl. Mater. Interfaces* **2017**, *9*, 7209–7216.

[42] P. Kissel, R. Erni, W. B. Schweizer, M. D. Rossell, B. T. King, T. Bauer, S. Götzinger, A. D. Schlüter, J. Sakamoto, *Nat. Chem.* **2012**, *4*, 287–91.

[43] R. Bhola, P. Payamyar, D. J. Murray, B. Kumar, A. J. Teator, M. U. Schmidt, S. M. Hammer, A. Saha, J. Sakamoto, A. D. Schlüter, B. T. King, *J. Am. Chem. Soc.* **2013**, *135*, 14134–14141.

[44] M. J. Kory, M. Wörle, T. Weber, P. Payamyar, S. W. van de Poll, J. Dshemuchadse, N. Trapp, A. D. Schlüter, *Nat. Chem.* **2014**, *6*, 779–784.

[45] P. Kissel, D. J. Murray, W. J. Wulftange, V. J. Catalano, B. T. King, *Nat. Chem.* **2014**, *6*, 774–778.

[46] R. Z. Lange, G. Hofer, T. Weber, A. D. Schlüter, *J. Am. Chem. Soc.* **2017**, *139*, 2053–2059.

[47] J. F. Dienstmaier, D. D. Medina, M. Dogru, P. Knochel, T. Bein, W. M. Heckl, M. Lackinger, *ACS Nano* **2012**, *6*, 7234–7242.

[48] D. Cui, J. M. MacLeod, M. Ebrahimi, D. F. Perepichka, F. Rosei, M. Schmittel, M. Lackinger, Q. D. Zeng, C. Wang, K. Kern, V. Parasuk, D. Jiang, *Chem. Commun.* **2015**, *51*, 16510–16513.

[49] L. Xu, X. Zhou, W. Q. Tian, T. Gao, Y. F. Zhang, S. Lei, Z. F. Liu, *Angew. Chemie Int. Ed.* **2014**, *53*, 9564–9568.

[50] D. Peyrot, F. Silly, *ACS Nano* **2016**, *10*, 5490–5498.

[51] K. J. Shi, D. W. Yuan, C. X. Wang, C. H. Shu, D. Y. Li, Z. L. Shi, X. Y. Wu, P. N. Liu, *Org. Lett.* **2016**, *18*, 1282–1285.

[52] M. Di Giovannantonio, M. Tomellini, J. Lipton-Duffin, G. Galeotti, M. Ebrahimi, A. Cossaro, A. Verdini, N. Kharche, V. Meunier, G. Vasseur, Y. Fagot-Revurat, D. F. Perepichka, F. Rosei, G. Contini, *J. Am. Chem. Soc.* **2016**, *138*, 16696–16702.

[53] L. Grill, M. Dyer, L. Lafferentz, M. Persson, M. V. Peters, S. Hecht, *Nat. Nanotechnol.* **2007**, *2*, 687–691.

[54] M. Abel, S. Clair, O. Ourdjini, M. Mossoyan, L. Porte, *J. Am. Chem. Soc.* **2011**, *133*, 1203–1205.

[55] L. B. Pártay, G. Horvai, P. Jedlovszky, *Phys. Chem. Chem. Phys.* **2008**, *10*, 4754–4764.

[56] A. Rapakousiou, R. Sakamoto, R. Shiotsuki, R. Matsuoka, U. Nakajima, T. Pal, R. Shimada, A. Hossain, H. Masunaga, S. Horike, Y. Kitagawa, S. Sasaki, K. Kato, T. Ozawa, D. Astruc, H. Nishihara, *Chem. - A Eur. J.* **2017**, *23*, 8443–8449.

[57] R. Matsuoka, R. Sakamoto, K. Hoshiko, S. Sasaki, H. Masunaga, K. Nagashio, H. Nishihara, *J. Am. Chem. Soc.* **2017**, *139*, 3145–3152.

[58] J. Liu, W. Zan, K. Li, Y. Yang, F. Bu, W. Bao, Y. Xu, *J. Am. Chem. Soc.* **2017**, jacs.7b05025.

[59] A. Braslau, M. Deutsch, P. S. Pershan, A. H. Weiss, J. Als-Nielsen, J. Bohr, *Phys. Rev. Lett.* **1985**, *54*, 114–117.

[60] P. Kissel, A. Schlüter, J. Sakamoto, *Chem. - A Eur. J.* **2009**, *15*, 8955–8960.

[61] P. Kissel, J. van Heijst, R. Enning, A. Stemmer, A. D. Schlüter, J. Sakamoto, *Org. Lett.* **2010**, *12*, 2778–2781.

[62] P. Payamyar, K. Kaja, C. Ruiz-Vargas, A. Stemmer, D. J. Murray, C. J. Johnson, B. T. King, F. Schiffmann, J. Vandevondele, A. Renn, S. Götzinger, P. Ceroni, A. Schütz, L.-T. Lee, Z. Zheng, J. Sakamoto, A. D. Schlüter, *Adv. Mater.* **2014**, *26*, 2052–8.

[63] D. J. Murray, D. D. Patterson, P. Payamyar, R. Bhola, W. Song, M. Lackinger, A. D. Schlüter, B. T. King, *J. Am. Chem. Soc.* **2015**, *137*, 3450–3453.

[64] P. Payamyar, B. T. King, H. C. Ottinger, A. D. Schluter, H. C. Öttinger, A. D. Schlüter, K. Jousten, R. R. Nair, E. W. Hill, D. W. Boukhvalov, M. I. Katsnelson, R. A. W. Dryfe, I. V. Grigorieva, H. A. Wu, A. K. Geim, P. Smith, N. Stingelin, J. Sakamoto, A. D. Schlüter, *Chem. Commun.* **2016**, *52*, 18–34.

[65] G. Binnig, C. F. Quate, C. Gerber, *Phys. Rev. Lett.* **1986**, *56*, 930–933.

[66] Y. Martin, H. K. Wickramasinghe, *Appl. Phys. Lett.* **1987**, *50*, 1455–1457.

[67] C. C. Williams, H. K. Wickramasinghe, *Appl. Phys. Lett.* **1986**, *49*, 1587–1589.

[68] J. Varesi, A. Majumdar, *Appl. Phys. Lett.* **1998**, *72*, 37–39.

[69] M. F. Sykes, J. W. Essam, *J. Math. Phys.* **1964**, *5*, 1117–1127.

[70] D. Stauffer, A. Aharony, *Introduction to Percolation Theory*, 2nd editio, Taylor & Francis, London, **2010**.

[71] S. Feng, P. N. Sen, *Phys. Rev. Lett.* **1984**, *52*, 216–219.

[72] D. McMullan, *Scanning* **2006**, *17*, 175–185.

[73] M. von Ardenne, *Zeitschrift für Phys.* **1938**, *109*, 553–572.

[74] R. J. Young, G. N. A. van Veen, A. Henstra, L. Tuma in *Low Volt. Electron Microsc.* John Wiley & Sons, Ltd, Chichester, UK, **2012**, Chapter 3, pp. 57–71.

[75] E. Ruska, M. Knoll, *Zeitschrift für Tech. Phys.* **1931**, *12*, 389–400.

[76] M. Knoll, E. Ruska, *Zeitschrift für Phys.* **1932**, *78*, 318–339.

[77] M. G. Burke in *Transm. Electron Microsc.* Springer International Publishing, Cham, **2016**, pp. 81–102.

[78] G. Binnig, H. Rohrer, *IBM J. Res. Dev.* **1986**, *30*, 355–369.

[79] J. Ferguson, A.-H. Mau, *Mol. Phys.* **1974**, *27*, 377–387.

[80] J. Fritzsche, *J. für Prakt. Chemie* **1866**, *97*, 290–303.

[81] H. D. Roth, *Angew. Chemie Int. Ed. English* **1989**, *28*, 1193–1207.

[82] R Calas, R Lalande, F Moulines, J. G. Faugere, *Bull. Soc. Chim. Fr.* **1965**, 121–&.

[83] C. A. Coulson, L. E. Orgel, W Taylor, J. Weiss, *J. Chem. Soc.* **1955**, *0*, 2961–2962.

[84] H. Bouas-Laurent, J.-P. J.-P. Desvergne, A. Castellan, R. Lapouyade, J.-P. J.-P. Desvergne, H. Andrianatoandro, M. Cotrait, en, *Chem. Soc. Rev.* **2000**, *29*, 43–55.

[85] A. R. Mallia, R. Ramakrishnan, M. A. Niyas, M. Hariharan, *CrystEngComm* **2017**, *19*, 817–825.

[86] S. Tsuzuki, T. Uchimaru, M. Mikami, *J. Phys. Chem. A* **2006**, *110*, 2027–2033.

[87] S. W. Watt, C. Dai, A. J. Scott, J. M. Burke, R. L. Thomas, J. C. Collings, C. Viney, W. Clegg, T. B. Marder, *Angew. Chemie Int. Ed.* **2004**, *43*, 3061–3063.

[88] S. L. Cockroft, C. A. Hunter, K. R. Lawson, J. Perkins, C. J. Urch, *J. Am. Chem. Soc.* **2005**, *127*, 8594–8595.

[89] R. Xu, V. Gramlich, H. Frauenrath, *J. Am. Chem. Soc.* **2006**, *128*, 5541–5547.

[90] B. W. Gung, X. Xue, Y. Zou, *J. Org. Chem.* **2007**, *72*, 2469–2475.

[91] B. W. Gung, Y. Zou, Z. Xu, J. C. Amicangelo, D. G. Irwin, S. Ma, H.-C. Zhou, *J. Org. Chem.* **2008**, *73*, 689–693.

[92] S. L. Cockroft, J. Perkins, C. Zonta, H. Adams, S. E. Spey, C. M. R. Low, J. G. Vinter, K. R. Lawson, C. J. Urch, C. A. Hunter, *Org. Biomol. Chem.* **2007**, *5*, 1062–1080.

[93] I Zouev, D.-K. Cao, T. V. Sreevidya, M Telzhensky, M Botoshansky, M Kaftory, *CrystEngComm* **2011**, *13*, 4376–4381.

[94] T. Hinoue, Y. Shigenoi, M. Sugino, Y. Mizobe, I. Hisaki, M. Miyata, N. Tohnai, *Chem. – A Eur. J.* **2012**, *18*, 4634–4643.

[95] B. Stevens, E. Hutton, *Nature* **1960**, *186*, 1045–1046.

[96] J. B. Birks, *Rep. Prog. Phys.* **1975**, *38*, 903–974.

[97] D. O. Cowan, R. L. Drisko in *Elem. Org. Photochem.* Springer US, Boston, MA, **1976**, Chapter 2, pp. 19–74.

[98] H.-H. Perkampus, L. Pohl, *Zeitschrift für Phys. Chemie* **1964**, *40*, 162.

[99] M. Sugino, Y. Araki, K. Hatanaka, I. Hisaki, M. Miyata, N. Tohnai, *Cryst. Growth Des.* **2013**, *13*, 4986–4992.

[100] K. Nagarajan, S. K. Rajagopal, M. Hariharan, *CrystEngComm* **2014**, *16*, 8946–8949.

[101] M. Lehmann, S. Gloza, S. Roth, *Chem. Mater.* **2015**, *27*, 8181–8184.

[102] T. Seko, K. Ogura, Y. Kawakami, H. Sugino, H. Toyotama, J. Tanaka, *Chem. Phys. Lett.* **1998**, *291*, 438–444.

[103] S. Yamane, Y. Sagara, T. Kato, *Chem. Commun.* **2013**, *49*, 3839.

[104] Y. Sagara, T. Kato, *Angew. Chemie Int. Ed.* **2011**, *50*, 9128–9132.

[105] Y. Sagara, T. Kato, *Angew. Chemie* **2008**, *120*, 5253–5256.

[106] Y. Sagara, S. Yamane, T. Mutai, K. Araki, T. Kato, *Adv. Funct. Mater.* **2009**, *19*, 1869–1875.

[107] J. Chen, N. Voutier, J. Rajabi, A. Crochet, D. M. Bassani, K. M. Fromm, *CrystEngComm* **2017**, *19*, 5106–5113.

[108] P. Davidovits, M. D. Egger, *Nature* **1969**, *223*, 831–831.

[109] P. Davidovits, M. D. Egger, *Appl. Opt.* **1971**, *10*, 1615–1619.

[110] F. Balzarotti, Y. Eilers, K. C. Gwosch, A. H. Gynnå, V. Westphal, F. D. Stefani, J. Elf, S. W. Hell, *Science (80-.).* **2017**, *355*, 606–612.

[111] R. N. Jones, *Chem. Rev.* **1947**, *41*, 353–371.

[112] J. W. Sidman, *J. Chem. Phys.* **1956**, *25*, 115–121.

[113] D. P. Craig, P. C. Hobbins, *J. Chem. Soc.* **1955**, *0*, 2309–2319.

[114] D. P. Craig, P. C. Hobbins, *J. Chem. Soc.* **1955**, *0*, 539–548.

[115] E. A. Chandross, J. Ferguson, E. G. McRae, *J. Chem. Phys.* **1966**, *45*, 3546–3553.

[116] E. d. B. Barnett, J. W. Cook, T. E. Ellison, *J. Chem. Soc.* **1928**, *0*, 885–890.

[117] H.-H. Perkampus, *Zeitschrift für Phys. Chemie* **1957**, *13*, 278–297.

[118] H.-H. Perkampus, *Zeitschrift für Phys. Chemie* **1959**, *19*, 206.

[119] E. A. Chandross, J. Ferguson, *J. Chem. Phys.* **1966**, *45*, 3564–3567.

[120] N Abasbegović, N Vukotić, L Colombo, *J. Chem. Phys.* **1964**, *41*, 2575–2577.

[121] M. Nicol, M. Vernon, J. T. Woo, *J. Chem. Phys.* **1975**, *63*, 1992–1999.

[122] J. Räsänen, F. Stenman, E. Penttinen, *Spectrochim. Acta Part A Mol. Spectrosc.* **1973**, *29*, 395–403.

[123] H. K. Wickramasinghe, M. Chaigneau, R. Yasukuni, G. Picardi, R. Ossikovski, *ACS Nano* **2014**, *8*, 3421–3426.

[124] A. Einstein, *Ann. Phys.* **1905**, *322*, 132–148.

[125] P. Van der Heide, *X-ray Photoelectron Spectroscopy*, John Wiley & Sons, Inc., **2012**, pp. 1–13.

[126] J. H. Williams, *Acc. Chem. Res.* **1993**, *26*, 593–598.

[127] C. Y. Kim, P. P. Chandra, A. Jain, D. W. Christianson, *J. Am. Chem. Soc.* **2001**, *123*, 9620–9627.

[128] Y.-Y. Luk, N. L. Abbott, J. N. Crain, F. J. Himpsel, *J. Chem. Phys.* **2004**, *120*, 10792–8.

[129] E. V. Anslyn, D. A. Dougherty, *Modern Physical Organic Chemistry*, University Science Books, **2006**, p. 946.

[130] J. M. Klingsporn, N. Jiang, E. A. Pozzi, M. D. Sonntag, D. Chulhai, T. Seideman, L. Jensen, M. C. Hersam, R. P. V. Duyne, *J. Am. Chem. Soc.* **2014**, *136*, 3881–3887.

[131] X. Wang, J.-H. Zhong, M. Zhang, Z. Liu, D.-Y. Wu, B. Ren, *Anal. Chem.* **2016**, *88*, 915–921.

[132] M. D. Sonntag, D. Chulhai, T. Seideman, L. Jensen, R. P. Van Duyne, *J. Am. Chem. Soc.* **2013**, *135*, 17187–17192.

[133] Y. Xue, X. Li, H. Li, W. Zhang, *Nat. Commun.* **2014**, *5*, 4348.

[134] Neil M. Mackie, David G. Castner, E. R. Fisher, N. M. Mackie, D. G. Castner, E. R. Fisher, *Langmuir* **1998**, *14*, 1227–1235.

[135] D. T. Clark, D. Shuttleworth, *J. Polym. Sci. Polym. Chem. Ed.* **1980**, *18*, 27–46.

[136] D. T. Clark, M. Z. Abrahman, *J. Polym. Sci. Polym. Chem. Ed.* **1982**, *20*, 1729–1744.

[137] D. Clark, D. Kilcast, D. Adams, W. Musgrave, *J. Electron Spectros. Relat. Phenomena* **1972**, *1*, 227–250.

[138] C. Schmidt, T. Breuer, S. Wippermann, W. G. Schmidt, G. Witte, *J. Phys. Chem. C* **2012**, *116*, 24098–24106.

[139] D. Kozai, Y. Kabasawa, M. Ebert, S. Kiyonaka, Y. Otani, T. Numata, N. Takahashi, Y. Mori, T. Ohwada, *Mol. Pharmacol.* **2013**, *85*, 175–185.

[140] F. Cozzi, S. Bacchi, G. Filippini, T. Pilati, A. Gavezzotti, *Chem. - A Eur. J.* **2007**, *13*, 7177–7184.

[141] P. Muller, *Pure Appl. Chem.* **1994**, *66*, 1077–1184.

[142] J. K. S. Wan, R. N. McCormick, E. J. Baum, J. N. Pitts Jr, *J. Am. Chem. Soc.* **1965**, *87*, 4409–4414.

[143] S. Wiederhorn, H. Drickamer, *J. Phys. Chem. Solids* **1959**, *9*, 330–334.

[144] D. Vione, V. Maurino, C. Minero, E. Pelizzetti, M. A. J. Harrison, R.-I. Olariu, C. Arsene, *Chem. Soc. Rev.* **2006**, *35*, 441–453.

[145] K. J. Stine, Stine, K. J. in *Supramol. Chem.* John Wiley & Sons, Ltd, Chichester, UK, **2012**.

[146] G Weidemann, D Vollhardt, *Langmuir* **1996**, *12*, 5114–5119.

[147] D. Vollhardt, Brewster angle microscopy: A preferential method for mesoscopic characterization of monolayers at the air/water interface, **2014**.

[148] M. Moradi, L. G. Tulli, J. Nowakowski, M. Baljozovic, T. A. Jung, P. Shahgaldian, *Angew. Chemie Int. Ed.* **2017**, *56*, 14395–14399.

[149] T. Owen, *Fundamentals of modern UV-visible spectroscopy*, Agilent Technologies, **2000**, p. 52.

[150] T. Schmid, A. Messmer, B.-S. Yeo, W. Zhang, R. Zenobi, *Anal. Bioanal. Chem.* **2008**, *391*, 1907–1916.

[151] T.-a. Yano, T. Ichimura, S. Kuwahara, F. H'Dhili, K. Uetsuki, Y. Okuno, P. Verma, S. Kawata, *Nat. Commun.* **2013**, *4*, 2592.

[152] M. Li, F.-G. Klärner, J. Sakamoto, A. D. Schlüter, *Chem. - A Eur. J.* **2013**, *19*, 13348–13354.

[153] L. Opilik, P. Payamyar, J. Szczerbiński, A. P. Schütz, M. Servalli, T. Hungerland, A. D. Schlüter, R. Zenobi, *ACS Nano* **2015**, *9*, 4252–4259.

[154] P. Payamyar, M. Servalli, T. Hungerland, A. P. Schütz, Z. Zheng, A. Borgschulte, A. D. Schlüter, *Macromol. Rapid Commun.* **2015**, *36*, 151–158.

[155] P. Payamyar, PhD thesis, **2015**.

[156] B. Branchi, P. Ceroni, V. Balzani, M. C. Cartagena, F.-G. Klärner, T. Schrader, F. Vögtle, A. Ueno, W. C. Still, V. Vicinelli, F. Vögtle, *New J. Chem.* **2009**, *33*, 397–407.

[157] T. Hayashi, N. Mataga, Y. Sakata, S. Misumi, M. Morita, J. Tanaka, *J. Am. Chem. Soc.* **1976**, *98*, 5910–5913.

[158] P. Kln, J. Wirz, *Photochemistry of Organic Compounds*, John Wiley & Sons, Ltd, Chichester, UK, **2009**.

[159] A. Lauer, A. L. Dobryakov, S. A. Kovalenko, H. Fidder, K. Heyne, J. P. Rostron, A. Harriman, *Phys. Chem. Chem. Phys.* **2011**, *13*, 8723–8732.

[160] W. Fudickar, T. Linker, F. Gobert, R. V. Bensasson, T. Ossowski, *Chem. Commun.* **2008**, *447*, 1771–1773.

[161] H. Bouas-Laurent, J.-P. Desvergne, A. Castellan, R. Lapouyade, H. D. Becker, S. M. Sarge, H. Dreeskamp, en, *Chem. Soc. Rev.* **2001**, *30*, 248–263.

[162] M. Baumgartner, K. Garello, J. Mendil, C. O. Avci, E. Grimaldi, C. Murer, J. Feng, M. Gabureac, C. Stamm, Y. Acremann, S. Finizio, S. Wintz, J. Raabe, P. Gambardella, *Nat Nano* **2017**, *12*, 980–986.

[163] W. Wang, N. Xie, L. He, Y. Yin, **2014**, *5*, 5459.

[164] J. J. L. Morton, A. M. Tyryshkin, R. M. Brown, S. Shankar, B. W. Lovett, A. Ardavan, T. Schenkel, E. E. Haller, J. W. Ager, S. A. Lyon, *Nature* **2008**, *455*, 1085–1088.

[165] K. Saeedi, S. Simmons, J. Z. Salvail, P. Dluhy, H. Riemann, N. V. Abrosimov, P. Becker, H.-J. Pohl, J. J. L. Morton, M. L. W. Thewalt, *Science (80-.).* **2013**, *342*, 830 LP –833.

[166] B. Náfrádi, M. Choucair, K.-P. Dinse, L. Forró, **2016**, *7*, 12232.

[167] Y. Erlich, D. Zielinski, *Science (80-.).* **2017**, *355*, 950 LP –954.

[168] O. Loebich, *Gold Bull.* **1972**, *5*, 2–10.

[169] D Axelrod, D. E. Koppel, J Schlessinger, E Elson, W. W. Webb, *Biophys. J.* **1976**, *16*, 1055–69.

[170] W. Fudickar, T. Linker, *Langmuir* **2010**, *26*, 4421–4428.

[171] T. M. Vember, V. G. Mitina, A. S. Cherkasov, *Theor. Exp. Chem.* **1971**, *4*, 238–241.

[172] D. E. Applequist, R. L. Litle, E. C. Friedrich, R. E. Wall, *J. Am. Chem. Soc.* **1959**, *81*, 452–456.

[173] G. W. Breton, X. Vang, *J. Chem. Educ.* **1998**, *75*, 81.

[174] M. Khorasaninejad, W. T. Chen, A. Y. Zhu, J. Oh, R. C. Devlin, C. Roques-Carmes, I. Mishra, F. Capasso, *IEEE J. Sel. Top. Quantum Electron.* **2017**, *23*, 43–58.

[175] W. T. Chen, A. Y. Zhu, V. Sanjeev, M. Khorasaninejad, Z. Shi, E. Lee, F. Capasso, *Nat. Nanotechnol.* **2018**, 1.

[176] E. A. Weiss, G. K. Kaufman, J. K. Kriebel, Z. Li, R. Schalek, G. M. Whitesides, *Langmuir* **2007**, *23*, 9686–9694.

[177] V. V. Naik, R. Städler, N. D. Spencer, *Langmuir* **2014**, *30*, 14824–31.

[178] D. Nečas, P. Klapetek, *Open Phys.* **2012**, *10*, 181–188.

[179] W. Dai, F. Shao, J. Szczerbiński, R. McCaffrey, R. Zenobi, Y. Jin, A. D. Schlüter, W. Zhang, *Angew. Chemie Int. Ed.* **2016**, *55*, 213–217.

[180] F. Shao, V. Müller, Y. Zhang, A. D. Schlüter, R. Zenobi, *Angew. Chemie Int. Ed.* **2017**, *56*, 9361–9366.

[181] S. Jiang, Y. Zhang, R. Zhang, C. Hu, M. Liao, Y. Luo, J. Yang, Z. Dong, J. G. Hou, H. G., *Nat Nano* **2015**, *10*, 865–869.

[182] R. Zhang, Y. Zhang, Z. C. Dong, S. Jiang, C. Zhang, L. G. Chen, L. Zhang, Y. Liao, J. Aizpurua, Y. Luo, J. L. Yang, J. G. Hou, *Nature* **2013**, *498*, 82–86.

Curriculum Vitae

Personal Data

Name: Vivian Clarissa Müller

Date of Birth: 09 June 1989

Nationality: German

Email: vivian.mueller@mat.ethz.ch

Education

June 2014–Current	PhD Thesis in the Polymer Chemistry Group, ETH Zurich, Zurich Thesis title: *Two-Dimensional Polymers from the Air/Water Interface: Synthesis, Characterization, And Application* Advisor: Prof. A. Dieter Schlüter
Februar 2014	Master of Science ETH in Interdisciplinary Sciences, ETH Zurich, Zurich Thesis: *Synthesis of Molecular Building Blocks for the Construction of Zinc Porphyrin Push–Pull Acceptor Dyads* Advisor: Prof. François Diederich
Sept-Dec 2013	Chemistry Internship at Roche, Basel Synthetic Medicinal Chemistry
July 2012	Bachelor of Science ETH in Interdisciplinary Sciences, ETH Zurich, Zurich.

	Thesis: *Detection of chlorpropham on potatoes using desorption electrospray ionization* Advisor: Prof. Renato Zenobi
June 2009–Feb 2013	Research Assistant in the Hilvert Group, ETH Zurich, Zurich Directed Evolution Studies, Working under Sterile Conditions, Preparation of Various Selective Agar Plates, Management of Lab Materials.
July 2007	Französisches Gymnasium Berlin/Lycée français de Berlin, Abitur and Baccalauréat

Publications

1. C. Berchtold, V. Müller, L. Meier, S. Schmid, R. Zenobi ”Direct detection of chlorpropham on potato skin using desorption electrospray ionisation” *J. Mass Spectrom.* **2013**, *48*, 587–593.

2. V. Müller, T. Hungerland, M. Baljozovic, T. Jung, N. D. Spencer, H. Eghlidi, P. Payamyar, A. D. Schlüter ”Ink-Free Reversible Writing in Monolayers by Polymerization of a Trifunctional Monomer: Towards Rewritable ’Molecular’ Paper” *Adv. Mater.* **2017**, *29*, 1701220.

3. F. Shao, V. Müller, Y. Zhang, A. D. Schlüter, R. Zenobi ”Nanoscale Chemical Imaging of Interfacial Monolayers by Tip-Enhanced Raman Spectroscopy” *Angew. Chemie Int. Ed.* **2017**, *56*, 9361–9366.

4. V. Müller, F. Shao, M. Baljozovic, M. Moradi, Y. Zhang, T. Jung, W. B. Thompson, B. T. King, R. Zenobi, A. D. Schlüter ”Structural Characterization of a Covalent Monolayer Sheet Obtained by Two-Dimensional Polymerization at an Air/Water Interface” *Angew. Chemie Int. Ed.* **2017**, *56*, 15262-15266.

Talks and Poster Presentations

June 2016:	Talk at the 2nd *International Symposium on Synthetic Two-Dimensional Polymers*, Nara, Japan.
June 2016:	Poster Presentation at the 2nd *International Symposium on Synthetic Two-Dimensional Polymers*, Nara, Japan.
April 2017:	Talk at the *American Chemical Society Meeting*, San Francisco, USA.

Extracurricular Activities

June 2015–June 2017	President of the Scientific Staff Association at the Department of Materials (SAM). **Tasks**: Organization of various events, such as the D-MATL colloquium, PhD and Post-Doc retreat 2017, Collaboration Day 2015, Collaboration Day 2016, Breakfast Career Event, and Social Events; Representative in the Department Commission and Teaching Commission; Contact Person for other Departmental Associations
Fall 2014	Organization of the Master Graduation Ceremony 2014; Speaker at the Master Graduation Ceremony
Fall 2012	Board Member of the Winafe Organization Committee. Responsible for graphic design (design of poster, T-shirt, flyer, wristband)
Spring 2007	Organization of the High School Graduation Ceremony

Languages

German:	Native Speaker
English:	Fluent
French:	Fluent
Latin:	Latinum

Spanish:	Intermediate Knowledge
Italian:	Intermediate Knowledge

Computer Skills

Languages:	C++, C#, LaTeX, Javascript
EDV:	Adobe Photoshop, Adobe Illustrator, Mestrenova, Chemdraw, Excel, Origin, Word, Gwyddion, Nanoscope, PowerPoint

Interests and Activities

Organic and Analytical Chemistry, Surface Sciences, Programming, Politics, Environmental Issues
Ski, Snowboard, Tennis, Inline-skating, Reading, Travelling